PACROFI XI

11th Pan-American Current Research on Fluid Inclusions Conference

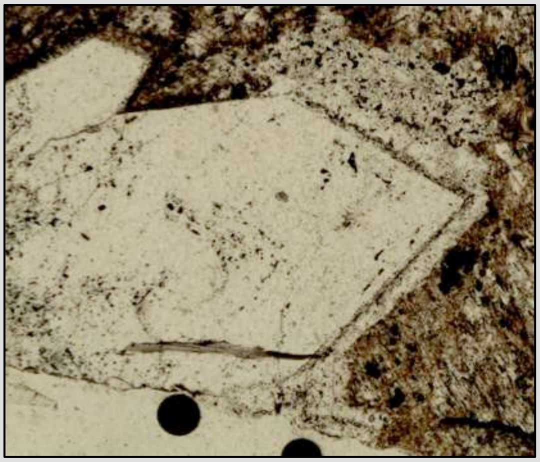

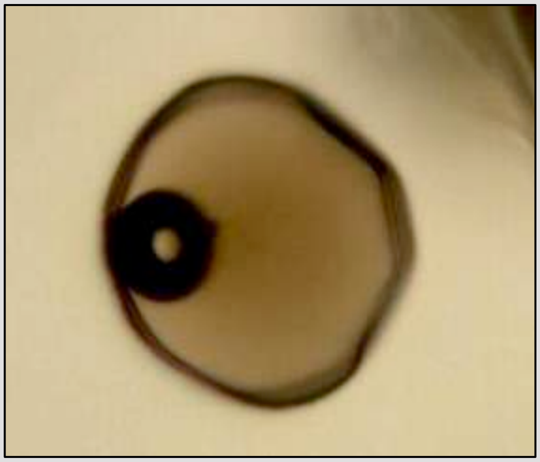

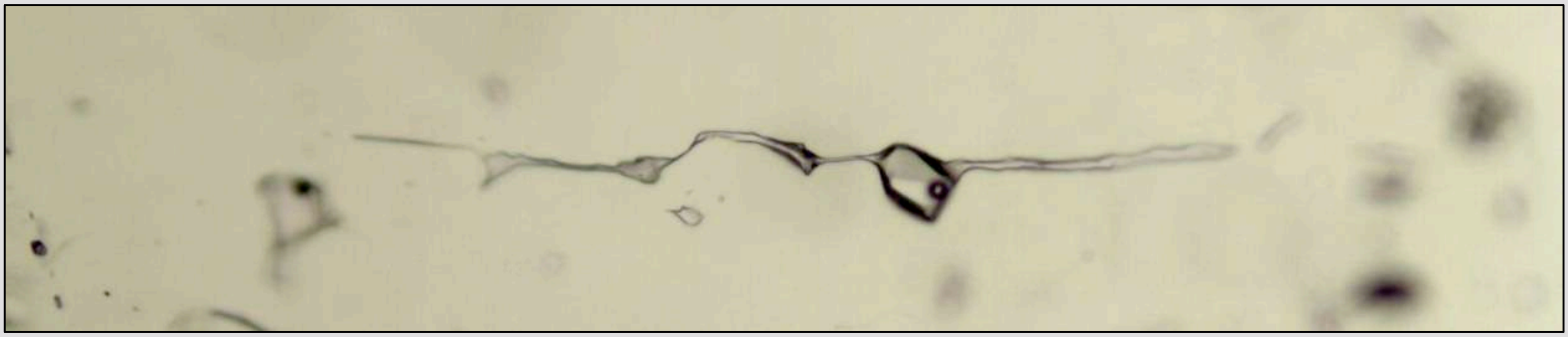

University of Windsor, Windsor, Ontario, Canada
June 18 - 20, 2012

PACROFI XI

11th Pan-American Current Research on Fluid Inclusions Conference

Abstracts with Program

18-20 June, 2012

University of Windsor
Windsor, Ontario, Canada

Iain Samson and Joel Gagnon
Conference Conveners

Edited by
Iain Samson, Joel Gagnon, Melissa Price

Preface

Welcome to Windsor and the 11th Pan-American Current Research on Fluid Inclusions conference (PACROFI XI). This year's conference mimics the character of past PACROFI meetings in representing a breadth of topics on fluid and melt inclusion research covering many different environments, including the mantle, plutonic and volcanic igneous rocks and processes, a range of mineral deposit types, sedimentary and surface environments, and even inclusions in meteorites. There is again representation from a variety of countries with delegates from Austria, Australia, Canada, China, Hungary, New Zealand, Poland, Switzerland, Turkey, and the United States.

The conference comprises 52 oral and poster presentations including six keynote talks by Adam Simon (UNLV), Csaba Szabó (Eötvös University), Steve Kesler (University of Michigan), Leonid Danyushevsky (University of Tasmania), Jacob Hanley (St. Mary's University), and Bob Burruss (USGS, Reston). Many thanks to each of them for agreeing to present a keynote talk. In addition, we are running an interactive workshop to allow demonstration and discussion of examples of fluid and melt inclusion petrographic relationships, interpretation, and documentation.

We would like to thank the organizations who have generously provided sponsorship: The Mineralogical Association of Canada (MAC), The University of Windsor, The Mineral Deposits Division (MDD) of the Geological Association of Canada, and The McCrone Group.

We hope that you will find the conference stimulating and your time in Windsor enjoyable.

Iain Samson and Joel Gagnon
June, 2012

Acknowledgements

The organizing committee would like to thank the following for their support of the PACROFI XI conference:

SCIENTIFIC COMMITTEE:

Iain Samson	University of Windsor
Joel Gagnon	University of Windsor
Robert Bodnar	Virginia Tech
Robert Linnen	Western University
Daniel Kontak	Laurentian University
Daniel Marshall	Simon Fraser University

INTRODUCTORY AND KEYNOTE SPEAKERS:

Robert Burruss	USGS, Reston
Leonid Danyushevsky	University of Tasmania
Jacob Hanley	St. Mary's University
Stephen Kesler	University of Michigan
Adam Simon	University of Nevada, Las Vegas
Csaba Szabó	Eötvös University

SPONSORS:

The McCrone Group
Mineral Deposits Division, Geological Association of Canada
Mineralogical Association of Canada
University of Windsor

LOCAL ORGANIZING COMMITTEE:

Iain Samson
Joel Gagnon
Sharon Horne
Alison Samson
Melissa Price

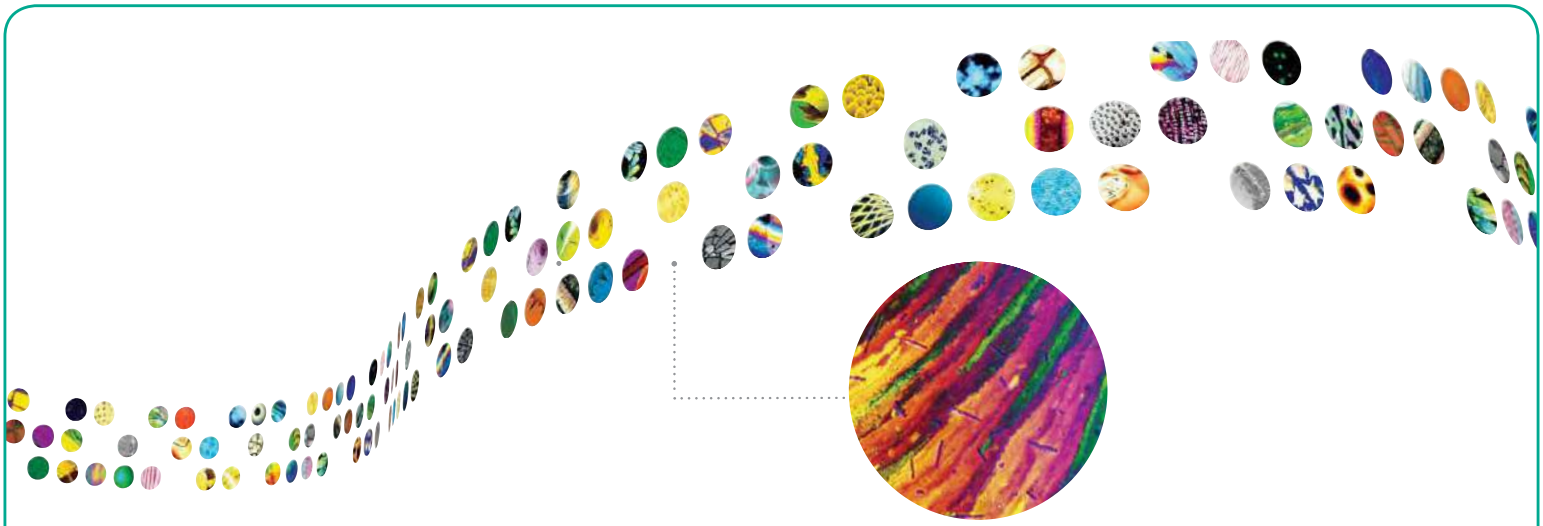

ECROFI-XXII

22ND BIENNIAL CONFERENCE

EUROPEAN CURRENT RESEARCH ON FLUID INCLUSIONS

5-9 JUNE 2013

ANTALYA

Cumhuriyet University

Istanbul University

Turkey

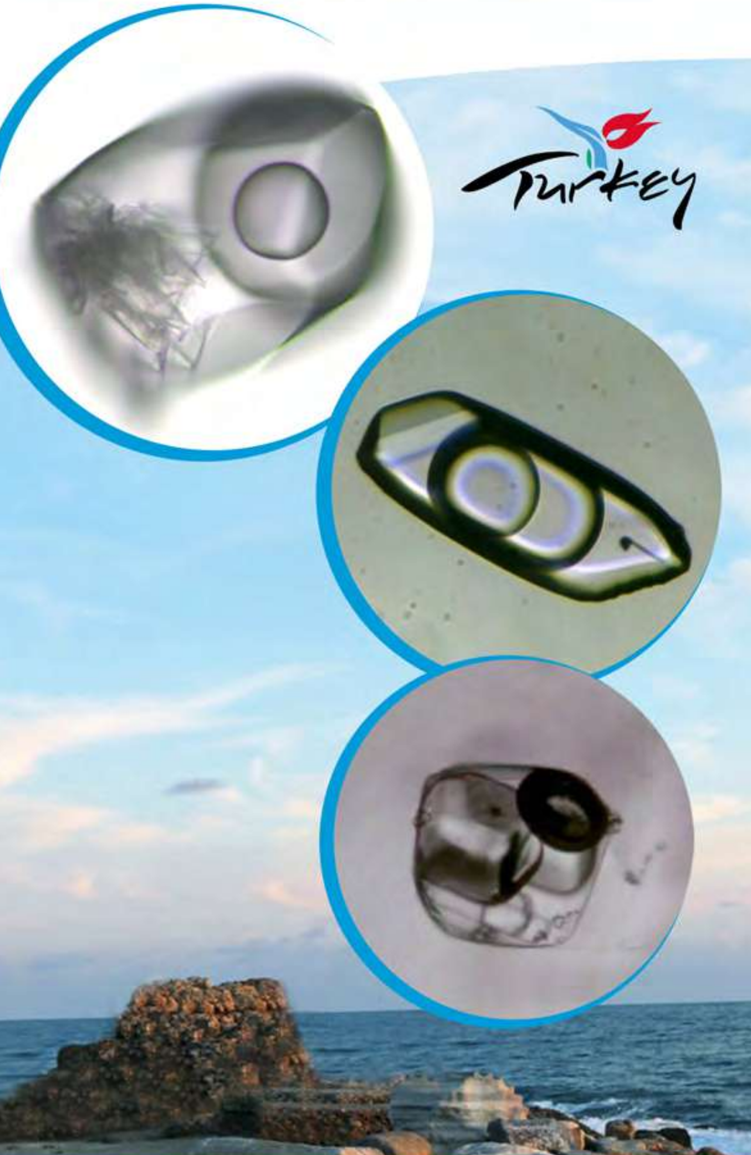

Scientific Secretariat
Cem KASAPÇI
Istanbul University Department of Geological Engineering,
Avcılar Campus, 34320 Avcılar-Istanbul / TURKEY
e-mail: ecrofi@ecrofi2013.org

www.ecrofi2013.org

FİGÜR

Organization Secretariat
Ayazmaderesi Cad. Karadut Sk. No:7 Dikilitas, Istanbul
Phone: +90 212 381 46 00 (pbx) Fax: +90 212 258 60 78
e-mail: ecrofi2013@figur.net

Conference Schedule PACROFI XI 2012

Sunday June 17	
5:00	**Icebreaker: Art Gallery of Windsor**

All oral sessions will be held in the Toldo Health Education Centre, Room 102

Monday June 18		
8:50	Introductory Remarks	
9:00	Simon, A. (Keynote)	Experimental insights into the variability of ore metal ratios in magmatic-hydrothermal systems
9:40	Lecumberri-Sanchez, P., Steele-MacInnis, M., Bodnar, R. J.	Experimental determination of the PVT properties of H_2O-NaCl-$FeCl_2$ fluids at magmatic-hydrothermal P-T conditions
10:00	Steele-MacInnis, M., Lecumberri-Sanchez, P., Bodnar, R.J.	PVTX properties of H_2O-$FeCl_2$ fluids
10:20	**Break**	
10:40	Doppler, G., Baumgartner, M., and Bakker, R.J.	Experimental re-equilibration studies of H_2O-D_2O-NaCl through quartz
11:00	Bakker, R.J.	Raman spectra of CO_2 and CH_4: resolution
11:20	Tattitch, B.C., Candela, P.A., Piccoli, P.M., Bodnar, R.J.	Determination of CO_2/H_2S ratios by Raman spectroscopy and model stability of mixed CO_2-H_2S clathrates in fluid inclusions
11:40	Mamedov, S., Adar, F., Tuschel, D., Koenig, A.	Applications of Raman microspectroscopy to fluid inclusion identification
12:00	**Lunch**	
1:30	Sun, R.	A new method for calculation of molar volume and bulk composition of CH_4-H_2O-NaCl fluid inclusions
1:50	Szabó, Cs (Keynote)	Significance of fluid, silicate and sulfide melt inclusions in mantle xenoliths from the Carpathian-Pannonian Region
2:30	Bodnar, R., Reynolds, J., Kontak, D., Fall, A.	Practical aspects of fluid inclusion data collection and interpretation (an informal session)
2:50	**Break**	
3:10	Poster introductions	
4:00	**Poster session**	
5:15	**Fluid inclusion workshop**	

Tuesday June 19		
9:00	Kesler, S.E. (Keynote)	A 50-year perspective on the role of fluid inclusion studies in ore deposit research
9:40	Ortelli, M., Kouzmanov K., Dilles J.H., Rusk B.G.	Fluid inclusion study in coexisting quartz and enargite from Main Stage veins at Butte, Montana
10:00	Marshall, D., Mavrogenes, J., Mernagh, T.	Melt inclusions of native silver and native bismuth at Cobalt, Ontario: an example of native-metal enrichments using experimental in situ melting studies
10:20	**Break**	
10:40	Simpson, M.P., Mauk, J. L., Bodnar, R. J.	The chemistry of fluid inclusions from the Waiorongomai epithermal Au-Ag vein deposit, Hauraki goldfield, New Zealand
11:00	Moncada, D., Bodnar, R.J.	An exploration model for precious metal deposits in the Guanajuato Mining District, Mexico, based on fluid inclusions and mineral textures
11:20	Bozkaya, G., Birlik, M.	Preliminary results on the origin of the fluids in the quartz veinlets related to hydrothermal alteration of the Eocene Kösedagi magmatics, northeast of Sivas, Turkey
11:40	Appold, M.S., Wenz, Z.J., Pelch, M.A.	Origin of Mississippi Valley-type deposits in the Ozark and Interior Low Plateaus, U.S. mid-continent: constraints from fluid inclusions
12:00	**Lunch**	
1:30	Danyushevsky, L.V. (Keynote)	The melt inclusion record of crystallisation of primitive mantle-derived magmas: an overview of the approach

Tuesday June 19

2:10	Severs, M.S., Gryger, K. J., Makin, S., Fedele, L., Bodnar, R.J., Bradford, W.	Long-term adakite generation and no evidence for magma mixing at Mount St. Helens based on melt inclusion analyses
2:30	Doherty, A., Bodnar, R.J., De Vivo, B., Messina, A.	Origin and evolution of the parent magmas of the Grey Porri Tuffs and selected lavas of Monte dei Porri, Island of Salina, Aeolian Islands, Southern Italy: a melt inclusion and geochemistry approach
2:50	**Break**	
3:10	Klébesz, R., Esposito, R., Bodnar, R.J., De Vivo, B., Lima, A., Petrosino, P., Török, K.	Origin of nodules in the 20 Ka Pomici di Base-Sarno eruption of Mt. Somma-Vesuvius, Italy, based on geochemistry of melt inclusions
3:30	Esposito, R., Hunter, J., Schiffbauer, J., Bodnar, R.J.	Depth profiling of the distribution of CO_2 and F in plagioclase-hosted melt inclusions from White Island (New Zealand)
3:50	Hofstra, A.H., Todorov, T.I., Adams, D.T., Marsh, E.E., Mercer, C.N.	Melt inclusion evidence for pre-eruptive enrichment and post-eruptive depletion of Lithium in silicic volcanic rocks — implications for the origin of Li-rich brines
4:10	Grzovic, M.L., Nabelek, P.I.	Li and B bearing fluid inclusions in the Harney Peak Granite, Black Hills, South Dakota
6:00	**Conference dinner: Sprucewood Shores Estate Winery**	

Wednesday June 20

9:00	Hanley, J.J., Ames, D.E. (Keynote)	The origin of early hydrothermal fluids associated with the Sudbury structure deduced from fluid inclusion Sr, C and H isotope analysis
9:40	Armstrong, J., Cline, J.S., Appel, K.	Evolution of ore fluids at the Batu Hijau porphyry copper-gold deposit, Sumbawa, Indonesia
10:00	Kontak, D.J., Ulrich, T., Kyser, K.T.	An integrated field, geochemical, thermometric and LA ICP-MS study of an intrusion-related Au setting: evidence for fluid mixing and rock dissolution
10:20	**Break**	
10:40	Burns, M., Kontak, D., Barrett, T.J.	Fluids in the Montclerg Archean mesothermal Gold system: an SEM-EDS evaporate mound approach to unravelling the chemistry and origin of different fluids
11:00	Xu, J.H., Xiao, X., Yang, R., Lin, L.H.	Fluid inclusion study on vein gold-copper mineralization at the Qiaxia-Sarekoubu area, southern Altaides, China
11:20	Burns, M.G.G., Kontak, D.J., Groat, L.A.	The role of fluids during alteration and mineralization of the highly evolved little Nahanni LCT-type pegmatite group: a fluid inclusion approach
11:40	Feng, Y., Samson, I.M.	The character of mineralizing fluids in the T-Zone, Thor Lake rare-element deposit, NWT, Canada
12:00	**Lunch**	
1:30	Burruss, R.C. (Keynote)	Analysis of hydrocarbon fluid inclusions in shale-gas systems: challenges and opportunities
2:10	Fall, A., Weisenberger, T. B., Eichhubl, P., Laubach, S. E., Davis, J.S., Bodnar, R. J.	Diagenetic controls on carbonate fracture cementation in tight-gas sandstones
2:30	Pottorf, R.J., Dreyfus, S., Siljeström, S., Pecheyran, C., Catalayud, B., Phan, N., Madincea, M., Reynolds, T.J.	Analysis of individual hydrocarbon fluid inclusions by femtosecond laser ablation and time of flight secondary ion mass spectrometry (ToF-SIMS)
2:50	**Break**	
3:10	Conner, A., Benison, K.C.	Observations of microorganisms and organic compounds in fluid inclusions from modern halite from Mars-analog Lake Magic, Western Australia
3:30	Zambito, J.J., Benison, K.C.	Reconstructing Permian hydrosphere, lithosphere, biosphere, and atmosphere from fluid inclusions in lacustrine halite: preliminary results from the Rebecca Bounds core, western Kansas
3:50	Discussion of future meetings	

Posters		
1	Bradford, W.B., Gryger, K.J., Makin, S., Fedele, L., Bodnar, R.J., Severs, M.S.	Investigation of volcanic processes during Cougar and Swift Creek Stages of Mount St. Helens
2	Espositio, R., Klébesz, R., De Vivo, B., Bodnar, R.J.	Volatile evolution of magma in the Campi Flegrei (Italy) volcanic system based on melt inclusions
3	Mercer, C.N., Hofstra, A.H., Marsh, E.E., Todorov, T.I., Koenig, A.E.	Tracking magmatic Molybdenum concentrations during evolution and degassing of the Hideaway Park rhyolite, Colorado: insights into Mo Partitioning in Climax-type deposits
4	Hanilçi, N., Aysal, N., Ceyhan, A., Şenkaya, S.	Preliminary microthermometric data on the Uludağ W-skarn deposit, Bursa, NW Turkey
5	Hewton, M.L., Marshall, D.D., Ootes, L., Loughrey, L.E.	Fluid conditions and possible sources for Devono-Mississippian beryl mineralization in the Mackenzie Mountains, Northwest Territories
6	Loughrey, L., Marshall, D., Ihlen, P.	Composition and formation conditions of fluid inclusions of the Byrud emerald deposit, Norway
7	Pandur, K., Ansdell, K., Halpin, K.	Preliminary petrographic observations on fluid inclusions in the Hoidas Lake REE deposit, Saskatchewan, Canada
8	Pandur, K., Molnár, F.	Hydrothermal evolution of the Recsk porphyry Cu ore system, Hungary, based on fluid inclusion studies
9	Smoke, R.P.S., Linnen R., Corcoran, P., Samson, I., Shahabi-Far, M., Good, D., Ames, D.	Petrography of fluid inclusions from the Marathon Cu-Pd deposit: the role of hydrothermal fluids in mineralization
10	Elmi Assadzadeh, G., Samson, I.M., Gagnon, J.E., Simpson, T.	The nature of daughter minerals in complex fluid inclusions in fluorite - insights from focused ion beam (FIB)-EDS analysis
11	Moncada, D., Bodnar, R.J.	Raman spectroscopic technique to determine the salinity of fluid inclusions
12	Steele-MacInnis, M., Lecumberri-Sanchez, P., Bodnar, R.J.	The numerical tool HOKIEFLINCS_H2O-NACL and its application in interpreting H_2O–NaCl fluid inclusion microthermometric data
13	Stewart, R.C., Kontak, D. J.	Nature, origin, and role of fluids trapped in the Granophyre Unit of the 1.85 Ga Sudbury Igneous Complex, Canada
14	Lamadrid, H.M., Bodnar, R.J., Lamb, W., Santosh M.	Water and hydrogarnet step-daughter minerals in CO_2-rich fluid inclusions in granulite facies rocks
15	Wolkowicz, K., Jackowicz E., Rzymelka, J.	Preliminary results of thermometric analysis of high temperature fluid inclusions in quartz in lithophysae agates from Nowy Kosciol (Sudety Mts., Poland)
16	Mathieu, J., Kontak, D.J., Turner, E.C.	Fluid inclusion study of hydrothermal dolomite and other late-stage cements in Neoproterozoic dolostone of the Wynniatt Formation (Victoria Island, NWT)
17	Zolensky, M.E., Bodnar, R.J., Fedele, L., Yurimoto, H., Itoh, S., Fries, M., Steele, A.	Analysis of direct samples of early solar system aqueous fluids

Abstracts

Origin of Mississippi Valley-type deposits in the Ozark and Interior Low Plateaus, U.S. mid-continent: constraints from fluid inclusions.

Appold, M.S.*, Wenz, Z.J.**, and Pelch, M.A.*

*Department of Geological Sciences, University of Missouri-Columbia, Columbia, MO, U.S.A.
**Minnesota Department of Natural Resources, St. Paul, MN, U.S.A.

Mississippi Valley-type (MVT) deposits have long been understood to be products of sedimentary basinal brines based on the bulk salinity, temperature, and major element composition of their fluid inclusions. Whether MVT mineralizing fluids resemble typical sedimentary brines with respect to ore metal content has until recently been far less certain and was a major concern of the present study. A further motivation for determining ore metal content in MVT mineralizing fluids is that ore metal content, together with pH, redox potential, and sulfur content, largely governs precipitation mechanism, which is also uncertain for many MVT deposits. Major element concentrations in MVT fluids reported in previous studies have largely been determined from bulk leachate analysis of fluid inclusions, where mixing of primary and secondary fluid inclusions and mineral matrix contributions are likely to have affected the reported results. Thus, another goal of the present study was to obtain improved measurements of major element concentrations, along with ore metal concentrations, through in situ analysis of individual fluid inclusions. These major element concentration data provide additional constraints on precipitation mechanism, fluid flow paths, and genetic relationships among deposits.

The focus of the present study was on fluid inclusions from the Southeast Missouri, Tri-State, Northern Arkansas, and Central Missouri districts of the Ozark Plateau, and the Illinois-Kentucky district of the Interior Low Plateau. A consistent feature found for these districts is that they contain populations of Pb-rich, sphalerite-hosted fluid inclusions (containing 100s to 1000s of ppm Pb) that probably reflect the intermittent invasion of Pb, and possibly overall metal-rich ore fluid into the districts during sulfide mineralization. High methane concentrations in both sphalerite- and gangue-hosted fluid inclusions indicate that mineralizing conditions were predominantly reducing, such that sulfide mineralization was probably caused by mixing of a Pb-rich ore fluid with a sulfide-rich fluid. Methane concentrations in fluid inclusions could be used to calculate minimum mineralization depths, which yielded a range from about 100 to 1500 m. Pb-rich ore fluids in all of the districts had dolomitizing Ca/Mg ratios, indicating that the fluids did not travel very far through the predominantly limestone aquifers in which sulfide mineralization is presently hosted. The Pb-rich ore fluids in the districts differed from one another with respect to major element composition indicating that, although all of the districts may have been formed from the same physical flow system, the ore fluids were chemically heterogeneous. In the Illinois-Kentucky district, the compositional distinctiveness of the ore fluid is consistent with inputs expected from local igneous activity contemporaneous with MVT mineralization.

Evolution of ore fluids at the Batu Hijau porphyry copper-gold deposit, Sumbawa, Indonesia.

Armstrong, J.*, Cline, J.S.*, and Appel, K.**

*University of Nevada, Las Vegas, Las Vegas, NV, U.S.A.
**Hamburger Synchrotronstrahlungslabor (HASYLAB) at Deutsches Elektronen-Synchrotron (DESY), Hamburg, Germany

Fluid inclusions contained within quartz veins from the Batu Hijau porphyry Cu-Au deposit in Indonesia were analyzed to track the evolution of fluid temperature, pressure, and composition throughout the deposit to better understand the formation of this and other Cu-Au porphyry deposits and to aid future exploration. The deposit contains an estimated 914 millions tonnes of ore containing 0.53 wt. % Cu and 0.40 g/t Au, making it one of the largest and richest porphyry Cu-Au deposits in Asia (Garwin, 2002). The fluid inclusions that were analyzed for this study are associated with intrusion of a series of tonalites between 3.76 ± 0.12 Ma and 3.67 ± 0.10 Ma into andesitic volcaniclastic rocks and a quartz diorite (Garwin, 2000). A combination of petrography, microthermometry, synchrotron x-ray fluorescence, and laser ablation-inductively coupled plasma-mass spectrometry (LA-ICP-MS) were used to determine the temperature, pressure, and compositional aspects of the deposit. Analyses focused on early A- and AB-type veins in samples that were collected over a vertical distance of greater than 1 km.

Four types of fluid inclusions were recognized based on the volume percent of the vapor bubble and the presence of halite (H), and were classified as VB35, VB20H, VB60, and VB85 inclusions. Results show that a high temperature, non-reactive fluid trapped in VB60 inclusions was introduced to the system first, was associated with only minor ore mineral precipitation, but may have contributed to early high temperature potassic alteration. A second, lower temperature, highly reactive fluid trapped in VB35 inclusions was subsequently introduced to the system and was likely responsible for the majority of ore mineral precipitation. This second fluid became immiscible during its ascent to the surface, forming a highly reactive brine and a non-reactive vapor, which were trapped in VB20H and VB85 inclusions, respectively.

Results further show that dense, two-phase VB35 inclusions, some of which contain opaque daughters, dominate in the deepest parts of the deposit, more than 800 meters below the surface. Inclusions at mid levels of the deposit, approximately 300 to 800 meters depth, are dominated by immiscible VB20H brine inclusions and low-density VB85 inclusions. Upper levels of the deposit are dominated by VB85 inclusions; however, VB20H brine inclusions are abundant. Homogenization temperatures of VB35 and VB20H inclusions were converted to trapping temperatures based on inclusion depth, assuming lithostatic pressure and no erosion of the young system. These corrections indicate that VB35 inclusions were trapped between approximately 250 and 400°C, with inclusions in the deepest part of the deposit being trapped at higher temperatures. Trapping temperatures for VB20H inclusions ranged from about 300 to 400°C. VB60 and VB85 inclusions homogenized by vapor bubble expansion and homogenization temperatures could not be determined (Sterner, 1992). Monitoring of vapor bubble expansion, however, suggested that homogenization of VB60 inclusions would have occurred at temperatures above approximately 500°C.

LA-ICP-MS analyses along with synchrotron analyses provided information on the reactivity of elements transported by the ore fluids trapped in inclusions. In general, Pb, Zn, and Mn were non reactive because elemental ratios were relatively constant in analyzed inclusions indicating that these elements were not variably fixed in or leached from the deposit. Alternatively, Cu is highly reactive and ratios between Cu and other elements vary widely across the deposit. Additional reactive elements that were fixed in the rock over time by fluid-rock reaction include Fe, Ca, K, Sr, and Ba. Analyses further show that the VB20H and VB35 fluids were the most reactive, because they exhibit significant changes in elemental ratios with respect to inclusion depth. Alternatively, VB60 and VB85 fluids were relatively non reactive and elemental ratios were fairly constant in these fluids. Although the deposit is a gold-rich porphyry, Au was quantified in only a single VB35 fluid inclusion analyzed using LA-ICP-MS, which contained 1.14 ppm Au.

REFERENCES

Fletcher, I. R., Garwin, S. L., McNaughton, N. J. (2000) SHRIMP U-Pb dating of Pliocene zircons. *In:* Beyond 2000: New Frontiers in Isotope Geoscience (eds. J.D. Woodhead,, J.M. Hergt, W.P. Noble), Abstracts and Proceedings. 73–74.

Garwin, S.L. (2000) The setting, geometry and timing of intrusion-related hydrothermal systems in the vicinity of the Batu Hijau porphyry copper-gold deposit, Sumbawa, Indonesia. Ph.D. thesis. University of Western Australia. 452p.

Garwin, S.L. (2002) The Geologic Setting of Intrusion-Related Hydrothermal Systems near the Batu Hijau Porphyry Copper-Gold Deposit, Sumbawa, Indonesia. Society of Economic Geologists Special Publication. Vol. 9. 333-366.

Sterner, M. (1992) Homogenization of fluid inclusions to the vapor phase: The apparent homogenization phenomenon. Economic Geology. Vol. 87. 1616–1623.

Pan-American Current Research on Fluid Inclusions (PACROFI-XI)
University of Windsor, Windsor, Ontario, Canada, June 18–20, 2012, Abstract Volume

Raman spectra of CO_2 and CH_4: resolution.

Bakker, R.J.

Resource Mineralogy, Department of Applied Geosciences and Geophysics, University of Leoben, Peter-Tunner-Str. 5, Leoben, Austria

The accuracy, precision, and uncertainty of peak positions in Raman spectra depend on the morphology of the spectra, as defined by the properties of best-fit curves (see also Bakker, 2011). Peak positions of CO_2 and CH_4 have been used to estimate the density of these gases in fluid inclusions (e.g., Lin et al., 2007, and Fall et al., 2011) in order to improve the characterisation of fluid properties in inclusions that contain homogeneous vapour phases, which cannot be studied by microthermometry. A clear shift in peak positions of CO_2 and CH_4 is observed as a function of density, or internal pressure in fluid inclusions. Mathematical equations were developed that describe the relationship between peak positions and density of pure CO_2 and pure CH_4. The present work has applied those equations to natural fluid inclusions in quartz from the Alpeiner Scharte (Olperer, Tauern Window, Austria), and H_2O-CO_2 fluid inclusions that were synthesized in the fluid inclusion laboratory of Leoben. The reliability of the equations is tested on individual fluid inclusions, and proposed improvements to this method are presented.

Quartz veins in gneisses from the Alpeiner Scharte contain abundant negative crystal shaped fluid inclusions that contain a vapour bubble (± 30 vol. %) and a liquid phase (± 70 vol. %) (Fig. 1). Raman spectroscopic analyses reveal only CO_2 in the vapour bubble (Fig. 2), and an H_2O-NaCl solution in the liquid phase. Microthermometric analyses of this inclusion reveal a T_m(clath) = +5.8°C and a T_m(ice) = -7.5°C.

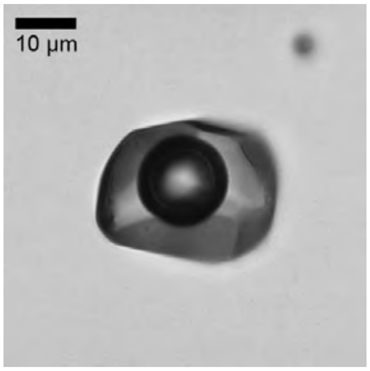

Figure 1. Two phase fluid inclusion at 20°C (Alpeiner Scharte).

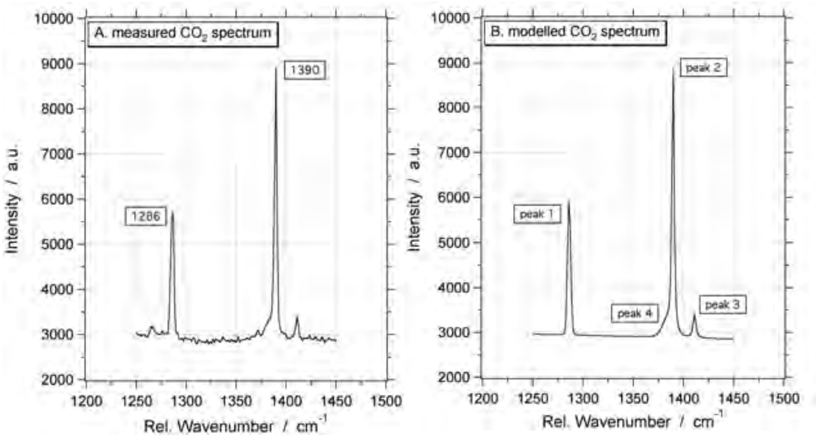

Figure 2. Observed (A) and modelled (B) Raman spectrum of CO_2.

The observed Raman spectrum of CO_2 (Fig. 2A) was modelled with best-fit equations for the individual peak positions with combined Gaussian-Lorentzian functions (Table 1):

Table 1.

Peak	Rel. Wavenumber	Width	Amplitude	% Gauss
1	1286.1432	3.5703	3071.85	0.9385
2	1389.6951	2.5784	6151.68	0.2456
3	1410.9938	3.2218	522.34	0.1682
4	1383.5372	11.3304	328.33	1

The obtained data are tested on consistency, i.e., the properties of fluid inclusions are calculated with microthermometric data using the program *ICE* (Bakker, 1997), and with Raman spectroscopic data using the wavenumber distance of the Fermi-double of CO_2 (Fall et al., 2011). The program ICE calculates a fluid inclusion bulk composition of $x(H_2O) = 0.9305$, $x(CO_2) = 0.0479$, and $x(NaCl) = 0.0216$, and a bulk molar volume of 26.23 $cm^3 \cdot mol^{-1}$. The density of the CO_2 vapour bubble is 0.1134 $g \cdot cm^{-3}$ at room temperature, corresponding to a $T_h(LV \rightarrow V) = +4.7°C$. The Fermi double of CO_2 (peaks 1 and 2) has a distance of 103.55 cm^{-1}, which corresponds to a CO_2 density of 0.3707 $g \cdot cm^{-3}$ according to Fall et al. (2011), and a $T_h(LV \rightarrow V) = +30.5°C$. At room temperature, a fluid inclusion with this property must contain a CO_2 liquid and vapour phase. Obviously, microthermometric experiments and observed phase assemblages in this fluid inclusion are in conflict with this model.

This apparent conflict results in the following queries: What is the resolution of a Raman spectrum? How well can a Raman spectrum be reproduced? What material is most appropriate for calibration of a Raman spectrum? The Raman detector (or spectral) resolution is defined by the wavenumber distance of two pixels (1.35 cm^{-1} for LABRAM and 0.46 cm^{-1} for LABRAM HR). In principle, the precision cannot exceed the spectral resolution. The calibration of the Raman spectrometer is usually performed with materials that have a well-defined spectrum (high intensity in a narrow wavenumber interval), such as neon, argon, diamond or silicon. These materials, however, have FWHW values of 1.8 cm^{-1} for the LABRAM and 0.7 cm^{-1} for the LABRAM HR. The FWHM is, in principle, a direct measure of the resolution of a spectrum. The analysis of spectra with distribution equations (e.g., Gaussian, Lorentzian) is a mathematical treatment of raw data, and may lead to a variety of peak positions. Consequently, these equations do not contribute to the resolution of raw data.

The Raman spectrum of CO_2 is re-examined in this study suing both a LABRAM and LABRAM HR. The spectra of the Fermi double of CO_2 are fitted to a Gauss-Lorentz distribution function. The spectra of CO_2 vapour bubbles in aqueous solutions are clearly influenced by the presence of dissolved CO_2 in water, and are introducing a larger uncertainty in the fitting procedures. The relationship between the wavenumber distance of the Fermi double and the density of CO_2 at a variety of temperatures cannot be described in a simple two-parameter equation (Fig. 3). At least three parameters must be involved to describe the pure CO_2 fluid properties. Below CO_2 homogenization conditions, uncertainties in peak estimations do not allow an accurate density calculation.

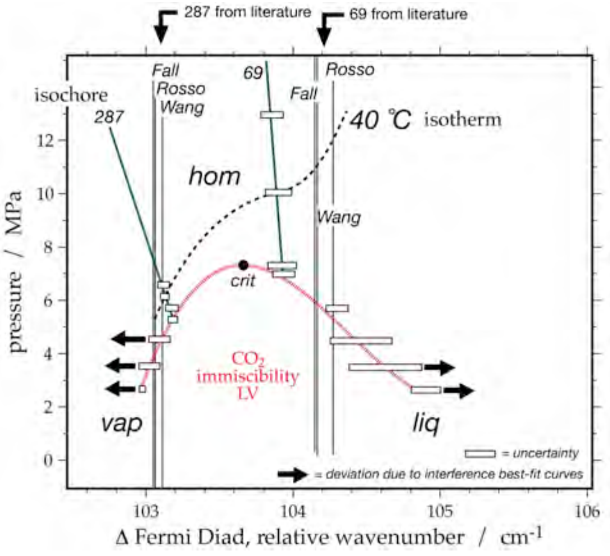

Figure 3. Pressure of CO_2 as a function of Fermi Diad (double). Constant values are indicated as obtained from literature. The isochores 287 and 69 $cm^3 \cdot mol^{-1}$ indicate the variation of the Fermi Diad in homogeneous fluid inclusions at variable temperatures. Below the critical point of CO_2, the immiscibility of liquid and vapour phases results in a large variation of Fermi double values, with a large uncertainty. The 40°C isotherm, i.e., at supercritical conditions, is a curved line within this diagram.

REFERENCES

Bakker R.J. (2011) ECROFI XXI Abstracts, Berichte der Geologische Bundesanstalt. 89, 32-33.
Bakker R.J. (1997) Computers & Geosciences. Vol. 23. 1-9.
Fall A., Tattich B., Bodnar R.J. (2011) Geochimica et Cosmochimica Acta. Vol. 75. 951-964.
Lin F., Bodnar R.J., Becker S.P. (2007) Geochimica et Cosmochimica Acta. Vol. 71. 3746-3756.
Rosso K.M., Bodnar R.J. (1995) Geochimica et Cosmochimica Acta. Vol. 59. 3961-3975.

Preliminary results on the origin of fluids in quartz veinlets related to hydrothermal alteration of the Eocene Kösedagi magmatics, northeast of Sivas, Turkey.

Bozkaya, G. and Birlik, M.

Department of Geological Engineering, Cumhuriyet University, Sivas, Turkey

The study area is located northeast of Sivas in north-central Anatolia. In this area, central Anatolian granitoids (Paleocene), syenitoids, and volcanics (Middle-Upper Eocene) were emplaced in relation to collision after the closure of Neotethys. Plutonic and volcanic rocks, known as Kösedag syenite (alkali feldspar syenite, syenite, and rare monzonite) and Karatastepe volcanics (basaltic trachy andesite, trachyte), occur in the study area.

Hydrothermal alteration was developed within both Karatastepe volcanics and Kösedag syenite due to 'hot-hot' contact. Hydrothermal minerals occur within the circular tension fractures in volcanic rocks, running parallel to the contact of plutonic and volcanic rocks. Hydrothermal alteration occurs in zones with a few square kilometers surface area (at most 30 km^2). The most common mineral parageneses in the argillic alteration zone in volcanic rocks are: 1) kaolinite + quartz + goethite + goyazite and/or alunite, and 2) kaolinite + quartz + jarosite + feldspar ± goethite and/or goyazite. Hypogene minerals are developed in two stages as early (kaolinite, pyrophyllite, illite, mixed-layered illite-smectite, smectite, quartz and opal-CT) and late (barite, ore minerals, alunite, goyazite, jarosite, chlorite, and mixed-layered chlorite-smectite) stage assemblages. Tourmaline and epidote are considered to be metasomatic in origin, but carbonates (calcite, dolomite, malachite, and azurite) developed as supergene minerals (Basibuyuk et al., 2007). In addition, Pb-Zn mineralization is also developed within the contact zone. Ore veins comprise mainly sphalerite, galena, chalcopyrite, fahlore, and covelline, with quartz and barite occurring as gangue minerals.

Fluid inclusion (FI) studies have been carried out on syenite- and volcanic-hosted quartz, and syenite-hosted barite from veins and the silica roof. On the basis of petrographic characteristics and the microthermometric behaviour of FIs, three types of FIs were identified: 1) primary inclusions in quartz crystals, 2) secondary inclusions in trails along healed fractures in quartz, and 3) primary inclusions in barite. In addition to common biphase (L+V) inclusions, monophase (V) and (L) FIs were also observed. Fluid inclusions occur in various sizes (mostly less than 5 to 10 µm) and shapes (rounded, semi-rounded and tabular).

The salinity of the fluids varies with different rock type: 1) 13.8 to 20.5 (avg. 16.4) wt.% NaCl equiv. for galenite-bearing quartz veins, 2) 9.8 to 16.9 (avg. 14.9) wt.% NaCl equiv. for syenite-hosted quartz veins, and 3) 10.7 to 15.3 (avg. 13.1) wt.% NaCl equiv. for syenite-hosted barite veins.

The average FI homogenization temperatures were 307.7ºC and 148.7ºC for primary and secondary inclusions, respectively, within the syenite-hosted, galena-bearing quartz veins. Average homogenization temperatures of 276.8ºC, 148.8ºC, and 268.3ºC were determined for primary inclusions in syenite- and volcanic-hosted quartz, and syenite-hosted barite occurrences, respectively. Syenite-hosted hydrothermal quartz shows relatively higher temperature and salinity values with respect to volcanic-hosted quartz. The different FI characteristics between syenite- and volcanic-hosted quartz occurrences were also confirmed by stable isotope data of hydrothermal clay occurrences in both host rocks (Basibuyuk et al., 2011). O and H isotope values were obtained for volcanic- (12.9 to 13.5 ‰ and -69 to -78 ‰, respectively) and plutonic-hosted (8.2 to 11.2 ‰ and -65 to -76 ‰, respectively) mixed-layered illite-smectite minerals.

Fluid inclusion data for quartz and barite minerals and stable isotope data for clay minerals indicate that the hydrothermal fluids responsible for syenite-hosted minerals were dominantly magmatic in origin, whereas these fluids were partly diluted with meteoric water in volcanic-hosted occurrences.

REFERENCES

Başıbüyük, Z., Yalçın, H., Bozkaya, Ö. (2007) Clay mineralogy related to hydrothermal alteration Eocene Kösedagi magmatics, Northeast of Sivas. 13th National Clay Symposium Proceedings. 44-64.

Başıbüyük, Z., Yalçın, H., Bozkaya, Ö. (2011) Mineralogical and geochemical properties for volcanic- and plutonic-rock-hosted hydrothermal illite-smectite occurrences, northeastern Sivas, Turkey. European Clay Conference Euroclay2011 Book of Abstracts, Antalya. 35.

Investigation of volcanic processes during Cougar and Swift Creek stages of Mount St. Helens.

Bradford, W.B.*, Gryger, K.J.*, Makin, S.*, Fedele, L.**, Bodnar, R.J.**, and Severs, M.S.*

**Environmental Science and Geology Program, Richard Stockton College of New Jersey, Galloway, NJ, U.S.A.*
***Department of Geosciences, Virginia Tech, Blacksburg, VA, U.S.A.*

Mount St. Helens (MSH) is the result of plate convergence between North America and the Juan de Fuca plate. Lying in the central axis of the Columbia River Embayment, MSH lies to the west of Mt. Adams, and may possibly have a direct effect on the magma being produced at Mt. Adams. The Cougar stage occurred 28 to 18 Ka ago and is considered the second most active period during the evolution of MSH after the Spirit Lake stage. After a brief period of dormancy (2 ka), the volcano erupted repeatedly during the Swift Creek stage from 16 to 12.8 ka (Clynne et al., 2008). These two periods of MSH genesis reflect a constant set of magmatic production mainly composed of dacitic composition, while the current Spirit Lake stage has produced a variety of mafic to felsic compositions during this same period. The main goal of this study is to investigate the magmatic processes that were dominant during the Cougar and Spirit Lake stages. In particular, the role of magma mixing and assimilation were considered in comparison to fractional crystallization. Additionally, the production of adakites at MSH was investigated to understand the role that slab melting may have had on the magma being produced. Adakites have been separated in two distinct petrogenetic categories: 1) melting of subducted hydrated basalt that is characterized as high silica andesite (HSA), and 2) low silica andesites (LSA) that are generated by melting of a mantle wedge region that has been metasomatized by slab melts rather than hydrous fluids (Martin et al., 2005). Samples of the eruptive periods mentioned above were collected from previously identified locations (Crandell, 1987; Smith and Leeman, 1987; Mullineaux, 1996; Clynne et al., 2008). Melt inclusion (MI) assemblages consisting of mostly small (5 to 40 μm) MI were located within plagioclase and pyroxene phenocrysts, These melt inclusions where analyzed by laser ablation-inductively coupled plasma mass spectrometry (LA-ICPMS) to determine their major and trace element abundances.

The geochemistry of the samples shows several trends. First, K_2O, CaO, and Al_2O_3 (Figure 1), and other major elements, show linear concentration trends with SiO_2 and lack any significant outliers. This suggests that magma mixing was not a major process during these stages at MSH; rather crystal fractionation was the dominant mechanism occurring within the magma chamber. That the melt inclusions found at MSH are of the HSA variety exclusively, suggesting that the magma was produced from slab melting during these periods. This is evident by plots of Sr/Y vs. Y, Nb vs. SiO_2%, and MgO% vs. SIO_2%, which are used to characterize the differences between LSA and HSA. Adakite genesis most commonly occurs during the early formation and final stages of the evolution of a volcano because this is when the conditions for slab melting are most optimal. Unusually, MSH adakites have occurred during these intermediate stages (Cougar/Swift Creek) of its history. Using the data collected, crystal fractionation models were performed on the primitive magma. These models yielded similar results to the geochemistry of our samples.

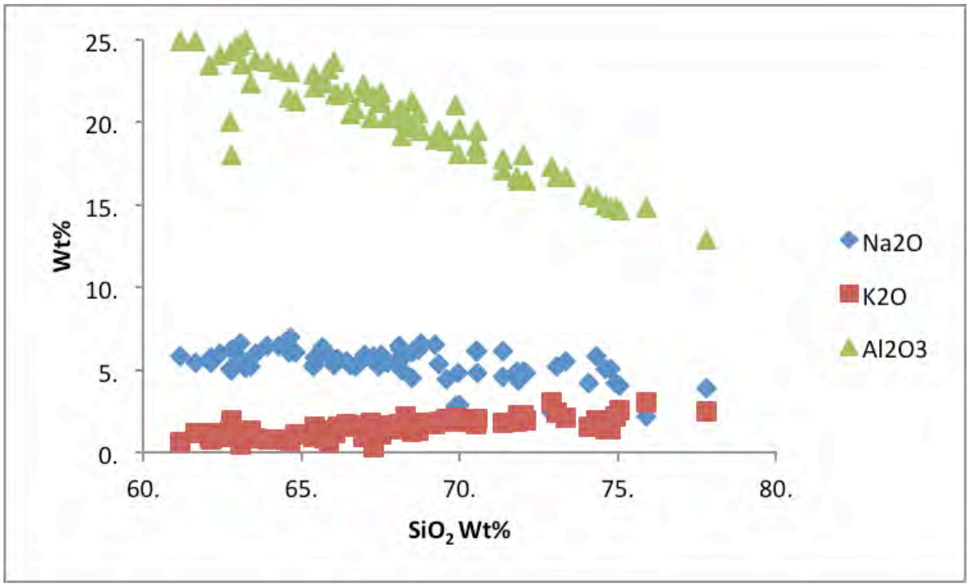

Figure 1.

REFERENCES

Clynne, M., Calvert, A., Wolfe, E., Evarts, R., Lanphere, M., Fleck, R. (2008) The Pleistocene Eruptive History of Mount St. Helens, Washington, from 300,000 to 12,800 Years before Present. US Geological Survey. Vol. 1750. 593-627.

Crandell, D. R. (1987) Deposits of pre-1980 pyroclastic flows and lahars from Mount St. Helens volcano, Washington. USGS Professional Paper. Vol. 1444 102p.

Martin, H., Smithies, R. H., Rapp, R., Moyen, J.-F., Champion, D. (2005) An overview of adakite, tonalite-trondhjemite-granodiorite (TTG), and sanukitoid: Relationships and some implications for crustal evolution. Lithos. Vol. 79. 1-24.

Mullineaux, D. R. (1996) Pre-1980 tephra-fall deposits erupted from Mount St. Helens, Washington. USGS Professional Paper. Vol. 1563. 99p.

Smith, D. R., Leeman, W. P. (1987) Petrogenesis of Mount St. Helens dacitic magmas. Journal of Geophysical Research. Vol. 92. 10313-10334.

The role of fluids during alteration and mineralization of the highly evolved Little Nahanni LCT-type Pegmatite Group: a fluid inclusion approach.

Burns, M.G.G.*, Kontak, D.J.*, and Groat, L.A.**

**Department of Earth Sciences, Laurentian University, Sudbury, ON, Canada, mg_burns@laurentian.ca*
***Department of Earth and Ocean Sciences, University of British Columbia, Vancouver, BC, Canada*

The 82 Ma Little Nahanni Pegmatite Group (LNPG), NWT, Canada, consists of a dike swarm of highly evolved LCT-type (**L**ithium, **C**esium, **T**antalum) pegmatites. This swarm contains several hundred, centimetre- to meter-scale, sub-vertical dikes over a strike length of approximately 15 km. The dikes intrude Precambrian to Lower Cambrian rocks of the Yusezyu and Narchilla formations, part of the Hyland Group, and are composed of siliciclastics and calcareous units formed in a passive margin setting. The pegmatites straddle the Yukon-NWT border in the Mackenzie Mountains with spectacular exposure, both vertically and along strike. Outcrop and drill core samples of the pegmatites record textures, mineralogy, and alteration (e.g., sodic) common to other well known LCT-type pegmatites (e.g., Tanco pegmatite, Manitoba).

The role of fluids and fluid-melt interaction during pegmatite formation has been, and remains, an important and debated issue. Through the analysis of fluid inclusions in samples from LNPG, this study aims to address the following: (1) whether or not fluids were present during pegmatite crystallization; (2) source of the fluids and contained solutes; (3) timing of fluids with respect to pegmatite evolution; (4) the role of fluids in pervasive sodic and phyllic alteration; and (5) the genetic association of fluids with oxide (Ta, Nb, Sn, W) mineralization. Two distinctly different fluids are observed in quartz: (1) a low-salinity, high-density aqueous fluid, and (2) an aqueous carbonic fluid with variable $X(CO_2)$. The aqueous carbonic fluid is interpreted from petrography to predate the aqueous fluid and is hosted in quartz, spodumene, K-feldspar, tourmaline, and cassiterite. Spodumene-hosted inclusions contain solids with high birefringence, interpreted to be stepdaughter phases.

An important observation in these pegmatites is the high degree of alteration present, manifested as secondary albite, muscovite, and lepidolite, which are common throughout the pegmatites. Mineralization, in the form of columbite-group oxides and cassiterite, is commonly associated with pervasive albite and muscovite altered regions of the pegmatite. Altered samples are inundated with secondary fluid inclusions in quartz, spodumene, and cassiterite. Thus, determining the chemistry, timing of fluid entrapment, and the fluid source is essential for understanding the nature of the alteration and mineralization in these and other highly evolved pegmatites.

Microthermometry for FIAs indicate secondary aqueous fluids have Th between 210° and 250°C (Fig. 1) and low salinities (<1 wt. % eq. NaCl). Aqueous carbonic inclusions have $X(CO_2)$ between 0.15 and 0.95 g/cc for quartz-hosted inclusions and 0.2 to 0.55 g/cc for spodumene-hosted inclusions. The depression of the CO_2 triple point to between -57° and -74°C is attributed to the presence of both methane and nitrogen in the carbonic phase, as confirmed by Raman spectroscopy (Fig. 2). The salinity of aqueous-carbonic inclusions are also low (<1 wt. % eq. NaCl), as indicated by clathrate melting temperatures.

The solute chemistry of the fluid inclusions was determined semi-quantitatively using the SEM-EDS evaporite method (Fig. 3). The salt mounds generated in this method were dominated by the major cations Na, K, and Ca (Fig. 4), with minor to trace amounts of Fe, S, As, F, and Zn (Fig. 4). Derivation from a pure NaCl salt occurs with Cl deficiency, which correlates with an increase in S and Fe. The chemistry of the salt mounds (Fig. 4) indicates the presence of elements exotic to pegmatites, the presence of which indicates the pegmatitic-hosed fluids must have exchanged with the country rocks. This interaction of the fluids with the wall rocks is also suggested by $\delta^{13}C$ values of -22‰ for fluid inclusion extracts.

The involvement and role of fluids at LNPG in both the pegmatite alteration and mineralization processes is not yet fully understood. Thus, although field observations directly relate late-stage hydrous mineral assemblages with narrow zones of high-grade oxide mineralization (Ta, Nb, Sn, W), the low-salinity and secondary nature of the inclusions precludes them from being directly related to mineralization. In additon, the lack of any primary fluid inclusions supports the London (2008) model in that the pegmatite melt may have remained water undersaturated during most of its crystallization history. Thus, this study supports, instead, the ingress of a late-stage sodic melt enriched in rare metals that is responsible for both the observed mineralization and extensive sodic metasomatism. That such a model is applicable to other evolved and mineralized pegmatite fields (e.g., Tanco pegmatite) is also suggested.

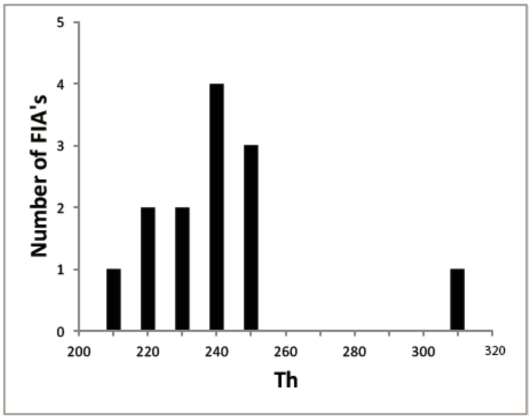

Figure 1. Homogenization temperatures for aqueous-type FIAs. All inclusions homogenized by bubble contraction.

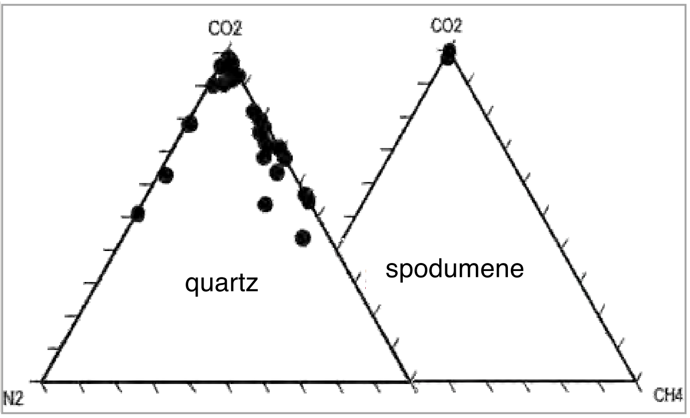

Figure 2. Ternary plots of gas compositions determined by laser Raman spectroscopy displayed by inclusion host.

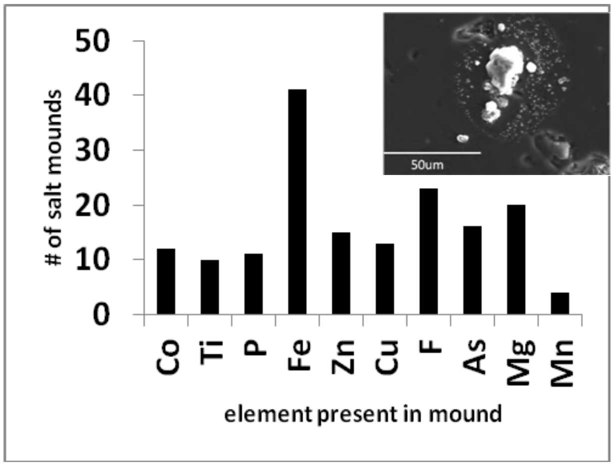

Figure 3. Decrepitate mound (inset) and histogram of evaporate mound data showing the relative presence of elements as solutes in quartz-hosted fluid inclusions.

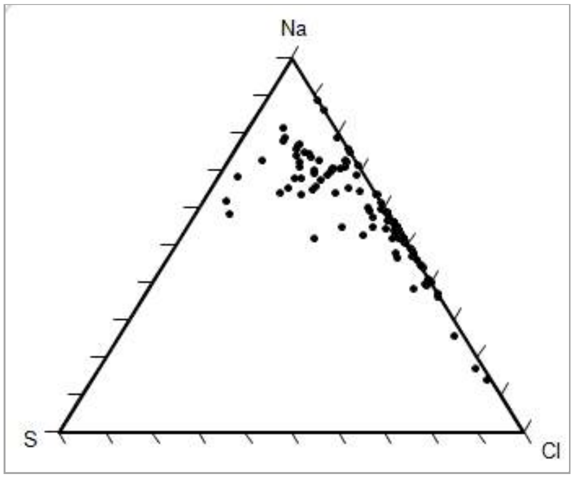

Figure 4. Na-S-Cl ternary plot for evaporate mounds. Note the increase in S content as Na:Cl ratio deviates from 1:1, which suggests input from a wall rock source.

REFERENCES

London, D. (2008) *Pegmatites.* The Canadian Mineralogist. Special Publication 10.

Fluids in the Montclerg Archean mesothermal gold system: an SEM-EDS evaporate mound approach to unravelling the chemistry and origin of different fluids.

Burns, M.*, Kontak, D.**, and Barrett, T.J.***

Department of Earth Sciences, Laurentian University, Sudbury, ON, Canada,
**mg_burns@laurentian.ca, **dkontak@laurentian.ca*
****29 Toronto St. S., Markdale, ON, Canada N0C 1H0, tjbarrett1@sympatico.ca*

This study summarizes detailed petrographic observations, fluid inclusion microthermometry, and SEM-EDS analysis of evaporate mounds performed on a suite of samples from the Montclerg gold property near Timmins, Ontario, Canada. The deposit represents an Archean-aged, auriferous, mesothermal quartz-carbonate ± sulphide (i.e., pyrite, arsenopyrite) vein system cutting a mixed sequence of mafic and felsic volcanic rocks, which are intruded by quartz-feldspar porphyry dykes. The purpose of the present study is to determine the types and origins of fluids present in the quartz veins via their thermometric and chemical properties, which can then be used to constrain trapping conditions and chronology of fluid entrapment.

Most Archean mesothermal or lode-gold systems, including Montclerg, experienced a complex deformational and metamorphic history, and were subjected to ingress of fluids of variable origin, which may be synchronous with or post-date mineralization. Petrographic observations reveal the presence of crack-seal textured quartz, open space infilling by different quartz generations (e.g., comb textures), and components of extensional shear veins. Rarely in these complex systems is it possible to unambiguously identify the mineralizing fluids due to multiple overprinting fluid events and re-equilibration of fluid inclusions, and Montclerg is no exception. In these cases, petrographic and microthermometric data cannot provide clear answers and thus an alternative approach to understanding fluids is required. In the samples studied, we used fluid salinity and fluid composition (i.e., two-phase H_2O, two- and three-phase H_2O-CO_2) to identify different fluid types versus liquid-vapour ratios (i.e., low- vs. high temperature), because the samples were variably recrystallized and most inclusion populations texturally modified. In addition, evaporate mounds were generated and analyzed by SEM-EDS in order to classify the chemistry of the solutes and identify different fluid types. The salt mound data were used together with ice melting temperatures and salinity data to relate the salt mound chemistry back to specific fluid inclusion types.

Thermometric measurements indicate three distinct fluids: (1) a low-temperature aqueous fluid, (2) an aqueous-carbonic fluid, and (3) a moderately saline, aqueous fluid. For the aqueous inclusions, the salinity of fluid inclusion assemblages varies from near 0 wt. % eq. NaCl (i.e., close to meteoric water) to 24 wt. % eq. NaCl, with the majority of the data below 12 wt. % eq. NaCl. In the moderately saline inclusions, first melting occurred at or above -21°C, thus Na is the dominant cation in solution (Figs. 1a, 2a). In contrast, first melting in the higher salinity inclusions occurred between -50° to -40°C, which suggests the presence of divalent cations, most likely Ca. In the aqueous-carbonic inclusions, CO_2 melted between -62.5° to -64°C, which indicates the presence of either CH_4 or N_2 (Fig. 1b), whereas clathrate melting occurred between 13° and 14.5°C (Fig. 1c), and is consistent with the presence of CH_4. The density of CO_2 varies, as indicated by the range for Th_{CO2}, both to the L or V phase, at between 0° and -17°C (Fig. 1d).

Results of the evaporate mound analysis agree with microthermometry measurements. In terms of the major solutes (Na, Ca, K), three types of mounds are recognized: Na-(Ca), Ca-Na, and K-Na (Fig. 2a). These ternary plots also show that certain mound compositions appear to dominate a single sample, rather than all types occurring uniformly within all samples. Thus, the K-rich mounds appear mainly in one sample, whereas Na- and Ca-rich mounds both occur in the other samples. Iron and F were detected in both the Na- and Ca-rich mounds, but were absent in the K-rich mound (Figs. 2b to e). A few mounds contained S at concentrations up to 5 to 10 wt. % (solutes normalized to 100%). Interestingly, Fe and S tend to occur in the same mounds (Figs. 2f, g, h). In summary, three distinct fluid types are indicated from analysis of the mounds: (1) Na-rich with minor Ca, Fe, and F; (2) Ca-rich with appreciable Na, and minor Fe and S; and (3) K-rich with some Na, but lacking Fe and Ca.

This study shows that simple inferences of fluid chemistry based on ice melting for complex mineralized vein systems is inadequate to characterize the fluid chemistry and, thus, to make inferences about the types of fluid present and their sources. The lack of well preserved fluid inclusions in many such settings also limits the evaluation and interpretation of the role of fluids in the mineralizing process. In addition, although many fluid inclusion studies have been done on typical mesothermal settings, the lack of solute chemistry limits interpretation of the results. To resolve this problem, we suggest an integrated thermometric-evaporate mound approach as illustrated here. This approach will provide more insight into the nature and, therefore, origin and role of fluids in the mineralizing processes in not only Archean quartz-carbonate ± sulphide systems, but also their younger analogues.

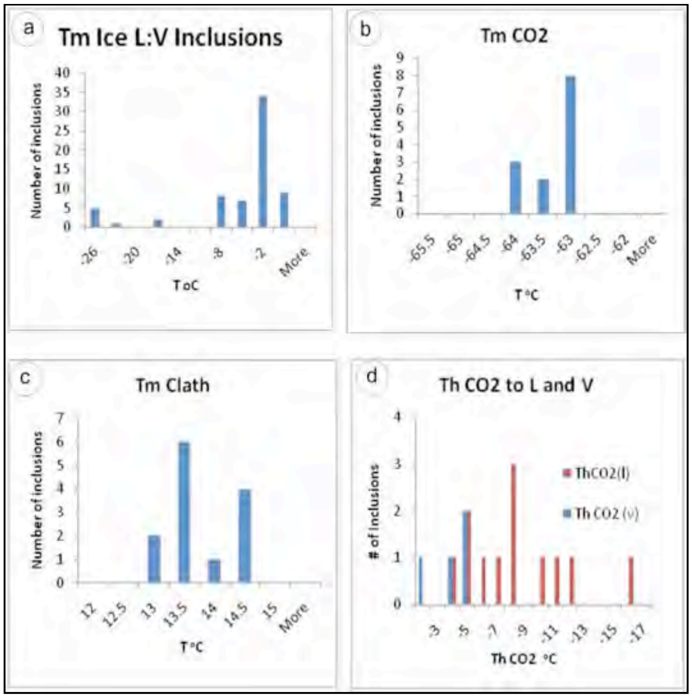

Figure 1a-d. a) Ice melting temperatures indicating a range in salinities. b) CO_2 melting temperatures indicate the presence of methane. c) Elevated clathrate melting temperatures also indicate the presence of methane. d) Very low Th CO_2 temperatures indicate the high density of the CO_2 phase of the inclusions.

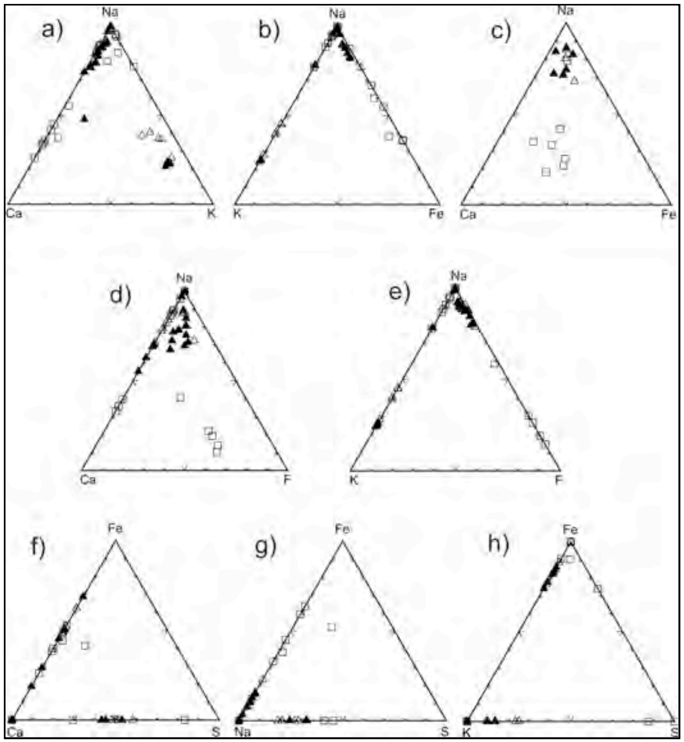

Figure 2a-h. Decrepitate mound results from three different samples plotted on ternary diagrams. Fig. 2a) Major solute (K, Na, Ca) plot revealing that certain samples (different symbols) contain only one fluid type. Fig. 2a through h) Three mound types are present: (1) Na-rich with minor Ca, Fe and F (filled triangles), (2) Ca-rich type with Fe, F and some Na (open squares), (3) K-Na mound with some S, lacking Fe and Ca (open triangles).

Analysis of hydrocarbon fluid inclusions in shale-gas systems: challenges and opportunities.

Burruss, R.C.

US Geological Survey, Reston, VA, U.S.A., burruss@usgs.gov

Studies of liquid oil hydrocarbon fluid inclusions (HCFI) over the past 30-plus years have advanced rapidly from basic presence/absence observations to identify migration pathways and timing of oil migration (Burruss, 1981) to sophisticated GC-MS correlations of inclusion compositions with reservoired oil (George et al., 1997) and models of reservoir filling using laser scanning confocal microscopy (LSCM), Fourier transform infrared adsorption spectroscopy, and equations of state (Thiery et al., 2002). Raman spectroscopy is important for analysis of gas-rich inclusions and gases in aqueous inclusions in reservoir rocks, but has had a limited role in analysis of HCFI due to interference from fluorescence of aromatic components in the oil.

As attention has shifted to gas resources within shales, issues have emerged that could be addressed with inclusion studies. For example, gases produced from high thermal maturity shale-gas systems have unusual geochemical characteristics, particularly carbon and hydrogen isotopic reversals (Burruss and Laughrey, 2010), that are inconsistent with conventional models of the origin of natural gas resources by progressive thermal cracking of organic matter. Furthermore, in foreland fold-and-thrust basins, such as the Appalachian basin where shales may have been buried to depths greater than 7 km before basin uplift, mudrocks rich in organic matter may have reached lower greenschist metamorphic conditions, possibly generating a late-stage, methane-rich gas that could have migrated to shallower reservoir rocks. Detailed analysis of gas-rich inclusions trapped in such formations could provide important clues to the origin of the gases that are currently being produced from these formations.

In mudstones, the only samples containing fluid inclusions are the fracture filling cements. A fundamental geochemical challenge is whether the gases produced after artificial fracturing (hydrofracking) of the shale can be correlated with the compositions of gases that were present in the natural fractures that were present during deformation and fluid flow in the basin. Inclusions are generally abundant in synkinematic fracture filling cements but in most cases primary inclusions are rare. Abundant secondary inclusions occur in multiple orientations of intersecting microfractures and separating out distinct generations of fractures that can be correlated with deformation history is difficult. We can use Raman spectroscopy to compare the molecular composition of gases in individual inclusions in specific assemblages with the GC analysis of the produced gases. However, analysis of a key geochemical parameter, stable isotopic composition, still requires crushing relatively large samples, on the order of 0.5 g (Luders et al., 2012). Such sample sizes may not be possible from drill core and when available always result in a mixture of multiple generations of gases.

The issues with bulk analysis of inclusion fluids are classic, long standing problems in fluid inclusion studies. These issues have largely disappeared for analysis of aqueous inclusions with advances in LA-ICP-MS of individual inclusions. We attempted to limit these problems in analysis of oil inclusions by using fluorescence microscopy to identify distinct generations of inclusions and high-grade samples to improve the yield of fluid relative to sample size. Recent work applying laser ablation to oil inclusions (Volk et al., 2010; Zhang et al., 2012) suggests that we may be reaching the ability to measure meaningful compositions of individual oil inclusions or discrete inclusion assemblages. In principle, these ablation methods could be applied to gas-rich inclusions.

Regardless of the analytical method, the most fundamental issue for integration of inclusion observations with the history of fluid flow and deformation is knowledge of the history of inclusion trapping and potential of later re-equilibration of the inclusions to different PTX conditions. The problems with identifying primary, secondary, and pseudo-secondary inclusions are well known but rarely acknowledged in most publications. Identifying a sequence of cross-cutting microfractures with distinct inclusion assemblages is equally challenging. A significant component of this problem is the fact that inclusions occur in minerals in three-dimensional arrays and we study them in two dimensions in the plane of focus of a microscope. Understanding and communicating the 3D geometric relationships of inclusions to the orientation of the host mineral or to different inclusion assemblages is a daunting challenge.

During proof-of-concept experiments on the potential of using coherent anti-Stokes Raman scattering (CARS) microscopy to image HCFI in 3D (Burruss et al., 2012 in review), two additional simultaneous imaging modes provided remarkable new views of inclusions. In particular, second harmonic generation (SHG) images of both inclusions and microstructures in 3D within quartz grains, provide the opportunity to examine the geometry of intersecting inclusion arrays and the relationship of inclusions to low angle grain boundaries, twinning, and growth zones. Another imaging mode, two photon excitation fluorescence (TPEF), creates images similar to epi-fluorescence LSCM of HCFI. The high sensitivity of this method revealed that some assemblages of CH_4-rich inclusions with low temperature phase behavior are weakly fluorescent. Re-evaluation of conventional Raman spectra of these inclusions revealed that the baseline of the inclusion spectra is elevated above the baseline of the spectra in the quartz adjacent to the inclusion. The elevated baseline appears to be related to the presence of TPEF. Careful reexamination of these gas-rich inclusions in widefield epi-fluorescence microscopy identified weak visible wavelength fluorescence consistent with the presence of trace amounts of high molecular weight aromatic hydrocarbons in the gas.

The ability to image fluid inclusions in quartz in 3-D with SHG presents a new opportunity to resolve questions of the timing of inclusion trapping and identification of inclusion assemblages. Detection of low intensity fluorescence in gas-rich inclusions through TPEF or by elevation of baseline in conventional Raman spectra provides new information on the role of late-stage cracking of high molecular weight hydrocarbons in gas genesis. Integration of conventional Raman spectroscopy of gas-rich inclusions combined with 3-D imaging to detect the orientation of chemically distinct inclusion assemblages offers the further opportunity to either identify high-grade samples dominated by distinct inclusion assemblages for bulk crushing and analysis or guide selection of inclusions for single inclusion analysis with ablation methods.

REFERENCES

Burruss, R. C. (1981) Hydrocarbon fluid inclusions in studies of sedimentary diagenesis. *In:* Fluid inclusions: Applications to petrology (eds. L.S. Hollister, M.L. Crawford). Volume Short Course Notes, Calgary. Mineralogical Association of Canada. Vol. 6. 138-156.

Burruss, R. C., Laughrey, C. D. (2010) Carbon and hydrogen isotopic reversals in deep basin gas: Evidence for limits to the stability of hydrocarbons. Organic Geochemistry. Vol. 41. 1285-1296.

Burruss, R. C., Slepkov, A. D., Pegoraro, A. F., Stolow, A. (2012) Unraveling the complexity of deep gas accumulations with 3D multimodal CARS microscopy. Geology. *In review.*

George, S. C., Krieger, F. W., Eadington, P. J., Quezada, R. A., Greenwood, P. F., Eisenberg, L. I., Hamilton, P. J., Wilson, M. A. (1997) Geochemical comparison of oil-bearing fluid inclusions and produced oil from the Toro sandstone, Papua New Guinea. Organic Geochemistry. Vol. 26. 155-173.

Luders, V., Plessen, B., di Primio, R. (2012) Stable carbon isotopic ratios of CH_4-CO_2-bearing fluid inclusions in fracture-fill mineralization from the Lower Saxony Basin (Germany) - A tool for tracing gas sources and maturity. Marine and Petroleum Geology. Vol. 30. 174-183.

Thiery, R., Pironon, J., Walgenwitz, F., Montel, F. (2002) Individual characterization of petroleum fluid inclusions (composition and P-T trapping conditions) by microthermometry and confocal laser scanning microscopy: inferences from applied thermodynamics of oils. Marine and Petroleum Geology. Vol. 19. 847-859.

Volk, H., Fuentes, D., Fuerbach, A., Miese, C., Koehler, W., Barsch, N., Barcikowski (2010) First on-line analysis of petroleum from single inclusion using ultrafast laser ablation. Organic Geochemistry. Vol. 41, 74-77.

Zhang, Z., Greenwood, P., Zhang, Q., Rao, D., Shi, W. (2012) Laser ablation GC-MS analysis of oil-bearing fluid inclusions in petroleum reservoir rocks. Organic Geochemistry. Vol. 43. 20-25.

Observations of microorganisms and organic compounds in fluid inclusions from modern halite from Mars-analog Lake Magic, Western Australia.

Conner, A. and Benison, K.C.

Department of Earth and Atmospheric Sciences, Central Michigan University, Mt. Pleasant, MI, U.S.A.

Lake Magic is one of the most extreme of hundreds of ephemeral acid-saline lakes in southern Western Australia. It has pH as low as 1.7, salinity as high as 32% TDS, temperatures ranging from 0 to 50°C, and some unusually high occurrences of SO_4 (up to 35,200 ppm), Si (up to 11,700 ppm), Al (up to 8,017 ppm), and Fe (up to 191 ppm)(Bowen and Benison, 2009). This environment exhibits parallel characteristics with Mars environments, including similarities in minerals, geochemistry, sedimentary textures and structures, and diagenetic features. Molecular studies of associated lakes in Western Australia have documented novel acidophilic, halophilic microorganisms (Mormile et al., 2009). Understanding fossilization of extremophiles in chemical sediments, such as halite and gypsum, precipitated in acid brines has implications for the search for past life on Mars. This ongoing study focuses on describing suspect microorganisms and organic compounds trapped in Lake Magic halite.

Optical petrography has been used to distinguish among minerals, prokaryotes, and eukaryotes within fluid inclusions in Lake Magic halite. Suspect prokaryotes, 1 to 3 microns in diameter, with rod and cocci shapes, have been observed. Larger, 4 to 6 microns in diameter, yellow spherules are suggestive of eukaryotic microorganisms, including *Dunaliella* algae. Algal suspects exhibit a thin gel outer layer. Transmitted light optical microscopy is the first step in identifying microorganisms because it provides morphological and color identification. Plane transmitted light and polarized light microscopy allow for distinction between minerals and suspect microorganisms, however, identification of organic compounds is limited by traditional microscopy.

UV-vis petrography was used to further confirm the presence of prokaryotes and eukaryotes, but also to detect some organic compounds. Exposure to UV visible light produces positive blue-green fluorescence of suspect prokaryotes and eukaryotes, and orange fluorescence of some organic compounds, such as beta-carotene.

Chemical analysis of the fluid inclusions and of the microorganisms was performed. Laser Raman analysis of microbial suspects yielded disordered, graphite spectra. Laser Raman spectroscopy of the orange-fluorescing solids confirm the presence of beta-carotene.

Our study has shown that microorganisms and organic compounds in extreme acid brines are trapped within fluid inclusions in halite and can be observed both optically and chemically. The search for life on Mars should incorporate such optical and chemical examination of Martian evaporites for possible microorganisms and/or organic compounds in fluid inclusions.

REFERENCES

Bowen, B.B., Benison, K.C. (2009) Geochemical characteristics of naturally acid and alkaline saline lakes in southern Western Australia. Applied Geochemistry. Vol. 24. 268-284.

Mormile, M.R., Hong, B.-Y., Benison, K.C. (2009) Molecular analysis of the microbial communities of Mars-analog lakes in Western Australia. Astrobiology. Vol. 9. 919-930.

The melt inclusion record of crystallisation of primitive mantle-derived magmas: an overview of the approach.

Danyushevsky, L.V.

CODES and School of Earth Sciences, University of Tasmania, Hobart, Tasmania, Australia

Crystallisation conditions of primary mantle-derived magmas at crustal levels differ from those of more fractionated magmas in two main aspects: 1) a high temperature contrast between the newly arrived magma and the plumbing system it enters, and 2) a large extent of chemical disequilibrium between the primitive melt and the phases present in the crustal plumbing system. This contribution will discuss the implications of these factors for the interpretation of melt inclusion compositional data. The presentation will focus on melt inclusions in olivine, since olivine is usually the first major mineral phase to form during crystallisation of primitive mantle-derived magmas.

1) The high temperature of crystallisation of such magmas leads to significantly faster diffusion rates within the early formed mineral phases, resulting in extensive post-entrapment re-equilibration of melt inclusions in primitive high-Fo olivine. These processes are capable of generating large changes in the concentrations of compatible elements within the initial volume of the trapped inclusion, and thus their understanding is essential for correct interpretations of melt inclusion data.

Relatively short diffusion distances required to generate significant changes to the trapped composition, compared to those required to change the composition of the entire host crystal, commonly lead to a situation where the inclusion composition is significantly altered, while the host crystal largely retains its original composition. Cooling of an inclusion after trapping results in crystallisation of olivine from the trapped melt, forming an olivine rim on the walls of the inclusion. The crystallising olivine rim is progressively enriched in Fe and Mn, and depleted in Mg and Ni, i.e., it has lower proportion of the forsterite component (Fo), resulting in a compositional gradient within the rim. The existence of this compositional gradient causes re-equilibration of the inclusion with its host. This re-equilibration is achieved by diffusion of Fe and Mn out of, and Mg and Ni into, the initial volume of the inclusion. This leads to a rapid decrease in Fe content of the residual melt inside the inclusion, a process referred to as “Fe-loss” by Danyushevsky et al. (2000). The extent of Fe-loss, i.e., the degree of re-equilibration, is defined as the amount of FeO* ‘lost’ by the residual melt relative to the amount that is ‘lost’ in the case of complete re-equilibration.

An example of olivine phenocrysts from an ~ 2.7 Ga Belingwe komatiite will be used to demonstrate the effects of Fe-loss on the composition of the inclusions and to discuss possible approaches to reversing the changes.

An extreme case of post-entrapment re-equilibration during slow cooling in a crustal magma chamber will be demonstrated using melt inclusions in olivine phenocrysts from an ~ 720 Ma sill within the Dovyren magmatic complex in Siberia.

Intrusion of a primitive melt into the plumbing system can lead to olivine grains containing melt inclusions being heated over the temperature of inclusion entrapment. In this case, host olivine around the inclusion would melt, increasing the Mg# of the melt inside the inclusion, and resulting in disequilibrium between the melt and host olivine. This leads to re-equilibration of the melt with the host, which is achieved by diffusion of Fe (and Mn) into, and Mg (and Ni) out of, the melt inside the inclusion. As a result, a rapid increase in the Fe content of the melt is observed, a process that can be referred to as ‘Fe-gain’. An example of olivine phenocrysts from a modern submarine volcanic province in the Southwest Pacific will be used to demonstrate the effects of Fe-gain.

2) High-Fo olivine phenocrysts, which crystallised within the magmatic plumbing system prior to eruption, often contain numerous, large melt inclusions, indicating fast crystal growth rates. In some relatively rare cases, such fast growth rates can be triggered within the entire body of a primitive melt, if the onset of crystallisation is caused by H_2O degassing. More often, however, the fast growth rates occur at the margins of the melt lens, where it is in contact with cooler wall rocks and/or pre-existing semi-

solidified crystal mush zones. The hotter, primitive melt causes partial dissolution (incongruent melting) of the mush zone / wall-rock phases, which are out of equilibrium with the primitive melt, and mixing of the reaction products with the primitive magma. These processes are referred to as dissolution-reaction-mixing (DRM) processes (Danyushevsky et al., 2004). The DRM processes also result in a rapid loss of heat from the primitive melt and thus cause localised rapid crystallisation of high-Fo olivines from the primitive melt, leading to entrapment of numerous, large melt inclusions. As a result, many of the melt inclusions in high-Fo olivine phenocrysts record DRM processes in progress, rather than the composition of the primitive melt, and can thus be referred to as ‘anomalous’ inclusions.

The DRM processes should have the largest impact on the compositions of melt inclusions trapped by olivine phenocrysts that crystallise early from hot primitive mafic magmas. In contrast, the more “evolved” (less forsteritic) olivine phenocrysts crystallise from melts that are comparatively cooler, and, therefore, have less reaction potential due to their reduced temperature and compositional contrast with the mush-zone phases. This can explain why the ‘anomalous’ inclusions are preferentially found in high-Fo olivine phenocrysts, relative to the evolved phenocrysts.

This mechanism for the formation of anomalous inclusions is consistent with the wider range of anomalous major element concentrations in inclusions from primitive subduction-related lavas relative to MORB. Primitive subduction-related magmas undergo more substantial fractionation than MORB (e.g., andesites and more evolved lavas are common in subduction-related settings, whereas erupted MOR melts are largely basaltic). Generally, this is because subduction-related magmas have higher H_2O contents and occur in settings with thicker crust. The larger extent of fractionation of the subduction-related magmas generally leads to a greater variety of mineral types in the mush zones within the plumbing systems. Thus, in the subduction-related settings, there are generally larger temperature differences and compositional disequilibrium between the primitive melts and the mush-zone assemblage, both facilitating DRM processes.

Melt inclusions in olivine phenocrysts from a variety of subduction-related and mid-ocean ridge settings will be used to demonstrate the effect of DRM processes.

REFERENCES

Danyushevsky, L. V., Della-Pasqua, F. N., Sokolov, S. (2000) Re-equilibration of melt inclusions trapped by magnesian olivine phenocrysts from subduction-related magmas: petrological implications. Contributions to Mineralogy and Petrology. Vol. 138. 68-83.

Danyushevsky, L.V., Leslie, R.A.J., Crawford, A.J., Durance, P. (2004) Melt inclusions in primitive olivine phenocrysts: the role of localised reaction processes in the origin of anomalous compositions. Journal of Petrology. Vol. 45. 2531-2553.

Origin and evolution of the parent magmas of the Grey Porri Tuffs and selected lavas of Monte dei Porri, Island of Salina, Aeolian Islands, Southern Italy: a melt inclusion and geochemistry approach.

Doherty, A.L.*, Bodnar, R.J.**, De Vivo, B.***, and Messina, A.*

**Università degli Studi di Messina, Messina, Italy*
***Virginia Tech, Blacksburg, VA, U.S.A.*
**** Università di Napoli Federico II, Naples, Italy*

Salina is the second largest of the Aeolian Islands and is located just north of Sicily in the Tyrhennian Sea. The island is composed of five volcanic edifices that formed between 430 and 13 Ka. Volcanic products on Salina exhibit a wide range in composition, with erupted products ranging from basaltic lava to rhyolitic pumice. The eruptions of Monte dei Porri were the last of the cone-building eruptions on Salina, occurring between 67 to 30 Ka, following approximately 60 Ka of repose. The eruptions marked the start of the second cycle of volcanism on the island and deposited the Grey Porri Tuffs (GPT). This cycle began with a series of explosive eruptions that Keller (1980) described as the most violent in the history of the Aeolian Islands. Outcrops attributed to the GPT are found throughout the Aeolian Islands and as distant as the Milazzo Peninsula on Sicily, approximately 30 km away.

Previous studies of Salina have focussed on the larger of the island's twin peaks, Fossa delle Felci and the rhyolitic explosion crater, Pollara, and little is known of the volcanic plumbing system of Monte dei Porri. The current study focuses on the origin and evolution of the magma(s) that produced the GPT and the lava units of Monte dei Porri.

The typical mineral assemblage for the GPT is calcic plagioclase, clinopyroxene (augite), olivine (Fo_{72-84}) and orthopyroxene (enstatite) ± amphibole and Ti-Fe oxides. The Monte dei Porri lava units exhibit a similar mineral assemblage but contain lower Fo olivines (Fo_{57-78}). The lava units also contain numerous mono- and multi-mineralic glomerocrysts, some of which contain quartz, K-feldspar and mica, sometimes associated with olivine. This is consistent with earlier studies, which suggested that crustal assimilation played a role in the evolution of the Monte dei Porri magma. Bulk-rock analyses identify the GPT host units as andesitic pumice (SiO_2 59.9 wt %) and high-silica basaltic scoria (SiO_2 53.4 wt%). Melt inclusions (MI) hosted in the GPT pumice unit show basaltic compositions (SiO_2 46.2 wt%) and MI hosted in the scoria unit show basaltic andesite (SiO_2 56 wt%) compositions (Fig. 1).

Both the Monte dei Porri lavas and the GPT contain silicate MI that vary in size, shape and degree of crystallisation, depending on the host phase and host unit. Electron microprobe (EMPA) and secondary ion mass spectrometry (SIMS) analyses of MI hosted in olivine, pyroxene and feldspar indicate a complex geological history. Scoria-hosted MI have more evolved compositions than their host, while pumice-hosted MI have more primitive compositions than their host (Fig. 1). This suggests that the more mafic, olivine-hosted MI in the GPT pumice unit more closely represent the parental magma composition of the GPT scoria unit. In addition, most MI trapped in the GPT scoria unit have a similar composition to the bulk rock composition of the Monte dei Porri lava units. This may further indicate that the MI in the GPT scoria unit represent the parental magma composition of the Monte dei Porri lava units. It appears that the parental magma composition of the andesitic GPT pumice unit is not represented by the MI sampled thus far. This may be due to the fact that the studied MI are hosted in olivine, and the GPT pumice parental magma was trapped in more evolved phases (i.e. pyroxene and feldspar) or because the parental magma of the GPT pumice unit intruded an existing magma body and triggered the eruption of the GPT (in a similar fashion to the Pollara eruptions which followed the Monte dei Porri eruption cycle) and, therefore, its composition was not preserved in MI.

SIMS analysis of 23 inclusions show olivine-hosted MI from the GPT pumice unit have higher average H_2O and S contents (4.53 wt % and 3790 ppm, respectively) than MI from the GPT scoria unit (2.7 wt % and 1772 ppm, respectively) but slightly lower F contents (659 ppm in MI from the GPT pumice unit and 875 ppm in scoria-hosted MI). Chlorine contents are fairly uniform, averaging 3339 ppm in scoria-hosted MI and 3559 ppm in pumice-hosted MI. The H_2O contents reflect the different intensities of the eruptive styles, with the more explosive pumice units showing higher H_2O contents than the scoria units. Multiple sampling points in large olivine-hosted MI show uniform CO_2 abundances of approximately 187 to 492 ppm in the GPT pumice unit and 233 to 576 ppm in the scoria unit. If the melt was saturated in CO_2 at the time of MI entrapment, analysis of CO_2/H_2O pairs indicate that the olivine hosts must have crystallised at different depths, approximately 6.5 km for the pumice unit and 4.8 to 6.2 km for the scoria unit.

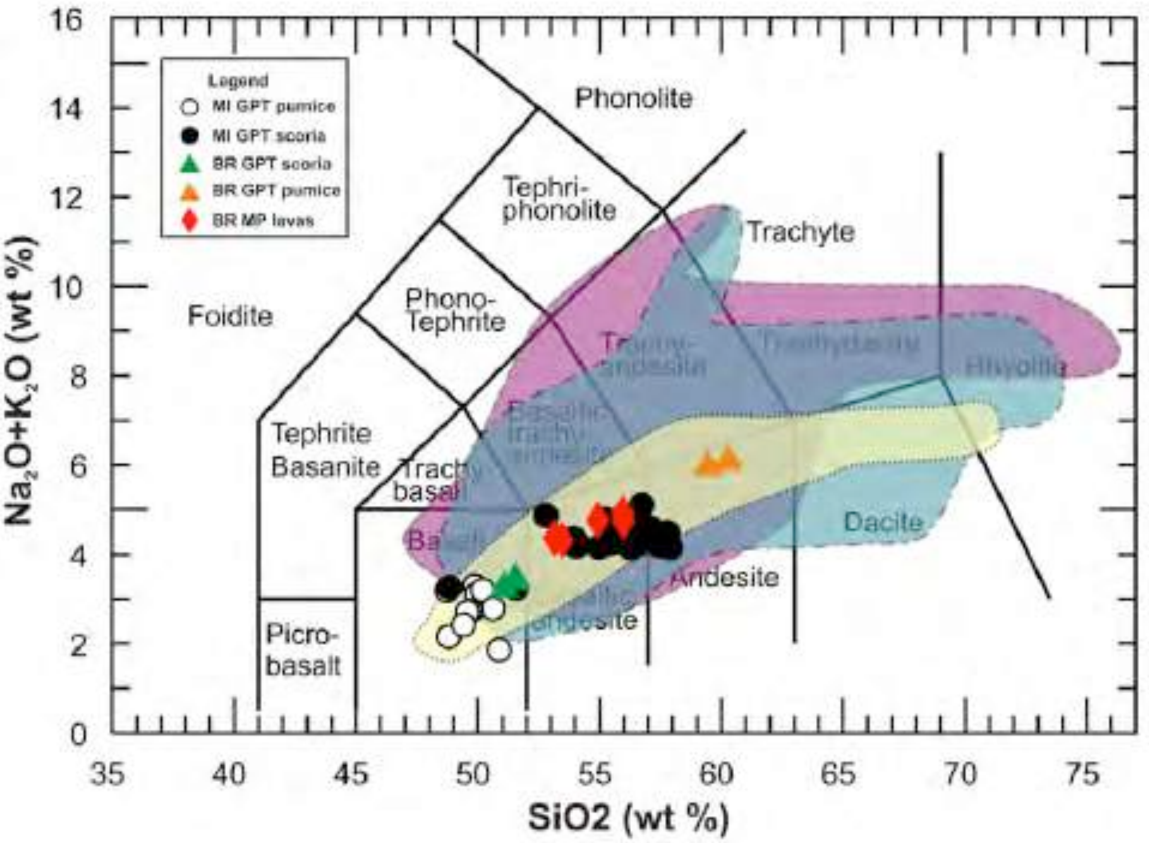

Figure 1. TAS diagram showing bulk rock composition of the Grey Porri Tuffs (GPT) and Monte dei Porri lava units and compositions of olivine-hosted MI in the GPT (Doherty et al., In press).

REFERENCES

Doherty, A.L., Bodnar, R.J., De Vivo, B., Bohrson, W. A., Belkin. H. E., Messina, A., Tracy, R. J. (*In Press*) Bulk rock composition and geochemistry of olivine-hosted melt inclusions in the Grey Porri Tuff and selected lavas of the Monte dei Porri volcano, Salina, Aeolian Islands, southern Italy. Central European Journal of Geosciences.

Keller, J. (1980) The island of Salina. Rendiconti della Societá Italiana di Mineralogia e Petrologia. Vol. 31. 489-524.

Experimental re-equilibration studies of H_2O-D_2O-NaCl through quartz.

Doppler, G.*, Baumgartner, M., and Bakker, R.J.

*Resource Mineralogy, University of Leoben, Austria, *gerald.doppler@unileoben.ac.at*

Fluid inclusions are assumed to be isolated containers trapped at specific *P-T* conditions. The use of fluid inclusions is generally based on the fact that the entrapped fluids retain their volume and composition after entrapment, however, there is evidence that entrapped inclusions do not always behave as closed systems. Experimental re-equilibration studies are performed with synthetic fluid inclusions in quartz to investigate diffusion processes of water and water-related species (D_2O) as well as salt (NaCl) through the quartz crystal structure at a constant pressure and temperature. With the chosen experimental setup, diffusion can be directly related to the activity of one fluid component. Therefore, we perform re-equilibration experiments with the aim of achieving the major factors that cause noticeable modifications of fluid inclusions in quartz. Precursor experiments have been performed with complex multi-component fluid mixtures and to not revert on the intensity of individual processes that take place during alteration. Thus, we currently perform specific re-equilibration experiments by using pure H_2O, pure D_2O, and NaCl-H_2O mixtures.

Initially synthesized fluid inclusions of well-known V_m-X properties (molar volume and composition) are synthesized in inclusion free Brazilian quartz crystals in cold seal pressure vessels under hydrothermal conditions. After the initial synthesis, fluid inclusion properties, such as composition, density, position within the crystal and inclusion shape, are characterized. Subsequently, the assemblages with the synthesized fluid inclusions are exposed to a different external fluid phase under hydrothermal conditions at the same pressure and temperature in re-equilibration experiments. Thus diffusion of the fluid species is only provoked by the compositional gradient between the entrapped inclusions and the surrounding fluid phase. The induced fugacity gradients act as the driving force of mass transfer in and out of the inclusions.

A series of synthesized pure H_2O inclusions are re-equilibrated by using pure D_2O as the external fluid phase with different re-equilibration times and at different temperatures. The results lead to the assumption that there are non-decrepitative changes of fluid inclusion properties, which can be directly related to: **1)** distance to the crystal surface; **2)** inclusion size, **3)** temperature, and **4)** time. Different concentration profiles within the crystal are characteristic for specific re-equilibration times and are related to the temperatures (Fig. 1).

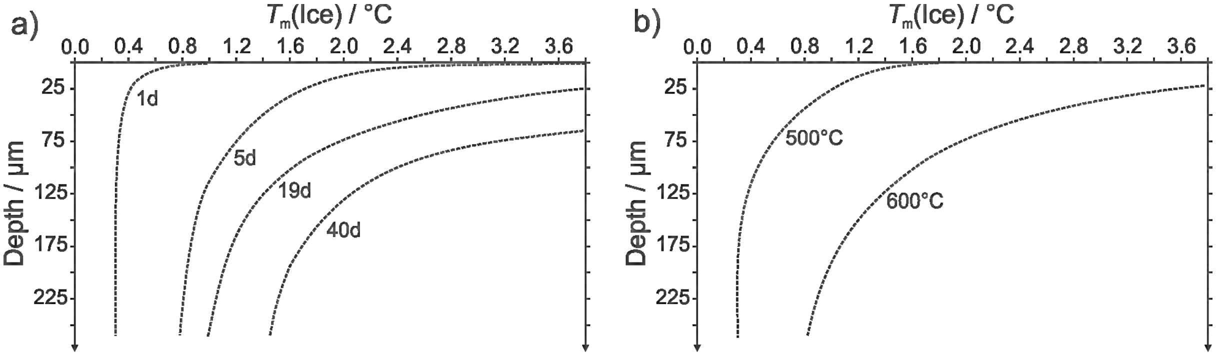

Figure 1. Concentration profiles after exposing initially synthesized pure H_2O fluid inclusions to pure D_2O during the re-equilibration process. The different envelopes represent the maximum melting temperatures T_m(Ice) after re-equilibration. Each experiment was performed at a pressure of 337 MPa. ***a)*** *time-dependant experiments;* ***b)*** *temperature-dependant experiments.*

Related to the diffusion experiments of the water-related species, synthetic NaCl-H_2O fluid inclusions with a composition of 10 and 20 mass % NaCl are exposed to pure H_2O during re-equilibration experiments. In relation to the experimental run time, a certain shift to higher salinities can be recognized by an increase of the ice melting temperatures (Fig. 2b and 2d). In addition, homogenization temperatures shift to higher temperatures, indicating a change in fluid density (Fig. 2a and 2c). The change in fluid properties can only be explained by the mass transfer of H_2O out of the inclusions, whereas NaCl seems to be immobile under experimental conditions.

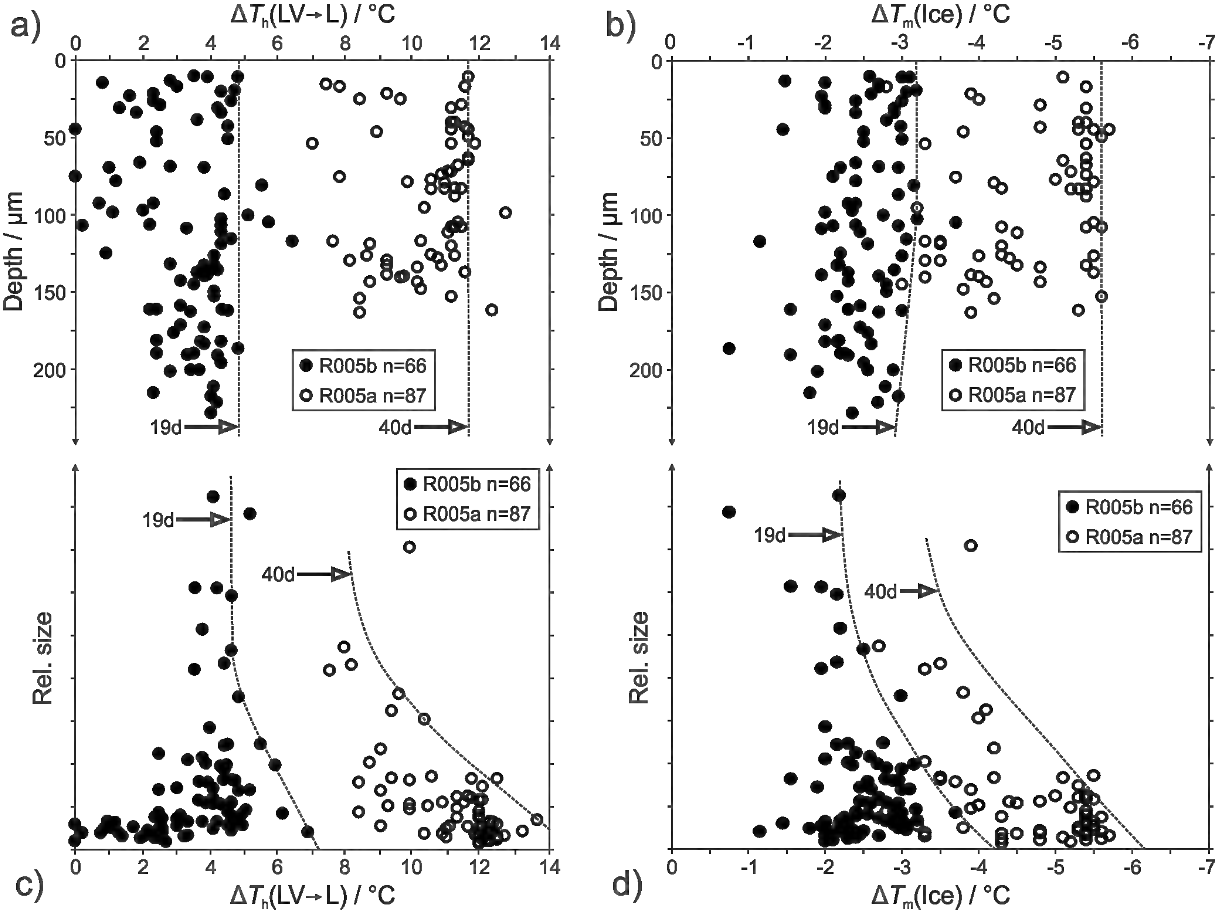

Figure 2. Concentration profiles after exposing initially synthesized 20 mass % NaCl fluid inclusions to pure H_2O during the re-equilibration process. The illustrated envelopes represent the maximum shift of $T_h(LV \rightarrow L)$ and $T_m(Ice)$ after re-equilibration. The pressure and temperature conditions of both experiments were 600°C at 337 MPa. a and b) illustrate the shift of homogenisation and melting temperatures as a function of distance to the crystal surface for two different re-equilibration run times. c and d) show the shift of T_h and T_m as a function of the relative fluid inclusion size.

We would like to thank the Austrian Research Fund (FWF) for the financial support of this project (project number P 22446-N21).

The nature of daughter minerals in complex fluid inclusions in fluorite - insights from focused ion beam (FIB)-EDS analysis.

Elmi Assadzadeh, G.*, Samson, I.M.*, Gagnon, J.E.*, and Simpson, T.**

*Department of Earth and Environmental Sciences, University of Windsor, Windsor, ON, Canada
**Department of Physics and Astronomy, Western University, London, ON, Canada

Focused ion beam milling, in conjunction with SEM-EDS spectroscopy, was used to determine the composition of solid phases within fluid inclusions in fluorite. Fluorite in the North Zone of the Mount Pleasant Sn(-W-Mo) deposit hosts primary liquid-vapour-solid fluid inclusions that contain at least nine optically different solid phases. Identification of these solids is important in understanding the chemistry of mineralizing fluids because the fluorite crystals are closely associated with cassiterite mineralization. These solids are daughter minerals because they all dissolve on heating. The optical properties and melting temperature ranges of the most abundant solids are:

A) square, isotropic, colourless, moderate relief (Tm = 251 to 375°C)
B) subhedral, equant, isotropic, colourless, low relief (Tm = 244 to 308°C)
C) anhedral, birefringent, colourless, low relief (Tm = 126 to 145°C)
D) acicular, high relief, birefringent, greenish (Tm = 341 to 386°C)
E) rhombic, colourless, moderate relief, birefringent (Tm = 56 to 140°C)

Due to the small size of the daughter minerals and the complex nature of these inclusions, optical microscopy has been of limited use in the identification of these minerals, as has Raman spectroscopy due to fluorescence of the host fluorite. SEM-EDS analysis of opened inclusions can determine the composition of solid phases, but such data cannot be easily related to the characteristics of solids in individual inclusions that had previously been studied optically, and therefore it is not possible to relate the composition of a solid with its optical properties. The SEM-EDS analyses showed that subhedral, equant solids are halite, and anhedral elongated solids are Fe(-Mn) chlorides. Based only on morphology and optical properties, either solid A or B could be interpreted as halite, however, on cooling, neither phase reacted to form a hydrate, indicating that neither solid is halite, or that hydrohalite did not form due to kinetic reasons. Of these two, solid A has the higher melting temperatures and is euhedral, suggesting that it is more likely to be halite.

Focused ion beam (FIB) milling in conjunction with EDS analysis allows characterization of solids and the fluid precipitate in situ, for previously chosen and studied inclusions (Figs. 1 and 2). These analyses show that solid B is halite and that solid C is an Fe-Mn-K chloride. The composition of solid A has yet to be determined. Other solid phases comprise Sn- and As-bearing compounds and Pb-, Zn-, and K-bearing chlorides. Residues precipitated from the inclusion fluids are enriched in Fe, Mn, K, Na, and Cl. Our data show that identification of solid phases based only on optical properties and, in particular, the interpretation of square isotropic solids with high melting temperature as halite, should be treated with caution because such interpretations can result in erroneous salinity calculations.

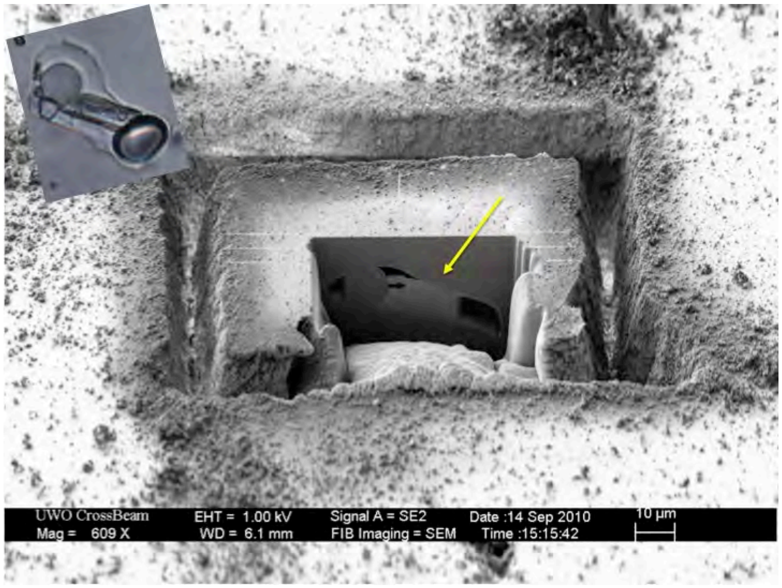

Figure 1. BSE image of a pit milled with a Ga focused ion beam. The pit in the centre shows the exposed inclusion (arrow). The inset shows an optical image of the same inclusion.

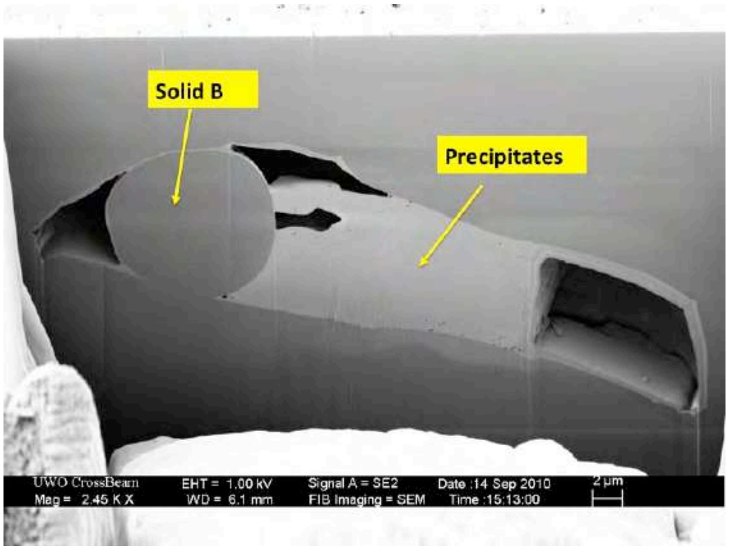

Figure 2. Close-up of the exposed inclusion shown in Fig. 1, showing solid B and residues precipitated from the fluid in the fluid inclusion.

Depth profiling of the distribution of CO_2 and F in plagioclase-hosted melt inclusions from White Island (New Zealand).

Esposito, R.*, Hunter, J.**, Schiffbauer, J.**, and Bodnar, R.J.*

**Department of Geosciences, Virginia Tech, Blacksburg, VA, U.S.A.*
***Nanoscale Characterization and Fabrication Labs, Virginia Tech, Blacksburg, VA, U.S.A.*

In the last several decades the number of publications describing the use of melt inclusions (MI) to determine the pre-eruptive volatile contents of magmas has increased significantly. In fact, MI provide the only reliable means of determining the volatile evolution before an eruption. In most MI studies, however, the volatile contents of the MI vary greatly. In particular, wide ranges in the concentration of CO_2 in MI are commonly reported, even for MI hosted in the same phenocryst or in the same growth zone within a phenocryst.

Our research group has studied melt inclusion assemblages (MIA) hosted in phenocrysts from White Island (New Zealand) and from Solchiaro (Italy) (Esposito & Bodnar, 2011). An MIA represents a group of MI that were all trapped at the same time (i.e., at the same temperature and pressure, and from a melt of the same composition), and as such, all of the MI in the assemblage should have identical volatile concentrations. The MI were analyzed by Secondary Ion Mass Spectrometry (SIMS) at Virginia Tech and at Woods Hole Oceanographic Institution to test the consistency of volatile abundances within an MIA. MIA from White Island are hosted in clinopyroxene, plagioclase, and orthopyroxene, while those from Solchiaro are hosted in clinopyroxene and olivine. In our previous studies, we found that H_2O, F, and Cl abundances were consistent in all MI within a given MIA. However, CO_2 and, to a lesser extent, S abundances showed wide variation in some MIA, but were consistent in others. The relatively wide variation in CO_2 content of MI that were presumably all trapped at the same time and location in the magma chamber is problematic, especially because trends in CO_2 versus H_2O are often used to infer a degassing path during magma evolution. In some of these earlier analyses of MI hosted in plagioclase, we sputtered completely through the MI and into the underlying host, based on depth profiles of the ions (^{12}C, ^{17}OH, ^{19}F, ^{30}Si, ^{32}S, and ^{35}Cl) analyzed by SIMS. When we examined these data, we noticed that ^{17}OH, ^{19}F, ^{32}S and ^{35}Cl counts remained relatively constant as the MI/host interface was approached, whereas ^{12}C counts sometimes appeared to increase at the MI/host interface.

In an attempt to better understand the distribution of volatiles within MI, and whether or not the CO_2 in particular is uniformly distributed within the MI, we have investigated the variation in CO_2 and F concentrations in three exposed MI and one unexposed MI hosted in plagioclase to test for the presence of a CO_2-rich layer at the MI/host interface. The MI that was not exposed at the surface was sputtered for ~ 10 hours to a depth of ~ 35 µm. This profile represents the whole section of the MI from the host crystal on one side, through the MI, and into the host below (Fig. 1).

The initial part of the profile is characterized by CO_2 enrichment and the CO_2 content decreases rapidly during initial sputtering. We have interpreted this feature to represent ^{12}C-contamination due to carbon in the air that was deposited on the sample surface before it was placed into the SIMS. During our routine MI analyses, we pre-sputter the sample before starting to collect the signal in order to remove the upper material that may be contaminated, either from exposure to the atmosphere or from sample preparation.

As predicted, the MI/host interfaces in the four MI (two interfaces in the unexposed MI and one each in the exposed MI) show an enrichment of ^{12}C. The apparent magnitude of the ^{12}C enrichment is likely due to the shape of the MI analyzed and the angle between the MI-face and the surface of the sample. In order to estimate the geometry of MI we have used a Focused Ion Beam (FIB) to excavate a vertical section through or adjacent to the MI. The sections were roughly 8 µm deep and MI shape was observed to vary from ovoid to prismatic. The MI shape can only be approximated because of the unknown variation in the third dimension. All MI profiles show some enrichment at the MI/host interface. We interpret the CO_2 enrichment at the interface to be the result of some small but unknown amount of crystallization on the MI wall to produce a CO_2-rich layer at the interface. Owing to the relatively slow rate of diffusion of CO_2 through the melt, the enriched boundary is “frozen in” as the MI cools. We note that fluorine, which is a smaller ion and which probably diffuses more rapidly in melts, does not appear to be enriched at the interface. These results have important implications concerning the reliability of CO_2 measurements in MI.

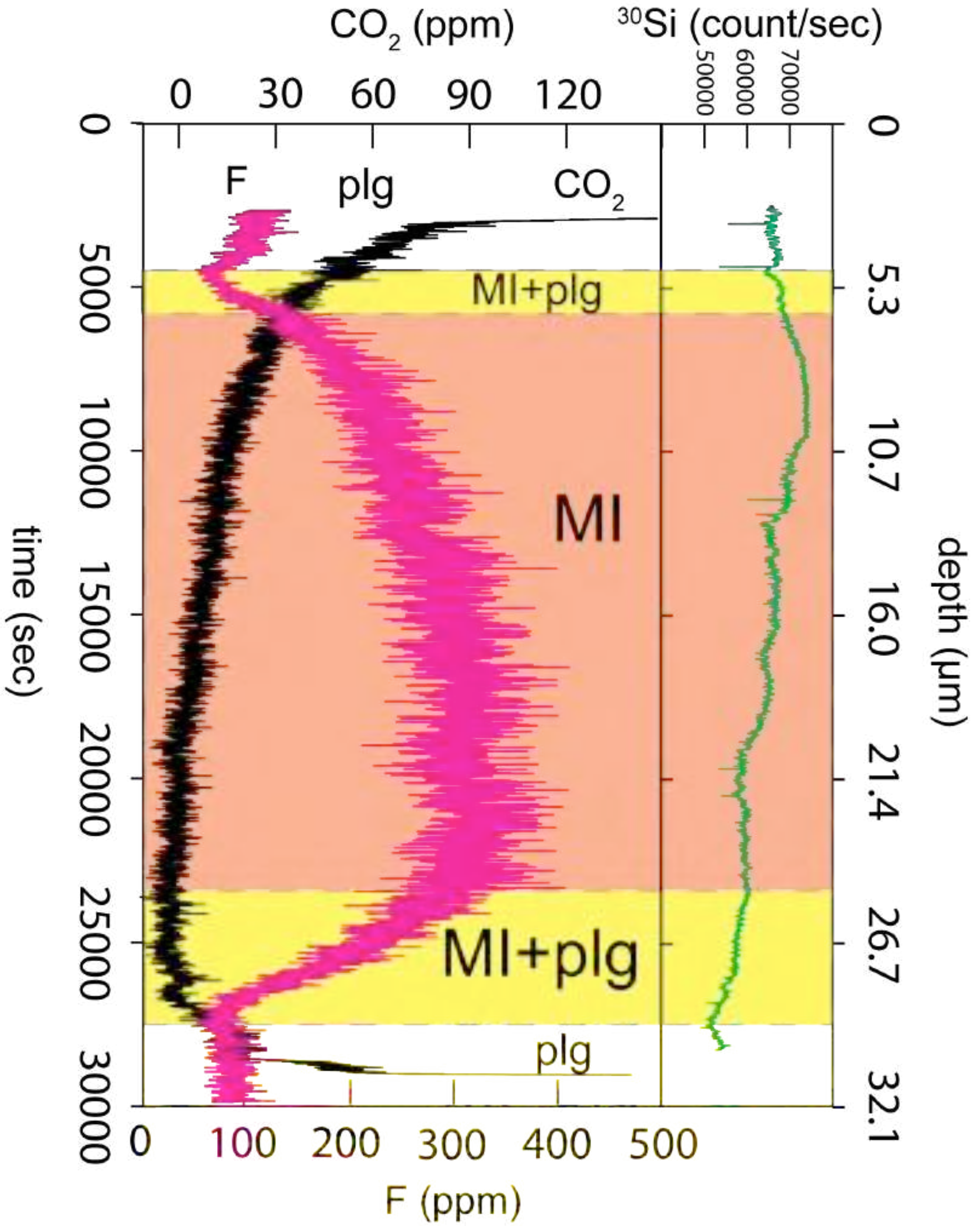

Figure 1. CO_2 and F concentration profiles and ^{30}Si counts of a non-exposed MI hosted in plagioclase. Note the contrasting behavior of CO_2 relative to F. MI = melt inclusion; plg = plagioclase.

REFERENCES

Esposito, R., Bodnar, R. J. (2011) Do melt inclusions record the pre-eruptive volatile content of magmas? Mineralogical Magazine. Vol. 75. 817.

Volatile evolution of magma in the Campi Flegrei (Italy) volcanic system based on melt inclusions.

Esposito, R.*, Klébesz, R.**, De Vivo, B.**, and Bodnar, R.J.*

*Department of Geosciences, Virginia Tech, Blacksburg, VA, U.S.A.
**Dipartimento di Scienze della Terra, Università degli Studi di Napoli Federico II, Napoli, Italy

Campi Flegrei (CF) is one of the most studied active volcanic complexes. Its proximity to Naples and the towns surrounding Pozzuoli Bay (1.5 million inhabitants) necessitates an understanding of its potential volcanic hazard. The area has been the site of volcanic activity for more than 60 ka, and contains many volcanic centers (cinder cones, tuff rings, calderas), some of which have erupted in historical times (Monte Nuovo and Solfatara). Some of these eruptions have been extremely violent (e.g. Campanian Ignimbrite).

In the last several decades, the number of studies based on melt inclusions (MI) has substantially increased because the MI technique offers many advantages relative to the bulk rock approach. In fact, pre-eruptive volatile contents are preserved and recorded by MI because host phenocrysts act as an insulating capsule preserving MI from geochemical variations during ascent and crystallization of the magma. In contrast, the bulk rock often represents a degassed or altered sample of a previously volatile-rich magma parent coming from deep in the crust. In contrast to bulk rock, some authors have argued that MI are able to record small-scale heterogeneities, especially those present in the mush zone near the walls of a magma chamber.

For these reasons, in this study we have reviewed all MI data published on the CF system in order to show the potential of the MI technique in understanding magmatic processes, with major focus on the evolution of volatile elements. In addition, we present new MI geochemical results for some eruptions of the CF (Campanian Ignimbrite, Neapolitan Yellow Tuff, Solchiaro, Bacoli, Agnano-Monte Spina, Solfatara, Astroni, Fossa Lupara). First, we have compared the data obtained from MI with data from the bulk rock. Moreover, we have investigated the geochemistry of MI from different eruptions at CF to determine if the eruptive style, type of sample, eruption age, and type of host are associated with different volatile compositions.

The new data presented here, combined with data from the literature, represent 11 eruptions out of a total of 64 eruptions that have been documented in the CF. The studied eruptions range from ~ 39 to 3.4 ka in age, and represent different eruptive styles and, thus, different types of samples (scoriae, pumice, and tuff). MI studied are hosted in several different types of phenocrysts, including sanidine, clinopyroxene, plagioclase, and olivine. Several different types of MI were observed in all phases. Some MI contained only glass, others contained glass plus one or more bubbles, and some contained glass plus bubbles plus crystals. Some MI were reheated in the lab to produce homogeneous glass inclusions, but most of the MI were naturally quenched to a homogeneous silicate glass.

Electron microprobe analysis of MI plus data from the literature shows compositions varying from trachy-basaltic (Solchiaro) through shoshonite (e.g., Fondo Riccio) to trachyte/phonolite (e.g., Bacoli). In contrast to bulk rock analyses, MI do not show gaps for intermediate compositions. MI compositions are continuous throughout all crystallization trends. MI showing intermediate compositions, however, are less abundant than those showing primitive and more evolved compositions. Although MI compositions overlap with those of the bulk rock, MI show wider concentration ranges for most of the major, minor, and trace elements relative to bulk rock, as has been reported for other magmatic systems. Generally, MgO, TiO_2, FeO_{tot}, and CaO behave incompatibly. In contrast to bulk rock compositions, however, P_2O_5 contents in MI are scattered for SiO_2 contents less than 56 wt% and are incompatible for SiO_2 contents greater than 56 wt%. In agreement with bulk rock compositions, MnO and Na_2O from MI show vertical trends when SiO_2 is approximately 60 wt%, but are random for SiO_2 less than 60 wt%. Al_2O_3 of MI is widely variable throughout the trend. Bulk rock K_2O shows as much variability as the K_2O content of MI and behaves incompatibly during magmatic evolution.

Laser ablation-inductively coupled plasma mass spectrometric analyses of MI from three of the eruptions (Solchiaro, Bacoli and Agnano-Mt Spina), in addition to data from the literature, suggest strong magma fractionation from the trachy-basalt to trachyte end member composition. MI with evolved compositions exhibit a negative Eu anomaly, however, the same anomaly is mostly absent in MI with trachy-basaltic composition. As for major and minor elements, MI show trace element abundances spanning a wider range relative to bulk rocks.

Secondary ion mass spectrometric (SIMS) analyses from this study, combined with data from the literature, show that volatile contents do not change systematically through time during volcanic activity of CF. Volatile elements of MI show higher concentrations relative to bulk rocks, especially for S, however, H_2O and CO_2 data are not available for bulk rocks making comparisons impossible. Generally, the less evolved the MI composition, the less S and CO_2 they contain, suggesting that magmas were *volatile*-saturated (CO_2-S rich fluid) since the early stage of magmatic evolution. F and H_2O vs. crystallization indicators are more scattered relative to the other volatiles. In general, F behaves incompatibly throughout the entire magmatic evolution because it shows weak positive correlation with various crystallization indicators (e.g., CaO/Al_2O_3). Cl shows a different behaviour during magmatic evolution relative to the other volatiles. Considering SiO_2 as a crystallization indicator, Cl behaves incompatibly for compositions less than 60 wt% SiO_2 and compatibly for those greater than 60 wt% SiO_2 (e.g., MI from Bacoli). The decrease in Cl contents for highly evolved magmas suggests that Cl is partitioned into the fluid phase at later magmatic stages. H_2O does not show any correlation with crystallization indicators, but H_2O-rich MI are recorded in Monopoli 1, Fondo Riccio and CI eruptions. The H_2O vs. crystallization indicators variability cannot be due only to polybaric crystallization and there are various processes that can lead to variations of H_2O and CO_2 content other than crystallization (polybaric and/or isobaric). First, the solubility of these two volatile species is affected by the abundances and evolution of other volatiles (e.g., Cl, S, and F). Secondly, post-entrapment crystallization on the wall of MI can affect the volatile contents in the glass and result in an apparent decrease in CO_2 content in the melt. It is important to note that several MI included in the database contain bubble(s). Thirdly, the silicate melt composition can affect the H_2O-CO_2 solubility. In fact, CO_2 solubility decreases from a trachy-basalt to a trachyte composition in the H_2O-CO_2 silicate melt system. Also, CO_2 flux from deep reservoirs into shallower reservoirs can increase the CO_2 content in the melt. Finally, open or closed system behaviour affects the evolution of volatile solubility, and this is important because closed and open behaviours likely alternate in active volcanic systems.

The new MI data presented in this study, combined with MI data from the literature, show that all magmas in the CF likely have undergone crystallization in magma chambers located at two different levels in the crust, one deeper in the crust (~ 6 km assuming 27 MPa/km), and one at a shallower level (~ 2 km), based on H_2O-CO_2 systematics.

Diagenetic controls on carbonate fracture cementation in tight-gas sandstones.

Fall, A.*, Weisenberger, T. B.*, Eichhubl, P.*, Laubach, S. E.*, Davis, J.S.**, and Bodnar, R. J.***

**Bureau of Economic Geology, Jackson School of Geoscience, The University of Texas at Austin, U.S.A.*
***ExxonMobil, Upstream Research Company, Houston, TX, U.S.A.*
**** Fluids Research Lab, Department of Geosciences, Virginia Tech, Blacksburg, VA, U.S.A.*

Natural fractures formed under subsurface conditions in sandstones are commonly either lined with cement, and thus are partially open for fluid flow, or are sealed by cement, and thus potentially hydraulically inactive. Whether fractures are open or sealed can significantly influence fracture permeability for natural gas (Laubach, 2003). This study focuses on understanding cement accumulations in fractures, with particular focus on the geochemical aspects of calcite fracture cements, which frequently seal (i.e., degrade) porosity of large fractures. We determine how, why, and when calcite fracture cements formed relative to the host rock diagenesis in the tight-gas sandstones of the Piceance Basin, Colorado, by combining petrographic observations, isotopic compositions of pore and fracture cements, and analyses of fluid inclusions trapped in fracture cements.

Petrographic observations of the fractures and host rock carbonates of the Cretaceous Mesaverde Group sandstones suggest that pore cements precipitated in the sequence of: 1) ferroan-dolomite, 2) ankerite, and 3) calcite, followed by calcite fracture cements. Porous albite, K-feldspar, and calcite in the matrix have a patchy texture that is characteristic of albitization of detrital feldspars, indicating that carbonate pore cements formed as a result of breakdown of detrital Ca-bearing feldspar.

Sr-isotope ratios are distinctly above Cretaceous to Tertiary seawater composition in the basin, indicating that the Sr, and by analogy the Ca, source is predominantly radiogenic. Based on the textural evidence for feldspar dissolution, the likely source of Sr is K-feldspar, suggesting that dissolution of marine carbonates in the sedimentary pile does not contribute to fracture-filling calcite formation.

In the Mesaverde Group sandstones, natural fractures are either open and lined by quartz (Fall et al., in press), or they may be lined with quartz and sealed with calcite. Calcite fracture cements occur both as banded crack-seal and as sparry cement. The cements contain fluid inclusion assemblages of coexisting two-phase aqueous and single-phase hydrocarbon gas inclusions, similar to inclusions trapped in the quartz cements (Fall et al., in press). The homogenization (trapping) temperatures of the aqueous fluid inclusions range from ~135 to 165°C. Trapping pressures determined using Raman spectroscopy (Becker et al., 2010; Fall et al., in press) range from ~30 to 55 MPa. Textural relations of fracture cements and trapping T-P conditions of fluid inclusions in quartz and calcite suggest that calcite formation postdates the quartz fracture cements, and that calcite formed during exhumation.

Fluid inclusion temperatures were combined with calcite oxygen isotope composition and the fractionation equation of Friedman and O'Neil (1977) to calculate the oxygen isotope composition of the calcite precipitating fluids (Fig. 1). This results in a $\delta^{18}O_{SMOW}$ ranging from -2 to ~4‰ for the calcite precipitating fluids. These values are within the range of present-day meteoric waters. According to Dickinson (1987), the fluid in equilibrium with calcite is isotopically similar to modeled waters for a closed system with a low water/rock ratio.

Feldspar dissolution as the primary source of calcium in fracture calcite, and the inference of low water/rock ratios, suggest that calcite fracture cement precipitation was controlled by the composition of the surrounding detrital host rocks.

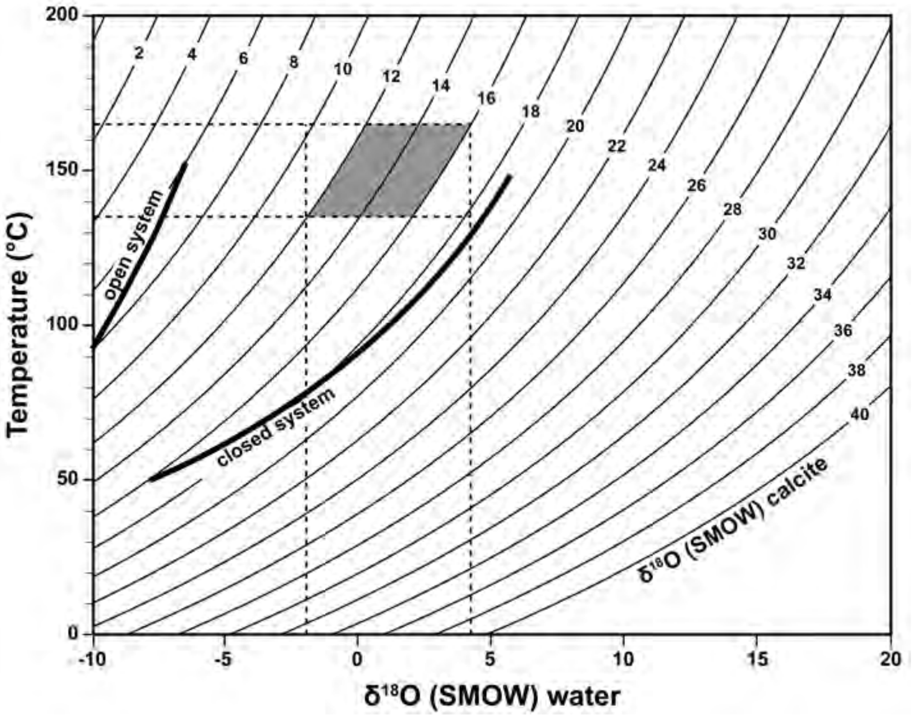

Figure 1. Oxygen isotopic composition of fracture calcite cements in cores from the Piceance Basin, Colorado, plotted against the fluid inclusion trapping temperatures. The oxygen isotopic composition is within the range of modern meteoric waters. Thick lines show the range in isotopic composition predicted for waters in open and closed systems (Dickenson, 1987).

REFERENCES

Becker, S. P., Eichhubl, P., Laubach, S. E., Reed, R. M., Lander, R. H., Bodnar, R. J. (2010) A 48 m.y. history of fracture opening, temperature, and fluid pressure: Cretaceous Travis Peak Formation, East Texas basin. GSA Bulletin. Vol. 122. 1081-1093.

Dickinson, W. W. (1987) An oxygen isotope model for interpreting carbonate diagenesis in nonmarine rocks (Green River Basin, Wyoming U.S.A.). Chemical Geology. Isotope Geoscience Section. Vol. 65. 103-116.

Fall, A., Eichhubl, P., Cumella, S. P., Laubach, S. E., Bodnar, R. J., Becker, S. P. (*In press*) Testing the basin-centered gas accumulation model using fluid inclusion observations: southern Piceance Basin, Colorado. AAPG Bulletin.

Friedman, I., O'Neil, J. R. (1977) Compilation of stable isotope fractionation factors of geochemical interest. *In:* Data of Geochemistry (ed. M. Fleischer), Volume 440-KK, U.S. Geological Survey Professional Paper.

Laubach, S. E. (2003) Practical approaches to identifying sealed and open fractures: AAPG Bulletin. Vol. 87, 561-579.

The character of mineralizing fluids in the T-Zone, Thor Lake rare-element deposit, NWT, Canada.

Feng, Y.* and Samson, I.M.**

Department of Earth and Environmental Sciences, University of Windsor, Windsor, ON, Canada
**fengl@uwindsor.ca, **ims@uwindsor.ca*

The Thor Lake REE-Zr-Nb-Ta deposit, located ~100 km southeast of Yellowknife, NWT, Canada, is one of the largest peralkaline pluton-related HREE-enriched rare-element mineral deposits in the world, and mainly consists of two mineralized zones, namely the Nechalacho deposit and the T-Zone. The T-Zone is zoned, and comprises from core to rim, a Quartz Core Zone (QCZ), an Upper Intermediate Zone (UIZ), a Lower Intermediate Zone (LIZ) and a Wall Zone (WZ). Pegmatitic textures are locally preserved in the LIZ and WZ, but the T Zone has seen a significant hydrothermal overprint such that most of the primary mineralogy has been replaced by hydrothermal minerals.

Primary fluid inclusion assemblages (FIAs) in the T-Zone comprise a mixture of liquid-rich, liquid-vapor (LV) and liquid-vapor-solid (LVS) inclusions. The distribution of solids in a given assemblage is inconsistent, the solids do not dissolve during heating, and co-existing LV and LVS inclusions show the same phase behaviour, suggesting that the solids are trapped, rather than daughter crystals. The assemblages can be classified into 6 types: (1) FIAs that are restricted to rare-element mineral-defined pseudomorphs encased within massive quartz; (2) FIAs that define sub- to euhedral domains (pseudomorphs) in massive quartz; (3) FIAs in growth zones of quartz crystals; (4) FIAs distributed in growth zones in fluorite associated with bastnäsite-group minerals; (5) isolated FIAs in quartz; and (6) FIAs in bastnäsite crystals.

Type 1 assemblages are mainly found in the UIZ, and can be subdivided into 3 groups based on the pseudomorph mineralogy, namely, those present in zircon-bearing pseudomorphs (Type 1a), bastnäsite-bearing pseudomorphs (Type 1b), and phenakite-bearing pseudomorphs (Type 1c) (Fig. 1a). Although the pseudomorphs are characterized by different minerals, they show similar prismatic to rhombic morphologies. Type 1 assemblages are restricted to the pseudomorphs and in some cases define the boundaries of a pseudomorph. Trapped solids in Type 1a assemblages have been identified as zircon using Raman spectroscopy. Trapped solids in Type 1b and 1c are typically birefringent and remain to be identified.

Type 2 assemblages occur in distinct domains that are rich in solid- and fluid-inclusions in massive quartz. Such domains exhibit an anhedral to subhedral habit and can be subdivided into two types: Type 2a occurs in pseudomorphs rich in rutile inclusions and, Type 2b are associated with albite inclusions. Compared to Type 1 assemblages, fluid inclusions in Type 2 FIAs are more abundant in the pseudomorphs, and may define the entire pseudomorph (Fig. 1b). In Type 2a assemblages, multi-solid inclusions are common and rutile has been identified as a common solid using Raman spectroscopy. Other solids are typically birefringent and remain to be identified. In LVS inclusions in Type 2b assemblages, rutile is absent and solids are typically birefringent.

Type 3 assemblages occur in growth zones in quartz that is associated with bastnäsite-group minerals (Type 3a) (Fig. 1c), oxides pseudomorphing aegirine (Type 3b), or an assemblage characterized by xenotime + thorite + iron oxides (Type 3c). **Type 4** assemblages are rare and occur in growth zones in fluorite that is associated with bastnäsite-group minerals and zircon in the UIZ. **Type 5** assemblages are also rare and are restricted to the central parts of quartz crystals and show no relation with secondary planes. **Type 6** assemblages occur in bastnäsite from the UIZ and are characterized by elongation that parallels the c-axis of the host mineral.

Raman spectroscopic analysis has been performed on the vapor phase in the primary fluid inclusions. CO_2 is present in Type 2a, 3a, 5 and 6 assemblages, whereas CH_4 has only occasionally been detected in Type 2a and 3a assemblages.

To date, microthermometric analysis has been performed on inclusions from FIA types 1a, 3a, 3c and 6 (Figs. 1d and 1e). TmICE values for LV and LVS inclusions indicate that the salinities are relatively consistent for Types 1 and 3, mostly lying between ~20 and 25 eq. wt % NaCl. Furthermore, the similarity in TmICE values for associated LV and LVS inclusions, is consistent with the conclusion that the solids are trapped. Inclusions in Type 6 assemblages show inconsistency in salinity and Th (LV→ L). One Type 6 FIA shows comparable salinities to inclusions of types 1 and 3 assemblages, whereas the other four assemblages exhibit lower salinity (5 ~ 15 eq. wt % NaCl). Th (LV→ L) values for types 1 and 3 show considerable scatter, with most data lying between 100 and 250°C, but ranging up to 400°C. Type 6 inclusions display relatively high and consistent Th (LV→ L) values that vary between 200 and 300°C. No CO_2 or clathrate melting was observed, possibly due to the small size of many of the inclusions. The microthermometric data show that the mineralizing fluids were mostly low-temperature and moderate-salinity fluids that transported or remobilized rare elements after the initial formation of the pegmatite. The difference in salinity and Th (LV→ L) values between Type 6 and the others indicate that the precipitation of the bastnäsite-group minerals was related to fluids that had a lower salinity and presumably a different genesis to those responsible for the precipitation of the other HFSE minerals.

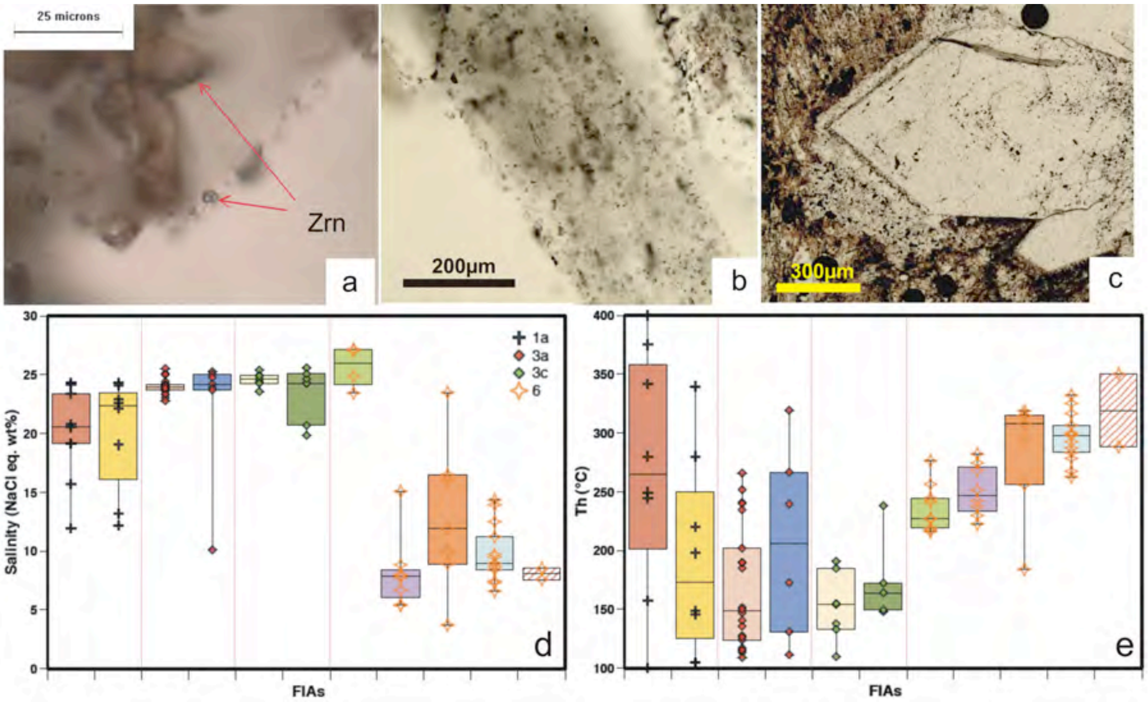

Figure 1a, b, and c: Photomicrographs of types 1a, 2, and 3a fluid inclusions. d and e: Box-whisker diagrams of the salinities and homogenization temperatures of inclusion types 1a, 3a, 3c and 6.

Li- and B-bearing fluid inclusions in the Harney Peak Granite, Black Hills, South Dakota.

Grzovic, M.L. and Nabelek, P.I.

Department of Geological Sciences, University of Missouri-Columbia, Columbia, MO, U.S.A.

Understanding the composition of magmatic fluids is important because the fluids can affect the differentiation of magma and the mobility of elements within these systems. High Li concentrations in magmatic fluids can inhibit crystal nucleation and reduce the viscosity of a magma, thus promoting the development of pegmatites (Nabelek et al. 2010). In the Harney Peak Granite (HPG) system, South Dakota, magmatic fluids were important in the formation of a broad pegmatite field, including Li- and B-bearing pegmatites. Wilke et al. (2002) hypothesized that fluids emanating from the HPG caused enrichment of Li and B in the granite's contact aureole. Individual fluid inclusions in quartz from different parts of the HPG pegmatite system were analysed using microthermometry and laser ablation (LA) ICP-MS. The goal of this study was to determine the role that the putative magmatic fluids played in the differentiation of the HPG and fluid flow in its aureole.

Concentrations of Li, B, K, Na, Rb and Cs were measured by LA ICP-MS in three types of fluid inclusions hosted by quartz. Types of fluid inclusions are: type 1 (H_2O-CO_2+salts), type 2 (H_2O+salts) and type 3 (CO_2-rich)(Sirbescu and Nabelek 2003). The LA ICP-MS data were reduced using AMS data reduction software (Mutchler et al. 2008).

Samples of quartz were taken from pegmatites and pegmatitic layers within the HPG and its satellite plutons. A tourmaline-bearing aplite-pegmatite in the Calamity Peak pluton was sampled, and has typical layering as described by Rockhold et al. (1987) and Duke et al. (1988), such as alternating layers of aplite and pegmatite. The aplite and pegmatite layers consist of quartz, plagioclase, potassium feldspar, tourmaline, and muscovite. Several samples were taken including: quartz within pegmatite layers, a quartz vein, and rose quartz from a nearby pegmatite dike. A pegmatite, with a relatively simple mineralogy comprising quartz, potassium feldspar, albite, and muscovite, was also sampled. Although tourmaline is not found in the pegmatite, it is found in the surrounding biotite-muscovite schist as a metasomatic mineral that has replaced biotite. The crystals of tourmaline are acicular and up to 150 mm in length. The quartz sample was taken from a large, meter-sized crystal.

Fluid inclusions in Calamity Peak aplite-pegmatite layers contain high concentrations of Na (up to 25.7 wt.%), K (up to 0.8 wt.%) and Li (up to 0.9 wt.%), and minor amounts of Rb (≤0.01 wt.%) and Cs (up to 0.05 wt.%). Generally, there is a negative correlation between the concentration of Na and Li. B concentrations were below the detection limits. Initial results indicate that secondary type 2 inclusions contain much higher concentrations of Li (average 0.3 wt.%) compared to primary type 1 inclusions (less than 0.1 wt.%), suggesting that Li was concentrated into the aqueous fluid phase during differentiation and unmixing of type 1 fluids.

In contrast, fluid inclusions from the tourmaline-absent pegmatite contain high concentrations of B (up to 7 wt.%). High B concentrations in the fluid explain the presence of tourmaline in the metasomatic aureole of the pegmatite. Elevated B concentrations in the fluids in this tourmaline-absent pegmatite may have been promoted by lack of scavenging by tourmaline crystallization in the pegmatite, whereas in the Calamity Peak aplite-pegmatite segregations, most B was scavenged by crystallizing tourmaline. The presence or absence of tourmaline was probably controlled more by the presence of Fe in the pegmatitic melt than the amount of B.

REFERENCES

Duke, E. F., Redden, J.A., Papike, J.J. (1988) Calamity Peak layered granite-pegmatite complex, Black Hills, South Dakota: Part I. Structure and emplacement. Geological Society of America Bulletin. Vol. 100. 825-840.

Mutchler, S. R., Fedele, L., Bodnar, R.J. (2008) Analysis management system (AMS) for reduction of laser ablation ICP-MS data. *In:* Laser-Ablation-ICPMS in the Earth Sciences: Current Practices and Outstanding Issues (ed. P. Sylvester). Mineralogical Association of Canada Short Course Series. Vol. 40. 318-327.

Nabelek, P. I., Whittington, A.G., Sirbescu, M-L. C. (2010) The role of H_2O in rapid emplacement and crystallization of granite pegmatites: resolving the paradox of large crystals in highly undercooled melts. Contributions to Mineralogy and Petrology. Vol. 160. 313-325.

Rockhold, J. R., Nabelek, P.I., Glascock, M.D. (1987) Origin of rhythmic layering in the Calamity Peak satellite pluton of the Harney Peak Granite, South Dakota: The role of boron. Geochimica et Cosmochimica Acta. Vol. 51. 487-496.

Sirbescu, M-L. C., Nabelek, P.I. (2003) Crystallization conditions and evolution of magmatic fluids in the Harney Peak Granite and associated pegmatites, Black Hills, South Dakota – Evidence from fluid inclusions. Geochimica et Cosmochimica Acta. Vol. 67. 2443-2465.

Wilke, M., Nabelek, P.I., Glascock, M.D. (2002) B and Li in Proterozoic metapelites from the Black Hills, U.S.A.: Implications for the origin of leucogranitic magmas. American Mineralogist. Vol. 87. 491-500.

Preliminary microthermometric data on the Uludağ W-skarn deposit, Bursa, Northwest Turkey.

Hanilçi, N., Aysal, N., Ceyhan, A., and Şenkaya, S.

Department of Geological Engineering, Istanbul University, Avcilar Campus, Istanbul, Turkey

Uludağ is located in northwest Turkey. The basement of the Uludağ Massive comprises Paleozoic-aged medium to high grade metamorphic rocks, such as amphibolites, gneisses and marbles. This metamorphic basement has been cut by Oligocene-aged (Okay et. al., 2008) Uludağ granodiorite. The Uludağ granitoid has modal compositions that are generally granodioritic, as do two outcropping stocks (two mica granodiorite and coarse-grained biotite granodiorite). The granitoid contains a number of xenoliths of the surrounding basement rocks with extensive metamorphic textures with amphibolitic composition (Yurdagül, 2004). The skarn zone has been developed along the granodiorite and marble contact. From the contact outward, the exoskarn zone comprises andradite, andradite+diopside, and diopside skarn zones, respectively. The skarn zones are enveloped by a tremolite-actinolite hornfels zone. The endoskarn zone has developed in a narrow area within the granodiorite and comprises epidote and hedenbergite. Quartz veins cut the skarn zones, represent a later hydrothermal event, and are host to W-mineralization. The aim of this study is to characterize the nature of the solutions that were responsible for the formation of the Uludağ skarn and the W-mineralization. For this purpose, the skarn zone has been sampled for fluid inclusion studies from the contact outward (Fig. 1).

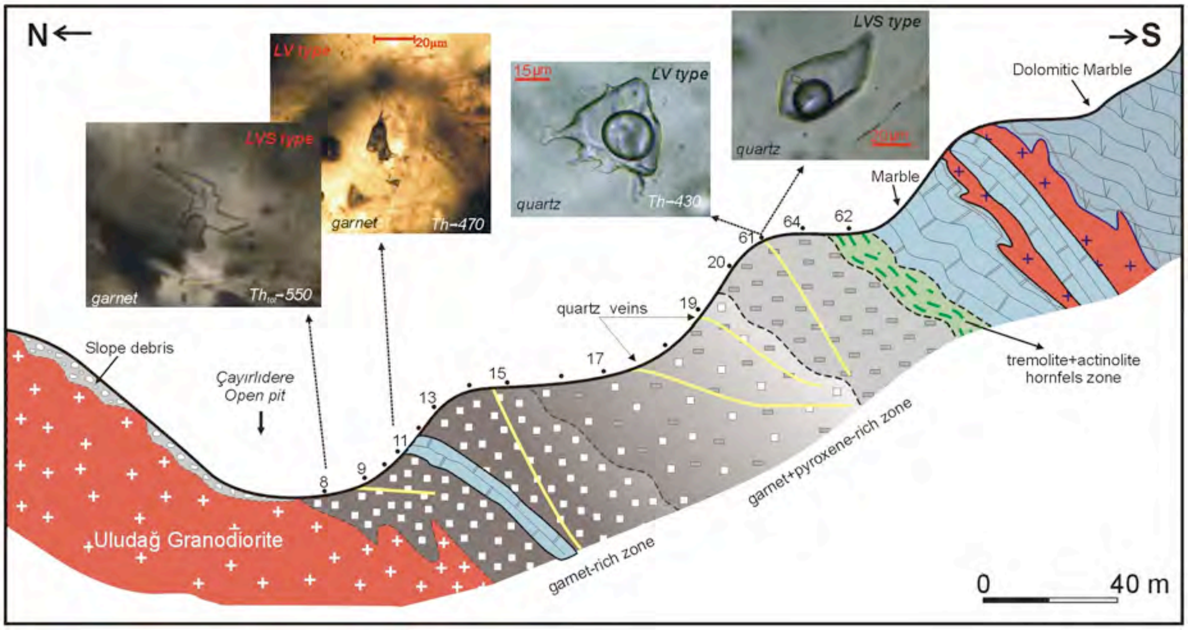

Figure 1. Cross-section of the Uludağ skarn zone in Çayırlıdere open pit, sample locations, and fluid inclusion types.

The preliminary fluid inclusion study was carried out in samples of garnet from an andradite skarn zone and quartz from the veins. At room temperature, two types of fluid inclusions were defined: type LV (liquid-vapor) and type LVS (liquid-vapor-solid) in the garnet and quartz minerals. The measurements were carried out on the primary inclusions, which occur as small clusters isolated in the garnet and quartz. The morphology of the inclusions is mostly irregular and they tend to be elongated in garnet, and mostly regularly-shaped in quartz. From the microthermometric results, the Te was between -43°C and -34°C for LV type in garnet, and between -58°C and -36°C for LV type in quartz. The average Tm_{ICE} value for LV type inclusions in garnet was -6.85°C, corresponding to 10.3 wt% NaCl equivalent, and the Tm_{ICE}

interval for LV type inclusions in quartz was between -12°C and -3°C, corresponding to 16 and 5 wt% NaCl equivalent. In some LV type inclusions in quartz, melting occurred between +8°C and +9°C, indicating the presence of CO_2 in the system. The average homogenization temperature of the LV type inclusions is 435°C for garnet, and 351°C for quartz. Generally, the solid phase (halite) of the LVS type inclusions did not melt until 600°C. Melting of halite was observed in only two LVS type inclusions in garnet at 545°C and 550°C, indicating a salinity of 65 wt% NaCl equivalent.

Preliminary microthermometric data indicate that the Uludağ skarn formation started at conditions over 600°C with high salinity (at least 65 wt% NaCl equiv.) solutions. The salinity of the solution dropped to 5% wt% NaCl equivalent with decreasing temperature to an average of 351°C during the late stage of the skarn formation, which is characterized by quartz veins and W-mineralization.

REFERENCES

Okay, A.,I., Satir, M., Zattin,M., Cavazza, W., Topuz, G. (2008) An Oligocene ductile strike-slip shear zone: The Uludağ Massif, northwest Turkey - Implications for the westward translation of Anatolia. Geological Society of America Bulletin. Vol. 120. 893-911.

Yurdagül, A. (2004) Lithogeochemical Investigation of the Uludağ Granitoide. Unpublished MSc thesis. Istanbul University, Institute of Science. 140p.

The origin of early hydrothermal fluids associated with the Sudbury structure deduced from fluid inclusion Sr, C and H isotope analysis.

Hanley, J.J.* and Ames, D.E.**

**Department of Geology, Saint Mary's University, Halifax, NS, Canada*
***Geological Survey of Canada, Ottawa, ON, Canada*

Footwall-style Cu-Ni-platinum-group element (PGE) ores along the northern margin of the Sudbury Igneous Complex (SIC) contain a diversity of barren and mineralized alteration veins that record magmatic-hydrothermal events associated with pre-impact regional metamorphism of the Archean country rocks, bolide impact, contact metamorphism of the country rocks and circulation of fluids during SIC cooling and ore emplacement, and post-SIC circulation of groundwater and neotectonic fluids.

Synchronous to the earliest stages of low sulfide, high PGE ore emplacement in the footwall was the precipitation of quartz-epidote-calcite(-garnet-sulfide-PGE) veins that host primary assemblages of coeval (immiscible, heterogeneously trapped) brine and hydrocarbon inclusions. LA-ICPMS analyses of single inclusions reveal that the saline fluid is a metal-rich (Cu-Ag-Pt-Bi-Au) aqueous brine (Ca-Na-Cl) with a bulk salinity of 33.5±2.6 wt% eq. NaCl [n=53, 1s], containing very high Sr but relatively low Rb bulk concentrations [4400 µg/g Sr; 110 µg/g Rb; Sr/Rb = 40; n = 18] and wt% concentrations of K, Fe, Mn, Zn, Pb and Ba. Microthermometry and GC analyses reveal that the hydrocarbon fluid consists of dominantly CH_4 with lesser amounts of higher order aliphatics and no CO_2, with relative abundances of hydrocarbon species following the Anderson-Schultz-Flory distribution, consistent with their formation via Fischer-Tropsch synthesis. Trapping conditions for the brine-hydrocarbon assemblages are estimated at P~0.5 kbar and ~200-250^{o}C. All available literature suggests that the fluid originated by mixing of a magmatic component (possibly from the SIC itself) and a groundwater component (Farrow, 1994; Molnar et al., 2001; Hanley et al., 2005, 2011 and authors therein).

To re-evaluate the source of this complex fluid we have recently determined initial (at 1.85 Ga) ^{87}Sr/^{86}Sr ratios in single brine inclusions by LA-MC-ICP-MS (at ETH Zurich; with F. Oberli and T. Pettke), and compound-specific d^{13}C and dD on bulk inclusion samples by GC/continuous flow isotope ratio MS (at Univ. Western Ontario; with J. Potter). Analyses of 62 brine inclusions yielded an average initial ^{87}Sr/^{86}Sr = 0.70536 ± 0.00068 (1SE), with a range from 0.70312 to 0.70677, varying by assemblage. Comparison of the data to suspected major reservoirs in the region (e.g., Figure 1a) show that obvious crustal sources (i.e., groundwaters, exsolved SIC magmatic volatiles;) had initial ^{87}Sr/^{86}Sr too high, and bulk Sr and ore metal concentrations far too low to be exclusive sources of the fluid. A major non-radiogenic component is required, and only two possibilities are considered (Figure 1a): (i) Proterozoic seawater covering the target area at the time of impact (Ames, 1999; Campos-Alvarez et al., 2010), or (ii) an exotic fluid sourced from the mantle. Inclusion d^{13}C$_{CH4}$ (-10 ‰) and dD$_{CH4}$ (-116 to -120 ‰) compositions support an abiogenic magmatic source (Figure 1b), consistent with the composition of hydrocarbons from MOR vent fluids, ophiolite complexes and agpaitic-alkaline complexes, and inconsistent with oceanic bacterial CO_2 reduction (see reference list for sources of data for comparison).

The results of this study show that early, metal- and abiogenic hydrocarbon-rich brines of probable mantle origin were trapped at the onset of low sulfide, footwall style ore formation at Sudbury. This is possibly the first direct observation of mantle-derived fluid at a terrestrial impact site, and the presence of ore metals in this fluid suggests that major revision to the ore-forming model for this giant magmatic sulfide system is warranted.

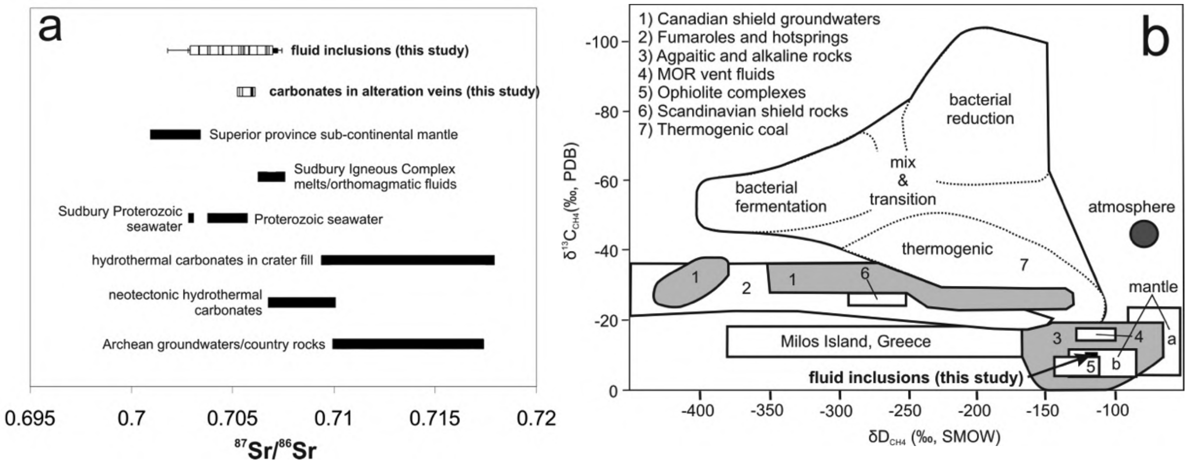

Figure 1. Summary of Sr, C and H isotope data for primary fluid inclusions from alteration veins formed at the onset of low sulphide footwall ore emplacement/precipitation. a). Sr isotope data for fluid inclusions and carbonates (this study) compared to other major reservoirs relevant to the Sudbury structure. b). C and H isotope data for CH_4 in fluid inclusions (this study) compared to other relevant compositional fields. Sources for data for comparison are summarized in reference list below.

REFERENCES

Abrajano,T.A., Sturchio, N.C., Kennedy, B.M. Lyon, Muehlenbachs, K., Bohlk, J.K. (1990) Applied Geochemistry. Vol. 5. 625-630.

Ames, D.E. (1999) Unpublished Ph.D. thesis. Carleton University, Ottawa, Ontario. 460p.

Botz, R., Stüben, D., Winckler, G., Bayer, R., Schmitt, M., Faber, E. (1996) Chemical Geology. Vol. 130. 49-64.

Campos-Alvarez, N.O., Samson, I.M., Fryer,B.J., Ames, D.E. (2010) Chemical Geology. Vol. 278. 131-150.

Dickin, A.P., Nguyen, T., Crocket, J.H. (1999) Geological Society of America Special Paper. Vol. 339. 361-371.

Fairbairn, H.W., Hurley, P.M., Card, K.D., Knight, C.J. (1969) Canadian Journal of Earth Sciences. Vol. 6. 489-497.

Farrow, C.E.G. (1994) Unpublished Ph.D. thesis, Carleton University Ottawa, Ontario. 373p.

Gibbins, W.A., McNutt, R.H. (1975) Canadian Journal of Earth Sciences. Vol. 12. 1990-2003.

Graser, G., Potter, J., Köhler, J., Markl, G. (2008) Lithos. Vol. 106. 207-221.

Hanley, J.J., Mungall, J.E., Pettke, T., Spooner, E.T.C., Bray, C.J. (2005) Mineralium Deposita. Vol. 40. 237-256.

Hanley, J., Ames, D., Barnes, J., Sharp, Z., Guillong, M. (2011) Chemical Geology. Vol. 281. 1-25.

Hurst, R.W., Farhat, J. (1977) Geochimica et Cosmochimica Acta. Vol. 41. 1803-1815.

Konnerup-Madsen, J. (2001) Geology of Greenland Survey Bulletin. Vol. 190. 159-166.

Marshall, D., Watkinson, D., Farrow, C., Molnár, F., Fouillac, A-M. (1999) Chemical Geology. Vol. 154. 1-19.

Molnár, F., Watkinson, D.H., Jones, P.C. (2001) Economic Geology. Vol. 96. 1645-1670.

Nivin, V.A., Devirts, A.L., Lagutina, Ye.P. (1995) Vol. 32. 65-71.

Paces, J.B., Bell, K. (1989) Geochimica et Cosmochimica Acta. Vol. 53. 2023-2035.

Potter (2000) Unpublished PhD thesis. Kingston University, London, UK. 296p.

Potter, J., Konnerup-Madsen, J. (2003) Geological Society of London Special Publications. Vol. 214. 151-173.

Schoell, M. (1988) Chemical Geology. Vol. 71. 1-10.

Sherwood-Lollar, B., Frape, S.K., Weise, S.M., Fritz, P., Macko, S.A., Welhan, J.A. (1993) Geochimica et Cosmochimica Acta. Vol. 57. 5087-5097.

Sherwood-Lollar, B., Westgate, T.D., Ward, J.A., Slater, G.F., Lacrampe-Couloume, G. (2002) Nature. Vol. 416. 522-524.

Veizer, J. (1989) Annual reviews of Earth and Planetary Sciences. Vol. 17. 141-167.

Veizer, J., Clayton, R.N., Hinton, R.W. (1992) Geochimica et Cosmochimica Acta. Vol. 56. 875-885.

Welhan, J.A., Craig, H. (1983) *In:* Hydrothermal processes at seafloor spreading centres (eds. P.A. Rona, K. Boström, L. Laubier, K.L. Smith) Plenum, New York. 391-409.

Fluid conditions and possible sources for Devono-Mississippian beryl mineralization in the Mackenzie Mountains, Northwest Territories.

Hewton, M.L.*, Marshall, D.D.*, Ootes, L.**, and Loughrey, L.E.*

**Simon Fraser University, Burnaby, BC, Canada*
***Northwest Territories Geoscience Office, Yellowknife, NT, Canada*

Milky green beryl (emerald variety) at the Mountain River showing in the Mackenzie Mountains, Northwest Territories, is found in extensional quartz-carbonate veins hosted by organic-poor deep marine sandstones and siltstones of the Neoproterozoic Windermere Supergroup. The section hosting the beryl-bearing veins is located in the hanging wall of a thrust fault above Paleozoic carbonates. The Mackenzie Mountains comprise the northern extent of the Cordilleran foreland fold and thrust belt and are composed of a thick package of Proterozoic to late Paleozoic siliciclastic, evaporitic, and carbonate rocks deposited during the rifting of Rodinia and development of the western margin of ancestral North America. Regional deformation during the Cretaceous and Tertiary resulted in very low grade sub-greenschist facies regional metamorphism and the development of anticlinal folds and thrust belts. No evidence of felsic magmatism in the Mackenzie Mountains has yet been reported. The Mountain River occurrence, therefore, does not conform to the accepted geological models of known emerald occurrences. The occurrence, however, does share some similarities with the Colombian-type model, where emeralds mineralized in organic-rich black shales from circulating hydrothermal sedimentary brines during regional deformation that mobilized Be, Cr, and V in situ. Thermochemical sulphate reduction by organic matter was key for mineralization of the Colombian emeralds, but inorganic reduction likely played the same role at Mountain River.

Fluid inclusion microthermometry was carried out on beryl and quartz chips from the beryl veins to determine mineralizing fluid conditions. Fluid inclusions are abundant but small and difficult to observe. The dominant population is of two-phase (liquid + vapour) fluid inclusion types (FITs). A less abundant three-phase population (liquid + vapour + salt crystal) was most frequently observed in quartz. Both FITs show relatively consistent phase ratios at room temperature, where the two-phase FITs consist of 15 to 20 vol. % CO_2 vapour and 80 to 85 vol. % brine, and the three-phase FITs consist of 15 to 20 vol. % CO_2 vapour, 15 to 20 vol. % salt crystal, and 60 to 70 vol. % brine. It was not obvious whether inclusions are along growth zones, along healed fractures, or as isolated inclusions, and thus all inclusions were identified as secondary.

In two-phase beryl-hosted inclusions, ice was generally observed to melt between -23.7 and -18.1°C, while a small number of inclusions had $T_{m\cdot ice}$ greater than -16.2°C. From the ice melting temperatures, salinity was determined to be greater than 21 wt% NaCl equivalent (Bodnar, 2003) for the majority of inclusions. Clathrate was measured in a small number of inclusions to melt at temperatures between -10.2 to -7.2°C. In two-phase FITs in quartz, ice melted between -26.1 to -19.1°C, with a small number of inclusions with $T_{m\cdot ice}$ greater than -17°C. Salinity was determined to be greater than 20.1 wt% NaCl equivalent for the majority of inclusions. Clathrate melted between -10.0 and -5.4°C. In many inclusions in both beryl and quartz, this phase transition displayed metastable behaviour. This transition is interpreted to be the melting of CO_2-clathrate as CO_2 has been confirmed by Raman analyses. Hydrohalite may have been observed as a small, rounded, slush-like phase in one of the inclusions in beryl, but this was difficult to confirm due to the small size of the inclusion.

Mineral separates of coeval beryl, quartz, and dolomite were also analysed for hydrogen, oxygen, and carbon isotopes to determine mineralization temperature and fluid source. Channel water extracted from beryl by step-wise heating has δD_{VSMOW} values in the range of -65 to -49‰. Framework $\delta^{18}O_{VSMOW}$ of beryl ranges from 16.2 to 17.2‰. $\delta^{18}O_{VSMOW}$ determined for quartz was in the range of 17.9 to 18.9‰. Dolomite was determined to have $\delta^{18}O_{VSMOW}$ of 17.2 to 18.1‰ and $\delta^{13}C_{VPDB}$ of -6.4 to 7.8‰. Mineral pair thermometry from quartz-beryl, quartz-dolomite, and beryl-dolomite pairs gave consistent equilibration temperatures in the range of 380 to 415°C. Isochores derived from these temperatures and fluid inclusion measurements indicates pressures of 2 to 4.5 kbar and corresponding depths of 6 to 12 km.

Results from isotopic analysis of channel water from emerald indicate moderately low δD values compared to other emerald occurrences (Fig. 1). Combined with calculated $\delta^{18}O$ values, the isotopic ratios of water from the Mountain River emeralds are inconsistent with the isotopic signature of magmatic waters, but within the bounds of metamorphic and sedimentary waters. Regional metamorphism is of sub-greenschist grade, and likely precludes any significant metamorphic fluid source being involved in mineralization. The most likely fluid source is determined to be regionally derived from the thick package of sedimentary and evaporitic rocks of the Mackenzie Mountains. A highly radiogenic Os_i value (3.2 ± 0.4) obtained from pyrite reflects a strong crustal contribution of Os and possibly other metals to the fluid system and provides further evidence of the sedimentary source for mineralizing fluids. This strong crustal contribution is not surprising given the thickness and recycled nature of the Mackenzie Mountains strata.

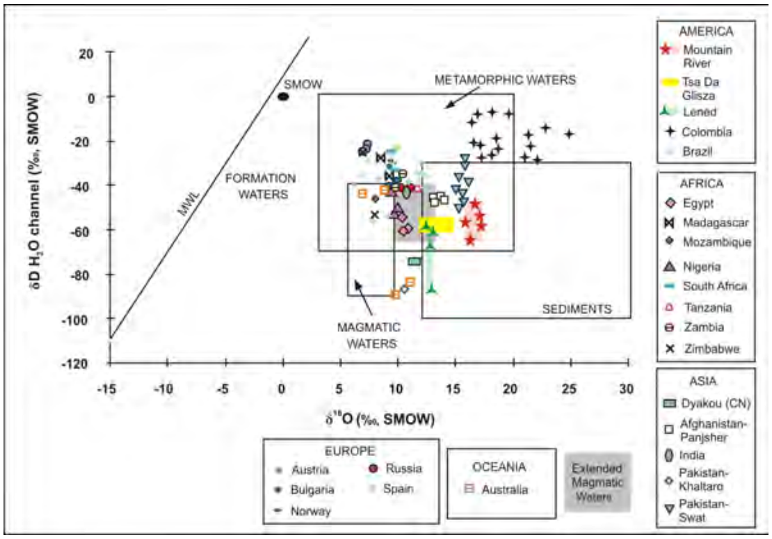

Figure 1. The isotopic values of channel water from beryl from the Mountain River (red stars) occurrence are distinct from other emeralds of the world. The isotopic values plot within ranges typical of sedimentary and metamorphic waters.

A Re-Os model 1 isochron age of 345 ± 20 Ma obtained from coeval pyrite indicates that emerald mineralization was contemporaneous with estimated ages of the Manetoe Facies dolomitization event (Morris and Nesbitt 1998) and extensive base metal mineralization in the northern Cordillera (Nelson et al., 2002). The Mackenzie Mountains host an extensive carbonate-hosted Zn-Pb district associated with the Manetoe Facies alteration, and comparable fluid inclusion observations in vein quartz from the Bear-Twit Zn-Pb showing (Gleeson, 2006) near the Mountain River beryl occurrence may suggest similar fluid conditions, if not a shared fluid source.

The conditions determined for emerald veins at the Mountain River occurrence indicate that basinal sedimentary brines, sourced regionally from the thick package of sedimentary rocks, were heated by deep burial and a high geothermal gradient, and scavenged Be, V, and Cr from host sediments. The inorganic reduction of sulphate to sulphide, and subsequent mineralization, was likely facilitated by iron-rich sediments. The Devono-Mississippian age puts the timing of emerald mineralization into an extensional back-arc environment. Following the northern Cordilleran metallogenic model proposed by Nelson et al. (2002), this high-temperature extension drove brines eastward toward the platform resulting in emerald and base metal mineralization. Thrusting during Cretaceous-Tertiary deformation placed the emeralds structurally above Paleozoic strata. This model is consistent with fluid inclusion and stable isotope results reflecting salinities, isotope ratios, and Os_i values typical of radiogenic sedimentary brines and conditions of mineralization of 380 to 415°C, 2 to 4.5 kbar pressure, and depths of 6 to 12 km.

REFERENCES

Bodnar, R. J. (1993) Revised equation and table for determining the freezing point depression of H2O-NaCl solutions. Geochimica et Cosmochimica Acta. Vol. 57. 683-684.

Gleeson, S. (2006) A microthermometric study of fluid inclusions in sulphides and carbonates from Gayna River and the Bear-Twit base metal prospects, Mackenzie Mountains, NWT. Northwest Territories Geoscience Office, NWT Open Report 2006-005. 9p.

Morris, G. A., Nesbitt, B. E. (1998) Geology and timing of palaeohydrogeological events in the Mackenzie Mountains, Northwest Territories, Canada. *In:* Dating and Duration of Fluid Flow and Fluid-Rock Interaction (ed. J. Parnell). Geological Society, London, Special Publications. Vol. 144. 161-172.

Nelson, J., Paradis, S., Christensen, J., Gabites, J. (2002) Canadian Cordilleran Mississippi Valley-Type deposits: A case for Devonian-Mississippian back-arc hydrothermal origin. Economic Geology. Vol. 97. 1013-1036.

Melt inclusion evidence for pre-eruptive enrichment and post-eruptive depletion of lithium in silicic volcanic rocks - implications for the origin of lithium-rich brines.

Hofstra, A.H.*, Todorov, T.I., Adams, D.T., Marsh, E.E., and Mercer, C.N.

*U.S. Geological Survey, MS-973, Denver, CO, U.S.A., *ahofstra@usgs.gov*

Lithium is an energy critical element used to manufacture lightweight rechargeable Li-ion batteries that power everything from cell phones to electric vehicles. It is produced primarily from brine (87%) in closed, arid, terrestrial basins on the Altiplano of South America, Tibetan Plateau of China, and Great Basin region of the western United States. Such basins also contain layers of Li-rich clay (hectorite) that may constitute an economic resource. Lithium supplies have significant geopolitical risks, because most of the world's resources are in Chile, Bolivia, and Argentina. Consequently, the USGS is conducting and supporting research to understand: 1) the source of Li in brine and hectorite, and 2) the processes that concentrate Li in evaporative basins.

Lithium is a lithophile element that is enriched in highly evolved silicic igneous rocks associated with hydrothermal deposits of Be, Mo, Sn, U, and F. Glassy varieties of these rocks frequently have higher Li abundances than devitrified, weathered and/or altered equivalents. The highest Li concentration ever reported in obsidian (3400 ppm) is from Macusani, Peru at the north end of the Bolivian Tin Belt. Li-rich glass in tuff (100-200 ppm) has been considered a possible source for Li-rich brine and clay (hectorite) at the only mine in the United States (Clayton Valley, Nevada). Laboratory simulations of weathering have shown that Li is easily leached from this tuff.

The small ionic radius of Li (0.076 nm) and 1+ charge give it a much higher diffusion rate than other cations in silicate melts, glass, and minerals, such as quartz. Rapid Li diffusion in quartz phenocrysts may result in equilibration between preexisting melt inclusions and surrounding magma prior to eruption. Rapid diffusion in melt and glass essentially guarantee significant Li loss from cracked melt inclusions and volcanic glass shards during eruption. Thus, melt inclusions in uncracked phenocrysts of rapidly cooled volcanic rocks are the only sample medium that may reflect the abundance of Li in pre-eruptive magmas.

The purpose of this investigation is to compare the Li content of melt inclusions to that of their host rocks to determine the proportion of Li lost to the environment during eruption, lithification, and weathering. We summarize previous results from the 0.8 Ma Bishop tuff (barren) in California, the 24.6 Ma Pine Grove tuff (Mo) in Utah, the 27.9 Ma Taylor Creek rhyolite (Sn) in New Mexico, and present new data from the 21.7 Ma Spor Mountain tuff (Be) in Utah and the 27.6 Ma Hideaway Park tuff (Mo) in Colorado. These data quantify pre-eruptive melt compositions and the magnitude of post-eruptive Li depletions that may generate significant Li-brine resources in arid terrestrial basins.

In previous studies, melt inclusions were analyzed using secondary ion mass spectrometry (SIMS). In this study, melt inclusions were analyzed at the Denver Inclusion Analysis Laboratory using established laser ablation inductively coupled plasma mass spectrometry (LA-ICP-MS) techniques with normalization to Al determined by electron microprobe (http://minerals.cr.usgs.gov/dial/index.html).

The distribution of Li abundances in melt inclusions from each locale generally have median values near the maximum and minima that approach, or are less than, those of the host rock (Fig. 1). Melt inclusion abundances that are less than the host rock suggest that Li diffused out of cracked inclusions into a low Li medium, such as air, during eruption. While median melt inclusion abundances range from 54 ppm in the Bishop tuff to 3710 ppm in the Spor Mountain tuff, corresponding host rock values have a much smaller range from 21 to 90 ppm (Fig. 1). Comparison of median melt inclusion values to those of their respective host rocks yield apparent Li depletions of 48 to 98%, with the largest depletions in samples containing the most Li.

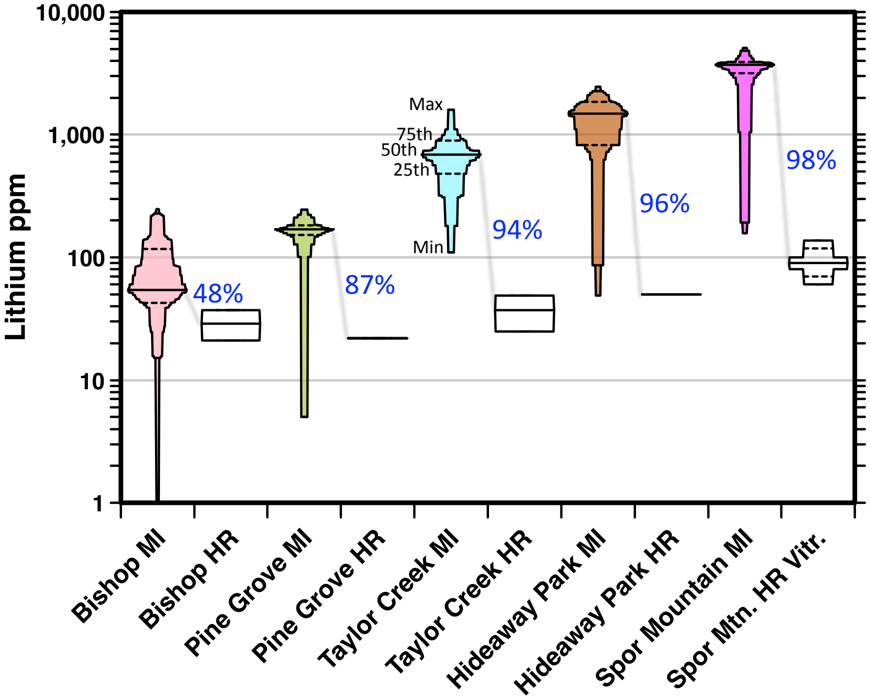

Figure 1. Range and percentile (25th, 50th=median, 75th) distribution of Li in melt inclusions (MI) and host rocks (HR) from each locale with apparent Li depletions in percent.

The Spor Mountain tuff is particularly informative because melt inclusions are remarkably enriched in Li, yet vitrophyre is 98% depleted (Fig. 1). The median Li abundance (3710 ppm) and extraction efficiency (98%), together with the estimated volume (10 km^3) and density (1.5 g/cc) of the tuff suggest that 54 Mt of Li was released into the local environment. If only 10% of this Li was collected in a closed basin and concentrated by evaporation, it would produce a world class Li-brine deposit with 5.4 Mt of Li. Larger volumes of less enriched rhyolite, such as the Bishop Tuff (>600 km^3, 54 ppm Li, 48% extraction), released about half as much Li into the environment (23 Mt Li), however, the tuff was erupted over a much larger area. Hence, the proportion of Li collected and concentrated in a basin from an eruption may be the critical factor for Li-brine formation, with successive eruptions conferring greater potential.

Melt inclusions contain more Li than volcanic glass. Vitrophyre and tuff, with 50 to 100 ppm Li, may be derived from magmas with 1000's of ppm Li. Melt inclusions in quartz phenocrysts from the Spor Mountain tuff have the highest Li abundance yet recorded (max 5080 ppm). Forty eight to 98% of the Li present in magmas may be lost to the environment during eruption, lithification, and weathering of tuff. Eruption of small volumes (10 km^3) of Li enriched rhyolite into closed basins can release enough Li to produce significant Li-brine deposits. Such localized eruptions may explain why brines in evaporative basins seldom have economic concentrations of Li. Rhyolites associated with hydrothermal deposits of Be, Mo, and Sn are often enriched in Li (1000's of ppm) and as such are ideal sources for Li-brines. Hydrothermal deposits of these metals may indicate potential for Li-brine deposits in nearby basins. Notably, the world's largest Li-brine resource in the Salar de Uyuni, with 8.7 Mt of Li, is flanked by Li-rich rhyolites of the Bolivian Tin Belt.

A 50-year perspective on the role of fluid inclusion studies in ore deposit research.

Kesler, S.E.

Department of Earth and Environmental Sciences, University of Michigan, Ann Arbor, MI, U.S.A.

Fluid inclusions have been the subject of research for almost 200 years, but their impact on our understanding of ore deposits has taken place largely during the last 50 years. The number of peer-reviewed research papers in Georef that mention fluid inclusions increased from 1 in 1960 to 552 in 2010, reaching a total of 8140 recorded papers (Fig. 1A). Before that, largely during the 1950s, considerable progress was made in the USSR by Khitarov, Lemmlein and others in literature that is captured only in part as peer-reviewed by Georef. The small number of peer-reviewed papers on fluid inclusions before the mid-1970s (Fig. 1A) belies the importance of early studies. In the west, things really started in the early 1950s when (F. Gordon) Smith at Toronto summarized the preceding 150 years of research showing that inclusions could be divided into aqueous and silicate types. Skinner suggested that fluid inclusions might leak, and Ingerson countered with arguments based on heating experiments. By the late 1950s, Smith had carried out numerous studies, including the use of decrepitation to study inclusions, and Roedder and Ames had published methods for extraction and bulk analysis of fluid inclusions. These were followed in the earliest 1960s by designs for heating and heating-freezing stages, respectively, by Little and Roedder.

At this point, people got to work measuring homogenization and freezing temperatures at individual deposits or deposit groups. Earliest attention went to the temperature, salinity, and source of fluids in Mississippi Valley-type deposits by Freas and Cameron at Cave-in-Rock (1961), Sawkins in the Pennines (1966), and Roedder at Pine Point, Hansonburg (1968), Southern Appalachians (1971) and Viburnum Trend (1977), with many of these studies noting that ore-forming fluids were just different enough from basinal brines to suggest some sort of additional input, possibly magmatic. The quest for evidence of a magmatic signature in inclusion fluids was aided by stable isotope measurements that started with analysis of D/H ratios of inclusion fluids by Hall and Friedman at Cave-in-Rock (1963) and Rye at Providencia (1964). By 1968, Rye had teamed with O'Neil to analyze O isotopes in fluid inclusions from Providencia, a development that facilitated efforts to identify the four types of ore fluids (connate/basinal, magmatic, meteoric, seawater) mentioned by White in his classic 1968 summary. Within the next decade, detailed studies involving homogenization and freezing temperatures, usually complemented by isotope analyses, were carried out at Baguio, Blue Bell, Casapalca, Climax, Echo Bay, Kuroko, and Pasto Bueno by Friedman, Hall, Kelly, Landis, Nash, Ohmoto, Robinson, Rye and Sawkins, with growing use of the now familiar O-H isotope diagram showing compositions of various types of ore fluids. This period saw publication of the Bingham-Butte-Climax porphyry deposit study (1971) by Roedder, which is the most-cited fluid inclusion study dealing directly with an ore deposit (Fig. 2), followed by work at Panasqueira by Kelly and Rye (1979) and Panguna by Eastoe (1979), also very widely cited. The trend toward use of fluid inclusions in integrated studies continued into the 1980s and beyond, and expanded to other deposit types including barite, Carlin-type, IOCG, orogenic gold, rare-earth element, skarn, sediment hosted copper, uranium, and active mid-ocean ridge deposits. The trend toward integrated ore deposit studies that included fluid inclusion measurements along with many other observations became so great by 1990 that the number of papers with fluid inclusion in the title (that is, those focusing exclusively on fluid inclusions) increased more slowly than the number of papers that mentioned fluid inclusions as part of a broader study (Fig. 1A). Among more recent integrated studies, the work by Hedenquist and others at Far Southeast-Lepanto (1998) and Arribas and others at Rodalquilar (1995) have been especially highly cited (Fig. 2).

Throughout this period, there was growing attention to special topics related to fluid inclusions in ore deposits. In 1968, Skinner and Roedder published experiments supporting Ingerson's contention that fluid inclusions did not leak, a conclusion that was to be partly contradicted for H_2, He, and even H_2O in the 1990s by Hall, Sterner, and Bodnar. This was followed by efforts by Banks, Bodnar, Bohlke, Boyce, Bray, Cuney, Dhamelincourt, Dubessy, Guha, Guilhaumou, Kesler, Li, Mironova, Naumov, Norman, Pasteris, Roedder, Samson, Shepherd, and Spooner to analyse major elements and gases in both bulk extracts and single inclusions using gas chromatography, quadrupole mass spectrometry, Raman and other methods. As studies of ore deposits increased in number, attention was given to important features of the fluid inclusion record, including inclusion assemblages and their relative ages, boiling or phase separation (in complex gas systems), halite saturation, fluid mixing, wall rock reactions, and melt inclusions, and their relation to aqueous/vapour inclusions. One early paper of this type by Roedder and Bodnar (1980) dealt with the role of immiscibility in inclusions and the possibility of using fluid inclusions as geobarometers, which remains a major challenge for ore deposit research. By the 1980s, progress was being made on two fluid inclusion related topics that provided important insights into the evolution of fluids during ore deposition, including: 1) the role in fluid inclusion observations of clathrates and CO_2 by Brenan, Brown, Collins, Hedenquist, Henley, Lamb, and Watson, and 2) phase equilibrium studies in various parts of the $NaCl$-KCl-$CaCl_2$-H_2O-H_2O-CO_2-CH_4 system by Bodnar, Bowers, Duan, Frantz, Helgeson, Sterner, Zhang, and others. Many of the phase equilibrium studies made use of the synthetic inclusion method developed by Bodnar, Sterner, and others. Papers on these topics have generally been more highly cited than those specifically dealing with ore deposits (Fig. 2).

By the 1990s, there was an increased drive to analyse inclusions, especially for their metal content, an effort that had started in the west with the 1963 neutron activation-crush-leach analyses of Czamanske, Roedder and Burns and the 1981 estimate based on size of opaque daughter minerals by Sawkins and Scherkenbach. Development of LA-ICP-MS and PIXE methods to analyse individual inclusions led to a new generation of integrated studies of ore deposits including recent work at Bajo de la Alumbrera, Bingham, Bismark, Nevados de Famatina, Mole granite (Sn-W) and southeast Missouri (MVT) by Appold, Audetat, Bakker, Einaudi, Gunther, Heinrich, Landtwing, Pettke, Redmond, Ryan, Ulrich and Wilkinson, among others. The analyses also resulted in a resurgence of interest in melt inclusions and their relation to formation of magmatic-hydrothermal fluids and ore deposits by many of the authors noted above, as well as Halter, Harris, Kamenetsky and others. Many of these papers are too young to have attracted numerous citations, although the 1998 and 1999 papers by Heinrich and others are prominent exceptions (Fig. 2).

It is no exaggeration to say that fluid inclusion studies have been essential to our current understanding of how ore deposits form. These studies have provided the basic information on the temperature and composition of ore fluids that was essential to efforts to understand the source of the fluids and their evolution. Although we have made impressive progress, much more remains to be done. We need to extend single-inclusion analyses to many more ore environments, develop methods to interpret and analyse smaller inclusions, improve our use of inclusions as geobarometers, link inclusion information more closely to actual ore deposition, and continue to help ore deposit geologists understand the movement of trace elements in the lithosphere.

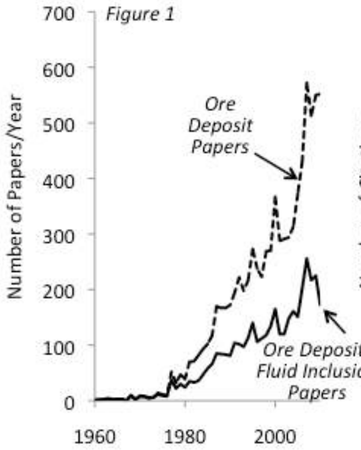

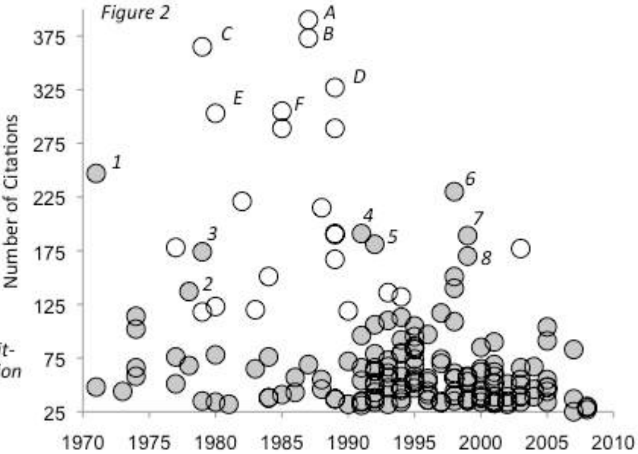

Figure 1. Georef cited papers mentioning "deposit" and "deposit and fluid inclusion". Fig. 2. Citations for "deposit+fluid inclusion" (gray) and experimental/theoretical aspects of fluid inclusions (white). 1-Roedder-porphyry deposits, 2-Eastoe-Panguna, 3-Kelly-Panasqueira, 4-Cerny-Pegmatite, 5-Heinrich-LAICPMS, 6-Hedenquist-clathrate, 7-Ulrich-LAICPMS, 8-Gunther-LAICPMS. A-Watson-CO_2, B-Zhang-Na-K-Ca-Cl-H_2O, C-Collins-clathrate, D-Brown-Flincor, E-Roedder-Pressure, F-Bodnar-NaCl-H_2O Synthetic.

Origin of nodules in the 20 Ka Pomici di Base-Sarno eruption of Mt. Somma-Vesuvius, Italy, based on geochemistry of melt inclusions.

Klébesz, R.*, Esposito, R.**, Bodnar, R.J.**, De Vivo, B.*, Lima, A.*, Petrosino, P.*, and Török, K.***

**University of Naples "Federico II", Naples, Italy*
***Virginia Tech, Blacksburg, VA, U.S.A.*
****Eötvös Loránd Geophysical Institute of Hungary, Budapest, Hungary*

Nodules (coarse-grained "plutonic" rocks) were collected from the uppermost, pyroclastic flow deposit of the ~20 ka Pomici di Base (PB)-Sarno eruption of Mt. Somma-Vesuvius, Italy. The studied samples have porphyrogranular texture with slight zonation and irregular edges on phenocrysts. The samples also contain crystallized melt pockets. These petrographic features are all consistent with the interpretation that the nodules represent the crystal-rich part of the mush-zone of the active plumbing system beneath Mt. Somma-Vesuvius, and were entrained into the erupting PB-Sarno magma.

Melt inclusions (MI) are abundant in clinopyroxenes in the nodules. All MI observed are partially to completely crystallized, suggesting slow cooling after trapping. Two types of MI can be distinguished based on petrography and composition. Type I MI consist of clinopyroxene, feldspar, mica, Fe-Ti-oxide minerals and/or dark green spinel, and a vapor bubble. We could not detect volatiles (CO_2, H_2O) in the bubbles by Raman analysis. Type II inclusions are generally lighter in color and contain subhedral feldspar and/or glass, and oxides. The two types are often spatially related (e.g., they appear in the same zone or area of the clinopyroxene) and both types of MI are randomly distributed in the crystals or they occur along a growth zone and are interpreted to be primary. MI were observed under the microscope during heating. MI homogenized between 1227°C and 1267°C, with most homogenizing at 1240 to 1250°C. As soon as the MI homogenized, they were quenched. Subsequently, the MI were analyzed to determine their major and trace element, and volatile compositions. Type I MI can be classified as phono-tephrite – tephri-phonolite – basaltic trachy-andesite, similar to the bulk rock composition of the old Somma eruptive products (Ayuso et al., 1998; Landi et al., 1999; Paone, 2006). Type II MI have a mainly basaltic composition and higher Mg and Ca content than Type I MI. The two different types of MI also show different trace element patterns. Type I MI are more enriched in incompatible elements compared to Type II MI. The trace element pattern of Type II MI is similar to that of the carbonates (Del Moro et al., 2001) underlying Mt. Somma-Vesuvius, but show higher concentrations. Secondary ion mass spectrometry analyses of homogenized MI show uniformly low H_2O-content (~0.15 wt%), but larger variations in the compositions of other volatile elements (CO_2, S, F, Cl). Only Cl and S show a positive correlation, with Cl increasing as the S content increases. In addition, the more evolved Type I MI tend to have higher Cl, F and S abundances than the basaltic Type II MI. One possible explanation for this behaviour is that the volatiles are retained in the melt phase during differentiation, suggesting that the melt did not reach volatile saturation.

The presence of spatially associated MI with different compositions in individual phenocrysts is commonly interpreted to represent small scale heterogeneities within the magma chamber due to reaction of the newly intruded magma with crystals and/or wall rock in the mush zone at the margin of the magma chamber (Danyushevsky et al., 2004). Our hypotheses is that the cooling and differentiating melt at the edge of the magma chamber reacted with the carbonates of the wall rock, leading to trace element patterns and small-scale heterogeneities that were recorded by the trapped MI.

REFERENCES

Ayuso, R.A., De Vivo, B., Rolandi, G., Seal, R.R., Paone, A. (1998) Geochemical and isotopic (Nd-Pb-Sr-O) variations bearing on the genesis of volcanic rocks from Vesuvius, Italy. Journal of Volcanology and Geothermal Research. Vol. 82. 53-78.

Danyushevsky, L.V., Leslie, R.A.J., Crawford, A., Durance, P. (2004) Melt Inclusions in Primitive Olivine Phenocrysts: the Role of Localized Reaction Processes in the Origin of Anomalous Compositions. Journal of Petrology. Vol. 45. 2531-2553.

Del Moro, A., Fulignati, P., Marianelli, P., Sbrana, A. (2001) Magma contamination by direct wall rock interaction: constraints from xenoliths from the walls of a carbonate-hosted magma chamber (Vesuvius 1944 eruption). Journal of Volcanology and Geothermal Research. Vol. 112. 15-24.

Landi, P., Bertagnini, A., Rosi, M. (1999) Chemical zoning and crystallization mechanisms in the magma chamber of the Pomici di Base plinian eruption of Somma-Vesuvius (Italy). Contributions to Mineralogy and Petrology. Vol. 135. 179-197.

Paone, A. (2006) The geochemical evolution of the Mt. Somma-Vesuvius volcano. Mineralogy and Petrology. Vol. 87. 53-80.

An integrated field, geochemical, thermometric and LA ICP-MS study of an intrusion-related Au setting: evidence for fluid mixing and rock dissolution.

Kontak, D.J.*, Ulrich, T. **, and Kyser, K.T.***

**Department of Earth Sciences, Laurentian University, Sudbury ON, Canada*
***Institute for Geoscience, Aarhus University, Hoegh-Guldbergs Gade 28000, Aarhus, Denmark*
****Department of Geological Sciences and Engineering, Queen's University, Kingston, ON, Canada*

This study compliments the previous work of Kontak and Kyser (2011), which documented the geological setting, petrology, isotopic (S, O, Pb) geochemistry, and fluid inclusion thermometry of an intrusion-related Au setting in Nova Scotia, Canada. At this location, regionally extensive quartz ± muscovite-sulphide greisens with anomalous gold (to 1 g/t Au) occur at the contact of the 380 Ma peraluminous South Mountain Batholith and metaturbidite rocks of the Cambro-Ordovician Meguma Supergroup. The inferred conditions of vein emplacement are estimated at 3.5 kbars based on contact metamorphic assemblages. Significantly, at this stratigraphic horizon the metasedimentary rocks are enriched in Ca, Fe, Mg, and Mn due to the presence of diagenetic carbonate. In this earlier study, which focused on an area where the quartz veins extended out from a late-stage pegmatite zone, a combined fluid inclusion and isotopic study indicated the following: 1) the presence of two fluid types. Type 1 fluid is a low-salinity (≤3 wt. % eq. NaCl) aqueous type with minor CO_2 and Th = 320 to 340°C ($P_{corrected}$ = 600 to 650°C), whereas Type 2 is a high-salinity (20 to 25 wt. % eq. NaCl) aqueous fluid with Th = 165 to 200°C ($P_{corrected}$ = 400°C), and enriched in $CaCl_2$ based on melting of ice and clathrates. Based on evaporate mound analysis, the two fluids coincided with Na- and Na+Ca-rich mounds, respectively (Fig. 1). Also of note was the presence of F in the Ca-rich, Type 2 fluid; and 2) that an initial magmatic-derived fluid with $\delta^{18}O_{H2O} \leq 10‰$ mixed with an external fluid having $\delta^{18}O_{H2O} \geq 15‰$. In addition, whereas $\delta^{34}S$ data indicated a direct igneous source for vein sulphides, Pb isotopic data for vein sulphides and pegmatitic K-feldspar indicated both magmatic and sedimentary reservoirs. Thus, these data supported a model whereby an initial magmatic fluid exsolved from the granite mixed with a second fluid, which had equilibrated with the metasedimentary wall rocks. In order to further document the chemical signature of these fluids, further stable isotopic analyses of vein quartz and LA ICP-MS analysis of the fluid inclusions identified above were undertaken.

The new $\delta^{18}O$ analysis of vein quartz was done across veins from margins to cores. The results for two transects (SP-06-02 and 09) are summarized in Figure 2, where it can be seen that unreasonably low temperatures of vein formation (i.e., 250°C) would be required to satisfy the $\delta^{18}O_{quartz}$ values. Furthermore, such inclusions with T_h = 100°C are lacking in the vein samples. Thus, the elevated $\delta^{18}O$ values for vein quartz require fluid mixing, with one of these fluids being enriched in ^{18}O. Such an ^{18}O enriched fluid could be generated by interacting with a rock containing carbonate because this phase is a sink for ^{18}O. Since the carbonate-rich layers in the local rocks are also enriched in Fe, Mg, and Mn, this provides an opportunity to identify this component by LA ICP-MS analysis of the fluid inclusions. Results for these analyses are summarized below and also some data are presented in Figure 3. Type 1 and 2 FIAs are easily distinguished, with Type 2 fluid relatively enriched in (ppm, max. values indicated) Na (<80,000), Ca (50,000), K (10,000), Mn (<3,000), Fe (<2,000), Li (2,000), Mg (<1,500), Ba (400), Cs (300), Rb (250), and Pb (<150), whereas Type 1 fluids are relatively enriched in B (<3000) and As (<500). Based on the SEM-EDS data (Fig. 1), enrichment of Type 2 fluid in F is also noted. Although enrichment of Type 2 fluid in Ca, Mn, Fe, and Mg was expected, the high concentrations of granophile elements (e.g., F, K, Li, Cs, Rb) in this fluid were not. The enrichment of granophile elements in the Type 2 fluids may be explained in one of two ways: 1) back reaction of Type 2 fluid with the greisens, which liberated these elements, or 2) late-stage exsolution of a magmatic fluid, which mixed with the Type 2 fluid. Regardless of the interpretation, two important conclusions can be taken from this study: 1) the potential complexity of the fluid chemistry in hydrothermal systems; and 2) that decoupling of elements within fluid inclusions is necessary, because the sources for solutes in apparently homogeneous fluids need not be the same and they may instead reflect involvement of different reservoirs.

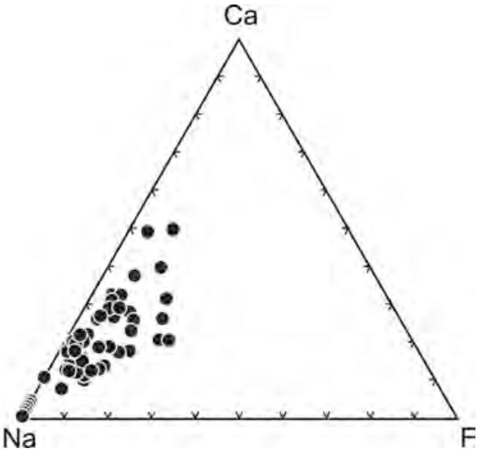

Figure 1. Ternary plot of Ca-Na-F for evaporate mounds in samples of vein quartz. Data are from Kontak and Kyser (2011).

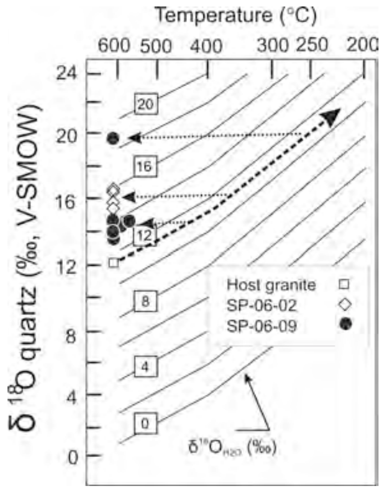

Figure 2. Plot of $\delta^{18}O_{quartz}$ vs. T with isopleths of $\delta^{18}O_{H2O}$ calculated using quartz-H_2O fractionation equation of Matsuhisa et al. (1979). The dashed arrow shows cooling trend of a fluid with an initial $\delta^{18}O_{H2O}$ value of 11‰. Other lines show points where vein quartz would precipitate from the cooling fluid to explain $\delta^{18}O_{quartz}$ values.

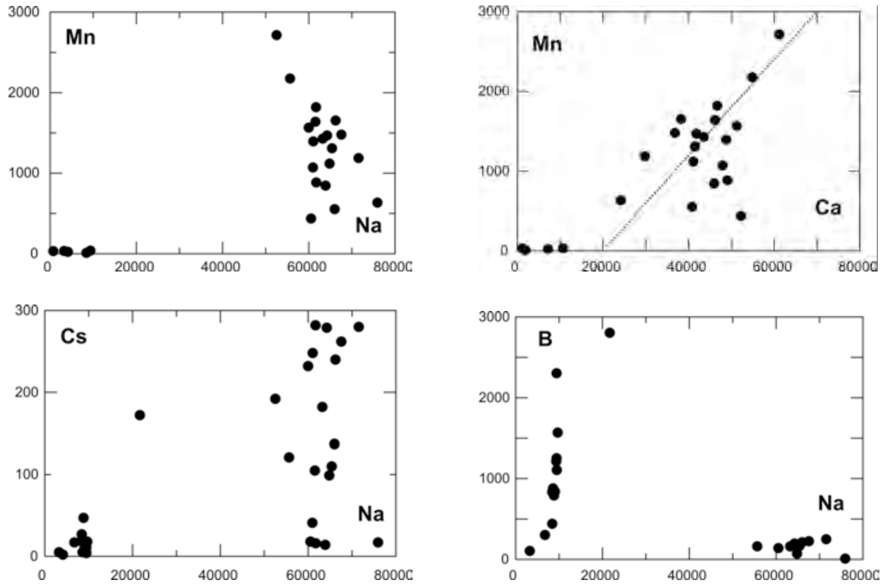

Figure 3. 1 Binary plots for solute contents (in ppm) for Type 1 and 2 fluid inclusions in this study. Type 1 fluids have the lower salinity values (i.e., <10,000 ppm Na). Note the enrichment of Type 1 fluids in B, but that Type 2 fluids are enriched in Mn and Ca, and that these two elements show a strong correlation.

REFERENCES

Kontak, D.J., Kyser, T.K. (2011) Fingerprinting multiple fluid reservoirs in a 380 Ma Intrusion-Related Gold (IRG) setting, Nova Scotia, Canada: Implications for the nature and origin of IRG deposits. Mineralium Deposita. Vol. 46. 337-363.

Matsuhisa Y., Goldsmith J.R., Clayton R.N. (1979) Oxygen isotopic fractionation in the system quartz-albite-anorthite-water. Geochimica et Cosmochimica Acta. Vol. 43. 1131–1140.

Water and hydrogarnet step-daughter minerals in CO_2-rich fluid inclusions in granulite facies rocks.

Lamadrid, H.M.*, Bodnar, R.J.*, Lamb, W.**, and Santosh M.***

**Department of Geosciences, Virginia Tech, Blacksburg, VA, U.S.A., lamadrid@vt.edu, rjb@vt.edu*
***Department of Geology and Geophysics, Texas A&M University, College Station, TX, U.S.A.*
****Department of Interdisciplinary Science, Faculty of Science, Kochi University, Kochi, Japan*

Granulite facies metamorphism is characterized by mostly anhydrous mineral assemblages that include orthopyroxene, plagioclase, garnet and quartz. The role of fluids during granulite formation has been the subject of intense debate for decades. The debate is centered on whether or not low a_{H_2O} fluids were present during metamorphism. Numerous workers have reported high-density “pure” CO_2 fluid inclusions as evidence that granulite facies fluids are carbonic and do not contain H_2O.

We show that H_2O is a common but minor fluid component in “pure” CO_2 fluid inclusions from various, previously well-studied granulites, as a fluid phase wetting the walls of CO_2-rich fluid inclusions in quartz and/or as a step-daughter mineral in the form of hydrogarnet covering the walls of CO_2-rich fluid inclusions in garnet.

Over a wide range of temperatures, CO_2 and H_2O are largely immiscible. Because of this, and because H_2O is the “wetting” phase, at room temperature small amounts of H_2O in CO_2-rich fluid inclusions occur as a thin film wetting the inclusion walls and are optically unresolvable. To overcome the difficulty in recognizing H_2O, the inclusions were analyzed at 150°C using a recently developed technique that involves a Raman microprobe coupled with a Linkam THSG 600 heating/cooling stage. Fluid inclusions were heated from room temperature (~25°C) to a temperature above the one-phase/two phase boundary (≈150°C), and the liquid H_2O phase that occurs as a thin film at room temperature evaporated into the vapor to produce a homogeneous H_2O-CO_2 fluid phase. Raman analysis of this homogeneous phase at elevated temperature revealed the presence of H_2O, as evidenced by a small but sharp peak at ~3641 cm^{-1} (Fig. 1).

In two of the samples, a peak was observed at about ~3665 cm^{-1}, or about 20 to 30 wavenumbers higher than that expected for the O-H vibration of H_2O (~3640 cm^{-1}). This spectrum was found to correspond to the O-H vibration of hydrogarnet (Fig. 1). Hydrogarnet is a hydrothermal mineral (~ 500°C) in which the hydroxide (OH) partially replaces silica (SiO_4), the Si^{4+} missing from the tetrahedral site is replaced by bonding of an H^+ to each of the four oxygens surrounding the vacant site $[(O_4H_4)^{4-}: (SiO_4)^{4-}]$.

The fluid inclusions that contain the hydrogarnet form arrays along healed cracks. The inclusions are CO_2-rich, range from 5 to 40 microns, and contain many solid phases. Some of the inclusions are irregularly shaped and others occur as randomly oriented, thin tubes that appear to be recrystallized and show evidence of necking down. The solid phases in the fluid inclusions (obtained by Raman spectroscopy) are mainly Fe- Mg-, Zn- and Cu-rich carbonates, hydrogarnet, pyrophyllite, micas and probable sulfide phases such as chalcopyrite. The hydrogarnet is thought to form by a reaction between the H_2O in the fluid phase and the host garnet during retrogression. The textural features of these inclusions and the composition of the solid phases suggest a possible high volatile-content carbonate melt that interacted with the rocks after the peak of metamorphism. Further work is necessary to determine the composition of the solid phases, and whether or not the fluid inclusions potentially represent immiscible carbonate melts trapped as melt inclusions.

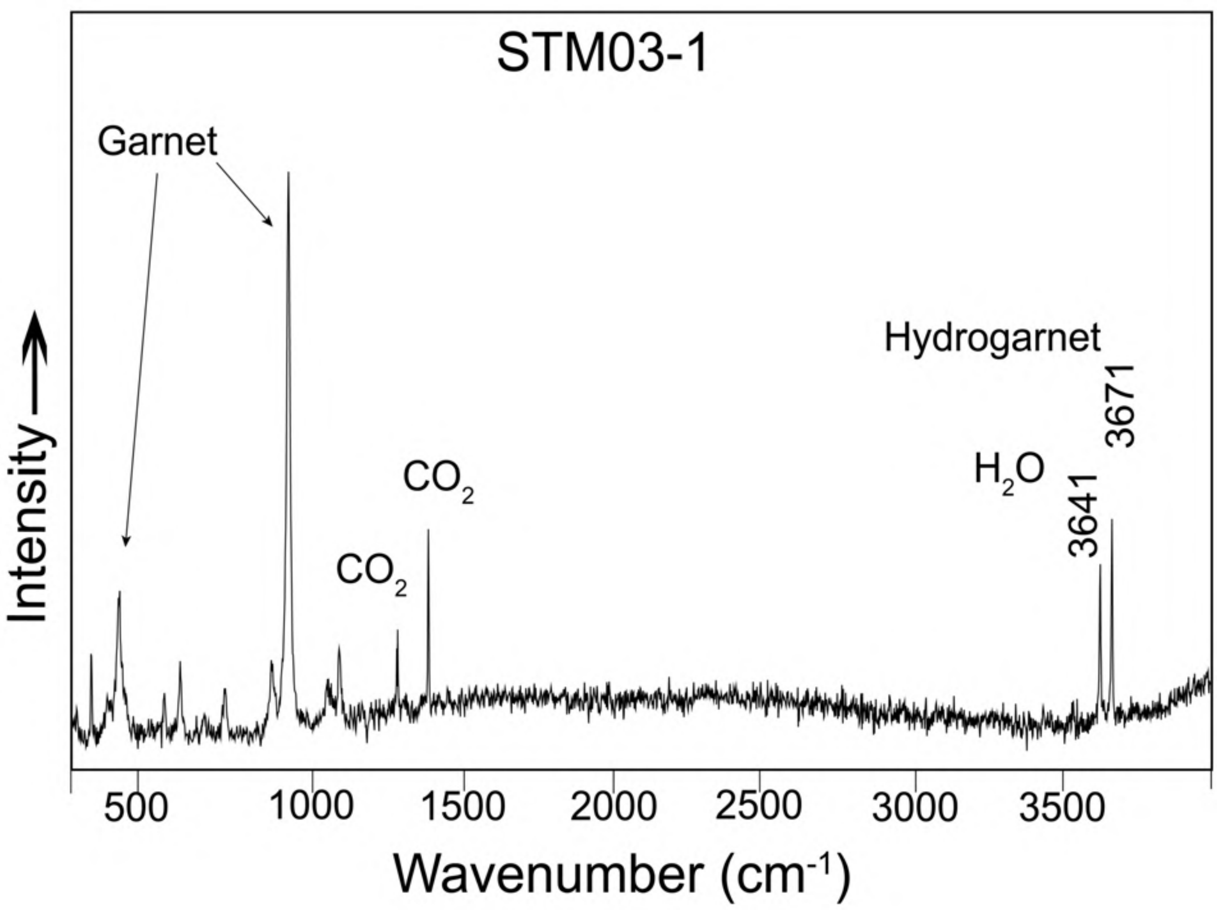

Figure 1. Raman spectrum showing peaks for H_2O and for hydrogarnet in a CO_2-rich fluid inclusion in garnet.

Experimental determination of the PVT properties of H_2O-NaCl-$FeCl_2$ fluids at magmatic-hydrothermal P-T conditions.

Lecumberri-Sanchez, P., Steele-MacInnis, M., and Bodnar, R. J.

Department of Geosciences, Virginia Tech, Blacksburg, VA, U.S.A.

Fluid inclusions are the most commonly used tool to determine the composition of geologic fluids and the pressure and temperature of geologic processes. Interpretation of thermometric data from fluid inclusions is based on the PVTX properties of the fluid in the inclusion. There is relatively abundant experimental data on H_2O-NaCl±KCl±$CaCl_2$±$MgCl_2$ fluids (which represent some of the most common salt components in geologic fluids (Yardley, 2005). However, while Fe is frequently one of the dominant cations in hydrothermal fluids, few experimental data on the PVTX properties of $FeCl_2$-bearing fluids are available.

The most commonly used system for the interpretation of fluid inclusions is the H_2O-NaCl system. The dissolution temperature of the last solid phase in the fluid inclusions is used to interpret the fluid salinity in terms of equivalent wt % NaCl. The liquid-vapor homogenization temperature is then used to determine the density and the slope of the inclusion isochore, based on the salinity determined from the solid dissolution temperature. The objective of this study is to determine the effect of adding iron to the H_2O-NaCl system, and the potential errors in salinity estimates and trapping pressure/temperature estimates that might result.

We have made synthetic fluid inclusions according to the methods described by Sterner and Bodnar (1984). The capsules were loaded with a mixture of deoxygenated, doubly distilled water, NaCl, $FeCl_2.4H_2O$ and pre-fractured quartz. The occurrence of magnetite in the bomb after the runs indicated that the fluid is likely in equilibrium with magnetite and therefore the dominant Fe species in solution is Fe^{2+} (Chou and Eugster, 1977). In addition, LA-ICPMS data from the synthetic fluid inclusions show Fe/Na ratios consistent with the nominal composition of the starting materials with precision similar to the analytical precision reported by Allan et al. (2005) for Fe analysis by LA-ICPMS. Because the bulk composition of the starting materials are consistent with the LA-ICPMS data from the synthetic fluid inclusions it is unlikely that iron oxides precipitated before the fluid was trapped in inclusions.

Fluid inclusions with a composition of 10 wt % $FeCl_2/(FeCl_2+H_2O)$ + 20 wt % NaCl/(NaCl+H_2O) have been synthesized at pressures of 1-3 Kbar and temperatures of 300-700°C. For these inclusions, the temperature of the last solid phase to melt during microthermometry (assumed to be hydrohalite based on the relative amounts of liquid and solid at the eutectic) yields a salinity of 25 wt % eq NaCl in the system H_2O-NaCl. This salinity is consistent with the eq wt % NaCl obtained from the known composition using the model of Heinrich et al. (1992). The data suggests that the liquid-vapor (LV) curve for the 10 wt % $FeCl_2/(FeCl_2+H_2O)$ + 20 wt % NaCl/(NaCl+H_2O) system varies little from the LV curve for 25 wt % NaCl. IsoTh lines have been plotted in PT space by using the known trapping conditions and the 25 wt% NaCl LV curve to interpret pressure at Th. The isoTh lines obtained by this method have slopes similar to those in the system 25 wt % NaCl.

REFERENCES

Allan M. M., Yardley B. W. D., Forbes L. J., Shmulovich K. I., Banks D. A., Shepherd T. J. (2005) Validation of LA-ICP-MS fluid inclusion analysis with synthetic fluid inclusions. American Mineralogist. Vol. 90. 1767-1775

Chou I. M., Eugster H. P. (1977) Solubility of magnetite in supercritical chloride solutions. American Journal of Science. Vol. 277. 1296-1314

Heinrich C. A., Ryan C. G., Mernagh T.P., Eadington P. J. (1992) Segregation of ore metals between magmatic brine and vapor: a fluid inclusion study using PIXE microanalysis. Economic Geology. Vol. 87 1566-1583.

Sterner S. M., Bodnar R. J. (1984) Synthetic fluid inclusions in natural quartz I. Compositional types synthesized and applications to experimental geochemistry. Geochimica et Cosmochimica Acta. Vol. 48. 2659-2668.

Yardley B. W. D. (2005) Metal concentrations in crustal fluids and their relationship to ore formation. Economic Geology. Vol. 100. 613-632.

Pan-American Current Research on Fluid Inclusions (PACROFI-XI)
University of Windsor, Windsor, Ontario, Canada, June 18–20, 2012, Abstract Volume

Composition and formation conditions of fluid inclusions of the Byrud emerald deposit, Norway.

Loughrey, L.*, Marshall, D.*, and Ihlen, P.

*Earth Sciences, Simon Fraser University, Burnaby, BC, Canada

The Byrud emerald deposit was first discovered in the early 1860s, at Byrud Farm located near Lake Mjøsa, southern Norway. From a geological, gemmological, and geochemical perspective, the Byrud emeralds are of great interest as they are vanadium-rich rather than chromium-rich, which is uncommon for the majority of emeralds worldwide. There are only a few emerald deposits that are vanadium-rich including Colombia; Lened in the Northwest Territories, Canada; Salininha in Bahia, Brazil; Dyakou in Yunnan, China; Panjshir, Afghanistan; and Gandao, Pakistan (Rondeau, 2008; Groat et al., 2008).

Emerald mining during the late 19th and early 20th century took place along flat-lying intrusive magmatic sills (maenaites), which range in size from 0.5 m to several meters thick. These sills intersect the sulphide-rich and carbonaceous Cambrian alum shale. At different levels the sills have been intruded by small pegmatites that also crosscut the black alum shales. The pegmatites are generally discontinuous and form lenses or dikes, ranging up to 30 cm in thickness (Rondeau, 2008). They consist of mainly K-feldspar and have an overall alkali syenitic composition. The pegmatites are likely associated with a large alkaline granite intrusion located west of Byrud. Previous work has determined that emerald mineralization occurs in the pegmatites, and rarely in the maenaites and alum shales, all of which are hosts rock to the pegmatites. It was hypothesized that the vanadium and chromium chromophores which give emerald its colour, were leached from the alum shales. In addition, there are 45 minerals reported from the deposit, with quartz, muscovite, plagioclase, pyrite, pyrrhotite, fluorite, topaz and beryl being the most common (Rondeau, 2008).

Two dominant Fluid Inclusion Types (FITs) have been observed from the Byrud emerald deposit. The first is a two-phase (vapour+liquid) assemblage. This FIT is abundant both in quartz and emerald, and consists of a brine and vapour bubble in variable amounts. The second FIT is comprised of three-phase inclusions commonly observed in quartz and to a lesser extent in emerald. These inclusions consist of a brine, vapour bubble, halite cube and rarely trapped accidental minerals. From previous work, the three-phase fluid inclusions have trapped several sulphide phases, such as pyrrhotite, galena, and sphalerite, which are distinctive to the Byrud emerald (Rondeau, 2008). The fluid inclusions in the samples studied occur as planes of inclusions along healed fractures, growth zones or as isolated inclusions. Minor growth zones observed in the emerald and quartz made it possible to conclusively identify primary fluid inclusions from both FITs, based on timing relationships between fluid inclusions and mineral growth characteristics.

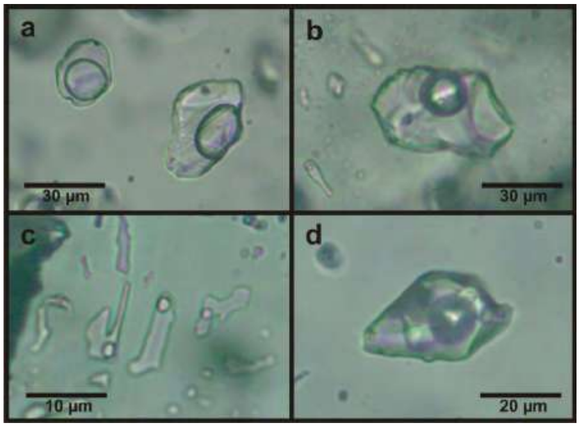

Figure 1. Fluid inclusions in emerald; a—c) two-phase fluid inclusions (liquid + vapour) and d) three-phase inclusions (liquid + vapour + halite). Photo taken in plane polarized light.

The dominant phase in the two-phase inclusions is the gaseous phase that occupies approximately 50-90% of the fluid inclusion volume, whereas the aqueous brine represents the remaining 10-50% of the volume, at room temperature. A second sub-FIT of two-phase inclusions displays fluid inclusion volumes where the gaseous phase occupies approximately 10-20%, and the aqueous brine comprising 80-90% of the remaining fluid inclusion volume. The inclusions display relatively consistent phase proportions within each FIT, generally, and range up to 60 microns in size. The main phase in the three-phase FIT is the aqueous brine that constitutes approximately 50-60% of the fluid inclusion volume, with 25-35% of the volume represented by the vapour phase and with halite occupying the remaining 15%. Also, a second sub-FIT of three-phase inclusions is present displaying fluid inclusion volume of 15% vapour phase, 10% volume halite cube and a remaining 75% volume aqueous brine. These inclusions can range up to 48 microns in size, and also display somewhat variable phase proportions.

Fluid inclusion microthermometric work on the two-phase FIT resulted in the nucleation of clathrate during rapid cooling at approximately -44°C and ice at approximately -55°C. In rare cases, solid CO_2 is formed at approximately -107°C. Upon further cooling to -160°C, no other phase changes were observed. Heating the inclusions from this temperature resulted in sublimation of solid CO_2 at approximately -58°C. Continued heating resulted in the first melting of ice over the temperature range -65°C to -54°C. Further heating resulted in the final ice melt temperatures which range from -5.8°C to 0.0°C, with clathrate final melt temperatures ranging between +9.1°C to +12.7°C. Heating the inclusions from room temperature resulted in a decrease in the volume of the vapour bubble, until the inclusions undergoes total homogenisation via vapour bubble homogenisation (Liquid + Vapour → Liquid) over a temperature range 161°C to 383°C. These results are consistent with previous work from Ventalon et al. (2009). Final ice melt and clathrate melt temperatures correspond to a range of salinities from 0.0 to 7.8 mass percent NaCl equivalent. Impurities in the CO_2 were detected via depression of the CO_2 triple point and CO_2, N_2, CH_4, and H_2S mole fraction estimates in the two-phase inclusions were obtained via Laser Raman spectroscopy and are on the order of 0.8974, 0.0261, 0.0354, and 0.0410, respectively.

Upon rapid cooling from room temperature to -160°C, the three-phase FIT nucleated clathrate at approximately -68°C and ice at approximately -87°C. No other phase changes were observed during cooling. Heating the inclusions resulted in the first melting of ice over the temperature range -58°C to -51°C. Final ice melt temperatures upon further heating occurred over the temperature range -29.4°C to -18.3°C, with clathrate final melt temperatures ranging between +10.3°C to +14.2°C. Heating the inclusions from room temperature resulted in a decrease in the vapour bubble and halite cube until final homogenization of the fluid inclusion to the liquid (and more rarely the vapour) phase over the temperature range of 152°C to 192°C for inclusions where total homogenisation is via halite melting (Liquid + Halite → Liquid), and over the range 231°C to 319°C for inclusions that undergo total homogenisation via vapour bubble homogenisation (Liquid + Vapour → Liquid). The halite melting temperatures measured in the three-phase inclusions correspond to a range of salinities from 29.8 to 31.5 mass percent NaCl equivalent.

The presence of two different saline fluids, represented by a low salinity two-phase (liquid+vapour) FIT and a highly saline three-phase (liquid+vapour+halite) FIT, is consistent with three possible scenarios to explain the observed fluid inclusions within the Byrud emeralds. The presence of the two FITs (Figure 2) supports either boiling and fluid inclusion trapping within a two-phase system, necking down, or the two different fluids have successively been trapped at the deposit. Since the Byrud deposit displays similarities to the Emmaville-Torrington emerald deposit in Australia, which has been interpreted as a boiling system (Loughrey et al., 2012) and the petrographic evidence for a boiling FIT (Figure 2), boiling is the preferred interpretation for the observed two FITs and is also consistent with the characteristic green and clear zones within some of the Byrud emerald.

Figure 2. Photomicrograph of a boiling assemblage in quartz consisting of a two-phase (vapour+liquid) and three-phase (liquid+vapour+halite) fluid inclusions. Photo taken in plane polarised light.

REFERENCES

Groat L.A., Giuliani G., Marshall D.D., Turner, D. (2008) Ore Geology Reviews. Vol. 34. 87-112.
Loughrey L., Marshall D., Jones P., Millsteed P., Main A. (2012) Central European Journal of Earth Sciences.
Rondeau B., Fritsch E., Peucat J.-J., Nordrum F.S., Groat L. (2008) Gems & Gemology. Vol. 44. 108-122.
Ventalon S., Dubois M., Rondeau B., Régnier S. (2009) European Current Research on Fluid Inclusions. 1-2.

Applications of Raman microspectroscopy to fluid inclusion identification.

Mamedov, S.*, Adar, F.*, Tuschel, D.*, and Koenig, A.**

*Horiba Scientific, Edison, NJ, U.S.A.
**US Geological Survey, Lakewood, CO, U.S.A.*

Raman spectroscopy is a powerful tool that has been applied widely to characterize a variety of fluid and solid materials. While microspot Raman analysis has been used with great success to identify and characterize materials, it has previously been less useful for characterizing minor components in samples and for characterizing sample heterogeneities. Minerals often contain fluids or gases in bubbles (inclusions) which have been trapped during the formation of the crystal and thus can provide information about the conditions existing during the mineralization as well as geological metamorphism- composition, temperature, and pressure. The size of inclusions ranges from less than a micrometer to several hundred micrometers in diameter. A Raman system coupled to a confocal microscope is required to obtain high spatial resolution and to analyse inclusions located below the surface without destruction. For a matrix having an index of refraction close to the glass, the use of a dry objective with cover slip correction is a solution to minimize the degradation of the lateral and axial resolution implied by the change of refractive index.

The recent development of high-speed, high resolution mapping capabilities now makes it possible to obtain high spectral, high spatial resolution Raman maps quickly and easily. Many fluid phases that are common in fluid inclusions, including H_2O, CO_2, CH_4, H_2S. etc., are easily recognized by Raman spectroscopy and in some cases quantified using their Raman band intensities and/or positions. Recently, there has been much interest in searching for small amounts of H_2O in FI that previously had been thought to contain only CO_2. Confirming the presence of even small amounts of water in fluid inclusions is important in understanding some upper mantle processes in which, as a result of exposure to high temperatures and pressures, hydrated minerals lose water that may then occupy fluid inclusions. At room temperature, the liquid H_2O phase occurs as a thin, sub-microscopic rim on the walls of the inclusion; it has therefore been diffficult, if not impossible, to locate the H_2O film using spot analysis. Raman mapping, however, facilitates the search for H_2O in these inclusions and provides a rapid method to survey a large number of fluid inclusions to see which, if any, contain H_2O. Multivariate analysis methods are used to construct the Raman maps and indicate the presence, in this case, of the water and other substances.

Several examples of fluid inclusions have been studied, and spectra of the gas phase, consisting of a mixture of CO_2 (1285 cm^{-1} and 1388 cm^{-1}), CH_4 (2914 cm^{-1}), N_2 (2331 cm^{-1}) and H_2S (2611 cm^{-1}) and liquid phase (3200-3700 cm^{-1}), will be shown.

Melt inclusions of native silver and native bismuth at Cobalt, Ontario: An example of native-metal enrichments using experimental in situ melting studies.

Marshall, D.*, Mavrogenes, J.**, and Mernagh, T.***

**Earth Sciences, Simon Fraser University, Burnaby, BC, Canada*
***Australian National University, Canberra, ACT, Australia*
****Geoscience Australia, Symonston, ACT, Australia*

Veinlets and trails of melt inclusions of both native bismuth (Fig. 1) and silver crosscut silicate and carbonate vein fill and alteration minerals in the five-element veins at Cobalt, Canada. The low melting temperature of bismuth (271 °C) is consistent with the current estimates of vein formation at Cobalt and melt textures are displayed by native bismuth (Bi) inclusions and trails. Native silver displays identical textures and these are also interpreted to have formed from a melt. However, native silver melts above 950°C, which is in direct conflict with current estimates of silver depositional conditions within the Cobalt camp. Despite the lack of experimental studies in the the Co-As-Ag ternary, the data from textural similarities in Bi and Ag melt inclusions, existing temperature evidence and recent advances in the study of melt inclusions from sulphide deposits all indicate that native silver can form as melt inclusions at temperatures as low as 350°C.

The silver within the five-element veins at Cobalt, Ontario has up to a few weight percent of dissolved mercury, antimony, and bismuth. Fluid inclusion evidence is also consistent with high salinity fluids at Cobalt. New experimental studies using silver compositions with high Cl contents, and minor amounts of Hg, Sb, and Bi utilize "gravity-dribble" experiments. These experiments place known mixtures of metals at the top of a graphite capsule, overlying a column of graphite spheres. The capsule is then placed within a piston-cylinder apparatus with a calibrated vertical temperature-gradient ranging from 550°C at the top of the capsule to 300°C at the bottom of the capsule. If the metal-salt mixture at the top of the capsule melts it dribbles down through the network of graphite spheres until either it cools sufficiently within the thermal gradient to partially solidify or it ponds at the bottom of the capsule. Our experiments have shown that the silver (+Bi +Hg +Sb +Cl) melts remain liquid at temperatures down to 375°C. The experiments are consistent with increased Sb and Hg concentrations in silver solidifying at higher temperatures, and slightly higher concentrations of Bi persisting in the silver melts to lower temperatures.

Veinlets of native bismuth and associated trails of metallic inclusions of native bismuth (Fig. 1) have been studied using a standard fluid inclusion heating-freezing stage coupled to a laser Raman microprobe to perform in-situ melt experiments of the bismuth solid inclusions from the silver deposits at Cobalt. The bismuth veinlets and solid inclusions exposed at surface have been analysed with an SEM equipped with an EDS detector and are virtually pure bismuth. Bismuth exposed at the surface of a doubly polished plate shows some laser damage and oxidation from Raman analysis and this develops a corresponding Raman peak at approximately 312 cm^{-1}. This peak is attributed to bismuth-oxide and is not seen and does not develop on a solid inclusion of native bismuth entirely contained within the host mineral. A single bismuth solid inclusion hosted within calcite was heated and the Raman spectrum recorded. Although thermoluminescence and fluorescence in the host calcite does present some analytical challenges, the 95 cm^{-1} Raman band does diminish and disappear at 175ºC indicating that the bismuth was molten by this temperature. This is well below the melting point of pure bismuth. Silver is Raman inactive, however, trace amounts of other unidentified compounds within solid silver inclusions display Raman peaks. These inclusions can be heated while collecting Raman spectra at various temperatures. When these peaks from the unknown compounds within the inclusions disappear and do not reappear on cooling to room temperature, it is interpreted that these solids have moved out of the beam path because the silver has melted. These experiments suggest that silver inside these solid-silver inclusions melts at approximately 300°C.

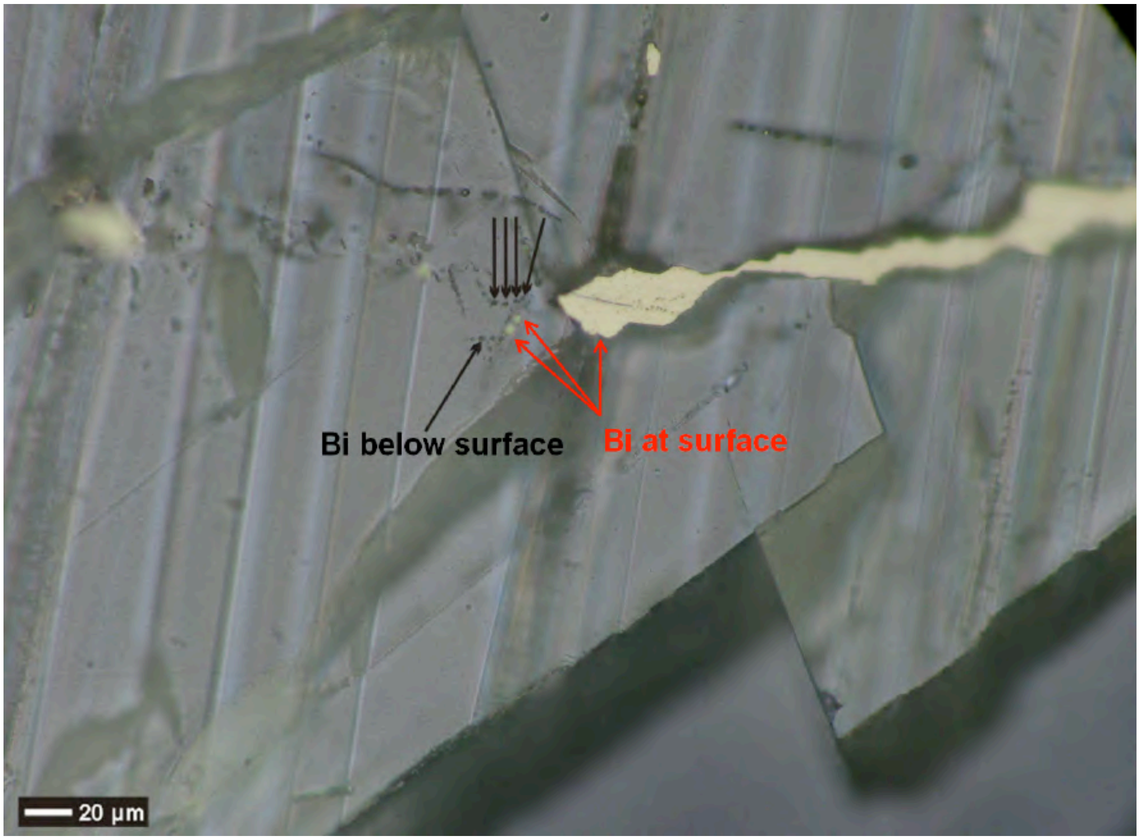

Figure 1. A veinlet of native bismuth terminating in a trail of native bismuth solid inclusions hosted within calcite. The bismuth exposed at surface (red arrows) is polished and reflective while the inclusions contained within the host calcite (black arrows) are dark.

The new evidence from dribble experiments and Raman data are consistent with the observed temperatures of formation for the silver veins at Cobalt, Ontario and that silver and bismuth were probably mobilized and concentrated as molten metals. The molten melts probably behaved an immiscible phase coexisiting with the highly saline hydrothermal brine previously documented at Cobalt. The mobilization and solidfication of the molten metals likely acted as a mechanism to concentrate both Bi and Ag within fractures (Fig. 1), while smaller amounts of the molten metal were trapped along healed fractures alongside or whithin fluid inclusions containing hydrothermal brine.

Fluid inclusion study of hydrothermal dolomite and other late-stage cements in Neoproterozoic dolostone of the Wynniatt Formation (Victoria Island, NWT).

Mathieu, J., Kontak, D.J., and Turner, E.C.

Department of Earth Sciences, Laurentian University, Sudbury, ON, Canada

Hydrothermal dolomite is commonly associated with base-metal deposition in carbonate host rocks (MVT) or with hydrocarbon migration. Fluid inclusions, coupled with various other techniques (e.g., SEM), provide detailed information about the composition and origin of a fluid and, hence, the conditions of base-metal mineralisation or hydrocarbon migration. This project aims to constrain the composition, origin, and evolution of fluids responsible for late-stage cements in the upper Wynniatt Formation (Shaler Supergroup), and thereby to assess the economic potential for hydrocarbons or base metals in this poorly known region. The Neoproterozoic Wynniatt Formation, exposed in the Minto Inlier on Victoria Island, Northwest Territories, consists of carbonate rocks that were locally karsted in the Early Cambrian. Sparry dolomite and calcite cements are present in the unit regionally, but appear to be most common near the karst surface and near regional normal faults that were active in the Cambrian. Petrographic relations suggest that the cements post-date karstification because some samples have saddle dolomite crystals that incorporate Cambrian sand.

Detailed petrography of samples near the karst surface has established a paragenesis of multiple phases, including, in decreasing age: dolomitised fine-grained matrix, coarse-grained saddle dolomite cement, ± coarse-grained brown dolomite cement, and white calcite cement. Some samples have late-stage quartz cement followed by brecciation and calcite precipitation. Associated with the quartz cement is framboidal pyrite, which appears repeatedly as a primary phase in growth zones in the quartz.

The paragenetic phases identified contain well-defined aqueous (A) and petroleum (P) fluid inclusion assemblages (FIAs) of primary and secondary types. Primary AFIAs are distributed along growth zones in both saddle dolomite and late-stage quartz cement, whereas the secondary AFIAs form both random groups of inclusions and clusters on healed fractures. Aqueous inclusion types present include L-V types with variable L:V ratios (in part due to necking), and monophase L- and V-types; only the L-V and monophase-V types are considered to represent trapping of primary fluids. P-type FIAs identified to date are monophase liquid, rarely with <2-3% L_{H_2O}, and are restricted to secondary trails in the late-stage quartz cement. These inclusions fluoresce a light beige-white under UV light (385 nm).

Preliminary measurements for AFIAs were limited to the L-V types from different paragenetic stages and yielded fluid densities of 0.75 g/cc and 0.9 g/cc. Metastability of the L-V inclusions in all phases was a problem, and despite repeated cycling between -100° and -140°C, freezing of the liquid did not occur, except in a few cases. For those inclusions in carbonate which did freeze (in brown dolomite and white calcite), detectable first melting took place at -21°C and 0.2°C, respectively. The few inclusions in quartz which froze showed first melting at -65°C and -1°C. Three populations of homogenisation temperatures were recorded for AFIAs in the carbonate phases: 100°, 115°, and 132°C, with variation in each FIA type of ≤3°C. In quartz, the AFIAs defined a single population of homogenisation temperatures at 130°C, again with little variation.

Decrepitated mounds generated in the different phases were analysed using the SEM-EDS method. Notably, the majority of decrepitated fluid inclusions from the carbonate phases did not produce evaporate mounds, possibly reflecting low salinities. The few mounds observed in the dolomite were dominated by Na with minor K (Na:K ratios of 10:1); the presence of Mg and Ca could not be determined owing to interference with the dolomite substrate. The white calcite phase yielded no mounds, which is again attributed to the low salinity of the inclusions. Data for quartz-hosted inclusions remain to be obtained.

Salinities obtained from fluid inclusion microthermometry indicate that at least two fluids were present during formation of late diagenetic carbonate cements in the Wynniatt Formation: a saline fluid (23 wt. % eq. NaCl) and a low-salinity fluid (near 0 wt. % eq. NaCl) of possible meteoric origin; mixing of these two fluids is also possible. The preliminary homogenisation temperature data for the FIAs suggest an increase in temperature during the evolution of the fluid, from the earlier saddle dolomite (100°C) to later white calcite and quartz (near 130°C). Burial depth calculations will be undertaken in order to determine if these temperatures were a function of burial, or if a hydrothermal fluid was responsible for the formation of the cements. The presence of petroleum inclusions along healed fracture planes in the quartz cement indicates that petroleum migration occurred after this cement formed and, possibly, after the rocks had experienced temperatures of at least 130°C. Future work will include isotope geochemistry and trace element analysis in order to better constrain the origin of the fluids.

Tracking magmatic Molybdenum concentrations during evolution and degassing of the Hideaway Park rhyolite, Colorado: insights into Mo partitioning in Climax-type deposits.

Mercer, C.N.*, Hofstra, A.H., Marsh, E.E., Todorov, T.I., and Koenig, A.E.

*U.S. Geological Survey, MS-973, Denver, CO, U.S.A., *cmercer@usgs.gov*

A key question in the study of Climax-type porphyry-Mo deposits is: what is the source and evolutionary path of metals and sulphur during the generation of mineralizing fluids? The origin of mineralizing fluids in these ore deposits is linked to immiscibility, or unmixing, of parental silicate magmas. Melt inclusions preserve "snapshots" throughout the evolution of parental magmas, providing a record of changing physical conditions and magmatic compositions. We present preliminary results from the first phase of an integrated study to investigate melt inclusions from the Hideaway Park rhyolite, Colorado. The goal of this work is to reconstruct the evolution of this high-silica magma (crystallization, mixing, degassing, etc.) and to track changes in metal concentrations (e.g., Mo) and volatile contents (H_2O, CO_2, S, F, Cl) during the course of magma evolution.

The source of Mo in Climax-type deposits is currently debated and may originate in the mantle and/or the crust. Once in a silicate melt, Mo partitions strongly into magmatic pyrrhotite and immiscible Fe-S-O melts (Mengason et al., 2011) and fractionation of these phases affect the metal budget of the parent magma. Solubility of molybdenite in aqueous fluids depends on temperature, salinity, S content, fO_2, and fS_2 (Zajacz et al., 2008; Zhang et al., 2012; Ulrich and Mavrogenes, 2008), all of which may vary during magma evolution. Understanding the partitioning of Mo into various magmatic phases relative to the timing of aqueous fluid saturation and Mo removal is important for estimates of metal budgets and source magma volumes.

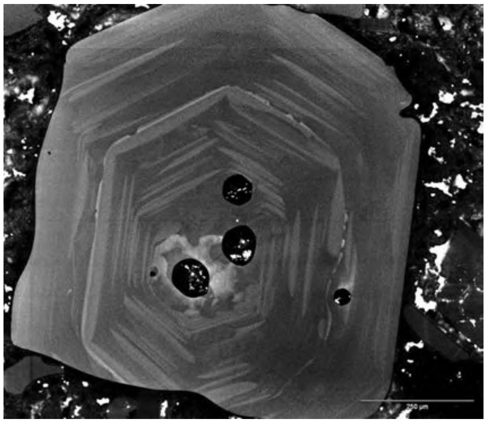

Figure 1. SEM-CL image of partially resorbed quartz phenocryst showing crystallized melt inclusions (scale = 250μm).

The Hideaway Park rhyolite is an ashflow tuff that is thought to be an extrusive expression of the Oligocene intrusive complex that formed the Henderson porphyry-Mo deposit, Colorado (Adams et al., 2009). The genetic link between the Hideaway Park rhyolite and the Henderson deposit offers a distinct advantage for a melt inclusion study of this porphyry system because the Hideaway Park melt inclusions did not undergo extensive hydrothermal alteration, and thus are relatively pristine compared to those typically found in porphyry ore rocks. Thus these samples provide a unique view into processes of magmatic evolution and metal transport in this Climax-type Mo system.

Most quartz-hosted melt inclusions in the Hideaway Park rhyolite are partially devitrified and/or crystallized so homogenization experiments are required to prepare them for microanalysis. Preliminary homogenization experiments have been carried out using a Linkam TS1500 heating stage to ascertain approximate homogenization experiments will be completed using a 1atm gas-mixing furnace and a rapid-quench cold seal pressure vessel. Pressurized homogenizations will be crucial to minimize volatile loss from the melt inclusions due to decrepitation or leakage (Student and Bodnar, 2004; Severs et al., 2007), allowing analysis of H_2O, OH, and CO_2 by FTIR and Raman spectroscopy. Major and trace element geochemistry, including S, F, and Cl will be determined by electron microprobe and LA-ICPMS.

SEM-cathodoluminescent (CL) images reveal distinct populations of melt inclusions trapped at various stages during quartz growth (Fig. 1). Melt inclusions are comprised of glass, devitrified glass, crystals, and vapour. Crystals typically include quartz, alkali feldspar, magnetite, fluorite, zircon, and monazite. At least three distinct populations of melt inclusions have been identified optically (Fig. 2). One group is typically dark brown with spherical to oblate shapes. Smaller inclusions of this group are glassy and transparent, while larger ones are devitrified, crystallized, and appear nearly opaque (Fig. 2A). Preliminary heating experiments (using slow heating rates (Student and Bodnar, 2004)) of an inclusion from this group resulted in dark brown glass with a large bubble (15 vol%) and several small bubbles that ruptured at ~1170°C, far exceeding temperatures expected for any high-silica melt. It is possible that this group represents lamprophyric melt that mingled with the high-silica rhyolite (e.g., Bookstrom et al., 1988).

Another group of inclusions are tan in colour and exhibit rounded, negative bipyramidal shapes (Fig. 2B). These inclusions are glassy to devitrified and contain clear to opaque crystals. Preliminary heating experiments of these inclusions resulted in formation of a bubble (5 vol%) during melting and vapour-melt homogenization to a clear glass between ~840-880°C, which is likely above their true entrapment temperature (if they are indeed rhyolitic).

The third group of inclusions are generally smaller in size, spherical to faintly bipyramidal, and are comprised of clear glass, clear and opaque crystals, and one or more bubbles (Fig. 2C). Heating experiments will be carried out on this group of inclusions shortly.

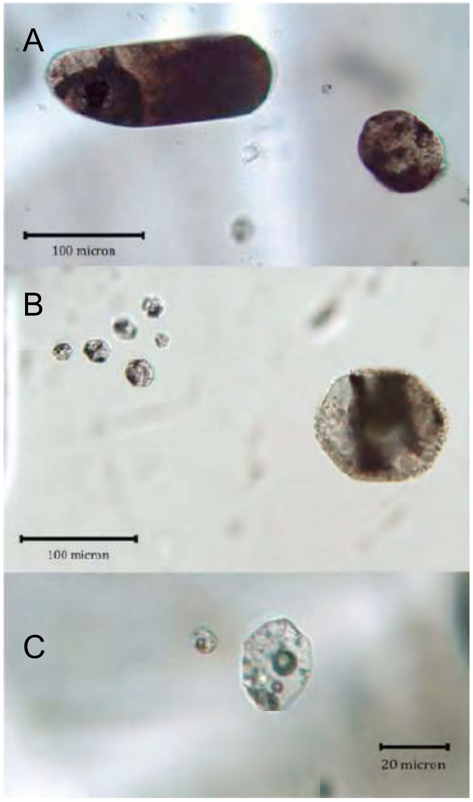

Figure 2. Optical microphotographs showing crystallized melt inclusions (before homogenization).

Preliminary trace element analysis by LA-ICPMS reveals a mantle-like Mo/Rb signature (>0.013). Inclusions have a modal Mo content of 10 ppm, but range from <3 to 115 ppm. This range may be indicative of two distinct processes of Mo distribution within the magma: (1) the magma may have been saturated with molybdenite (Audétat et al. 2011) and anomalously high Mo concentrations may be due to molybdenite platelets trapped in inclusions, and/or (2) the Mo content of the melt inclusions my fluctuate due to crystallization but may decrease upon saturation of an aqueous fluid and subsequent Mo separation. Further investigation will help elucidate these processes relative to the timing of aqueous fluid saturation and degassing, particularly of S, which enhances the aqueous solubility of Mo (Ulrich and Mavrogenes, 2008).

REFERENCES

Adams D.T., Hofstra A.H., Cosca M.A., Todorov T.I., Marsh E.E. (2009) GSA abstract. 93-7.
Audétat A., Dolejs D., Lowenstern J.B. (2011) Journal of Petrology. Vol. 52. 891-904.
Bookstrom A.A., Carten R.B., Shannon J.R., Smith R.P. (1988) Colorado School of Mines Quarterly. Vol. 83. 1-24.
Mengason M.J., Candela P.A., Piccoli P.M. (2011) Geochimica et Cosmochimica Acta. Vol. 75. 7018-7030.
Severs M.J., Azbej T., Thomas J.B., Mandeville C.W., Bodnar R.J. (2007) Chemical Geology. Vol. 237. 358-371.
Student J.J., Bodnar R.J. (2004) The Canadian Mineralogist. Vol. 42. 1583-1599.
Ulrich T., Mavrogenes J. (2008) Geochimica et Cosmochimica Acta. Vol. 72. 2316-2330.
Zajacz Z., Halter W.E., Pettke T., Guillong M. (2008) Geochimica et Cosmochimica Acta. Vol. 72. 2169-2197.
Zhang L., Audétat A., Dolejs D. (2012) Geochimica et Cosmochimica Acta. Vol. 77. 175-185.

An exploration model for precious metal deposits in the Guanajuato Mining District, Mexico, based on fluid inclusions and mineral textures.

Moncada, D.* and Bodnar, R.J.**

*Department of Geosciences, Virginia Tech, Blacksburg, VA, U.S.A., *moncada@vt.edu, **rjb@vt.edu*

Exploration geologists have been developing systematic approaches to search for mineral deposits since the time of Agricola. Applying new models and methods provides a competitive advantage in the search for mineral deposits because an explorationist can quickly evaluate potential targets and eliminate areas without good potential for mineralization. In our research we have developed a technique based on petrographic characteristics of mineral textures produced during boiling events in quartz, calcite and adularia, and fluid inclusions contained in these phases, that can be applied in exploration for precious metal deposits.

The Guanajuato mining district is one of the largest silver producing districts in the world. Ore shoots are localized along three major northwest trending vein systems, the La Luz, Veta Madre and Vetas de la Sierra (Figure 1). More than 1200 samples were collected from surface outcrops, underground mine, and historical and recent drill core. Traverses perpendicular to veins in all system were also conducted. The La Luz system samples were collected from the Plateros, Melladito, Intermediate, Nombre de Dios, Bolañitos, San José, Lucero, Karina, Daniela and Belén veins. The Veta Madre system extends over a strike length of 7 km and samples were collected from the Cebada, Guanajuatito, Cata, Tepeyac, Cata, Rayas, and San Vicente mines. The Vetas de la Sierra system samples were collected from the Monte San Nicolas, Villalpando, and San Nicolas veins. Mineralization in the district shows much variability between and within deposits, from precious metal-rich to more base-metal-rich zones, and from gold-rich to silver-rich zones. Ore textures also vary and include banded quartz veins, massive quartz veins and stockworks. Fluid inclusion and mineralogical features indicative of boiling have been characterized within all of the different mineralization styles from all three vein systems in the Guanajuato mining district. Most of the samples (approximately 90%) were also assayed for Au, Ag, Cu, Pb, Zn, As, Sb.

Features associated with boiling that have been identified in the Guanajuato mining district include colloform silica texture, moss silica texture, jigsaw silica texture, plumose silica texture, ghost-sphere silica texture, rhombic adularia, adularia, illite/sericite, lattice-bladed calcite, and lattice-bladed calcite replaced by quartz, coexisting liquid-rich and vapor-rich fluid inclusions, vapor-rich-only inclusions and liquid-rich inclusions with trapped illite. The fluid inclusions are hosted by jigsaw silica texture, plumose silica texture, and bladed calcite and rhombic calcite in secondary fluid inclusion assemblages; primary fluid inclusions are present only in euhedral quartz with no evidence of recrystallization. The La Luz area shows homogenization temperatures (T_h) from primary fluid inclusions in quartz from assemblages containing coexisting liquid-rich and vapor-rich inclusions that range from 209-211°C and salinity from 0.1-0.6 wt. % NaCl. Secondary fluid inclusion assemblages in quartz with coexisting liquid-rich and vapor-rich inclusions show a range in T_h from 180-320°C and salinity from 0.1-2.1 wt. % NaCl. Primary fluid inclusion assemblages in bladed calcite with coexisting liquid-rich and vapor-rich inclusions show a range in T_h from 160-188°C and salinity from 0.6-0.9 wt. % NaCl. Secondary fluid inclusion assemblages in quartz containing only vapor-rich inclusions show a range in T_h from 255-340°C and salinity from 0.5-1.5 wt. % NaCl. Primary liquid-rich inclusions with trapped illite in quartz show a range in T_h from 251-287°C and salinity 0.1-0.5 wt. % NaCl. Secondary fluid inclusions in quartz show a range in T_h from 286-289°C and salinity from 0.9-1.2 wt. % NaCl. In rhombic calcite T_h ranges from 159-197°C and salinity from 0.4-0.6 wt. % NaCl. Homogenization temperatures of fluid inclusions from the Veta Madre range from 184 to 300°C and salinities range from 0 to 5 wt.% NaCl. Secondary fluid inclusion assemblages in quartz with coexisting liquid-rich and vapor-rich inclusions show a range in T_h from 285-287°C and salinity from 0.3-0.7 wt. % NaCl. Secondary fluid inclusions in rhombic calcite range from 262-263°C, with salinity of 0.7 wt.% NaCl. Evidence of boiling based on fluid inclusions and mineral textures has been observed in most of the veins in the Guanajuato mining district and in most cases there is a close correlation between boiling and economic metal grades.

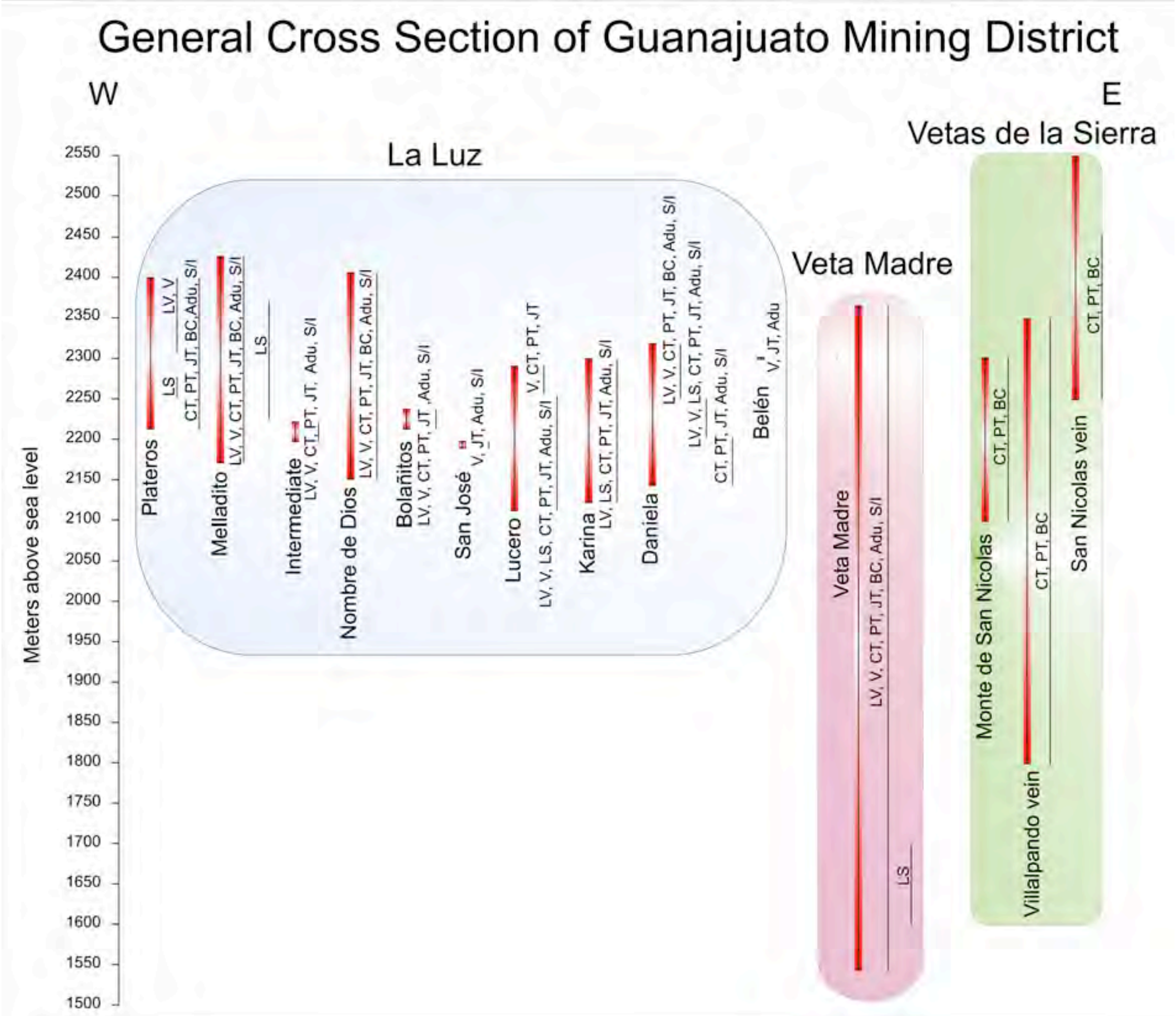

Figure 1. Schematic east-west cross section of the Guanajuato mining district showing the different veins and distribution of fluid inclusions and silica and calcite mineral textures present as a function of depth. (LV) Coexisting liquid-rich and vapor-rich inclusions, (V) Vapor-rich-only inclusions, (LS) Liquid-rich inclusions with trapped illite, (CT) Colloform silica texture, (PT) Plumose silica texture, (JT) Jigsaw silica texture, (BC) Bladed calcite replaced by quartz, (Adu) Adularia, (S/I) Sericite/illite smectite.

Pan-American Current Research on Fluid Inclusions (PACROFI-XI)
University of Windsor, Windsor, Ontario, Canada, June 18–20, 2012, Abstract Volume

Raman spectroscopic technique to determine the salinity of fluid inclusions.

Moncada, D.* and Bodnar, R.J.**

*Department of Geosciences, Virginia Tech, Blacksburg, VA, U.S.A., *moncada@vt.edu, **rjb@vt.edu*

Fluid inclusions provide the best tool available to determine the salinity of aqueous fluids in different geological environments. Most often, the freezing-point depression is used to calculate salinity (Bodnar, 1993, 2003), and this technique can be used for inclusions larger than about 5-7 μm in diameter (Goldstein and Reynolds, 1993). Determining the salinity from microthermometry for smaller inclusions is sometimes problematic owing to the difficulty in recognizing if the inclusion has frozen and/or when the ice phase melts. Additionally, many small moderate-to-high density inclusions fail to nucleate a vapor bubble during cooling from trapping conditions. The ice-melting temperature for such FI cannot be used to determine the salinity because the ice is not melting under vapor-saturated conditions. Here we describe a non-destructive technique using Raman spectroscopy to determine the salinity of fluid inclusions that can be applied to inclusions that are too small for microthermometric analysis.

Other workers have presented models based on Raman analysis to determine the salinity of fluid inclusions (Georgiev et al., 1984; Mernagh and Wilde, 1989). More recently, Furić et al. (2000), Dubessy et al. (2002) and Sun et al. (2010) described techniques and developed calibration curves for several electrolytes and presented equations to calculate salinity. However, these earlier studies do not discuss the acquisition time required to obtain Raman spectra. In the present study, it was found that longer than normal collection times are required to eliminate analytical uncertainty and to generate reproducible spectra. Raman spectroscopic analyses were performed using a JY Horiba LabRam HR800 high resolution, 800 mm focal length spectrometer in the Vibrational Spectroscopy Laboratory in the Department of Geosciences at Virginia Tech. Spectra were initially collected for various periods of time, increasing by five seconds each time and calculating the peak area ratio. I_A represents the weak hydrogen-bonded linear peak at 3450 cm^{-1} and I_B represents the strong hydrogen-bonded linear peak at 3220 cm^{-1}. It was found that the peak area ratio becomes constant and independent of time at around 300 seconds. Calibration data were collected from synthetic H_2O-NaCl fluid inclusions ranging from 0 to 22.5 wt. % NaCl. The peak area ratio area is plotted as a function of the salinity in wt. % NaCl in Fig. 1. Equation 1 relates the salinity to the peak area ratio.

$$\text{wt. \% NaCl} = 119.01333 \text{ X } (I_A/I_A+I_B) -73.83646 \qquad (1)$$

The Raman method was applied to natural fluid inclusions from two different environments. The results show that salinities determined by Raman agree well with those predicted from microthermometric analysis (Fig. 2).

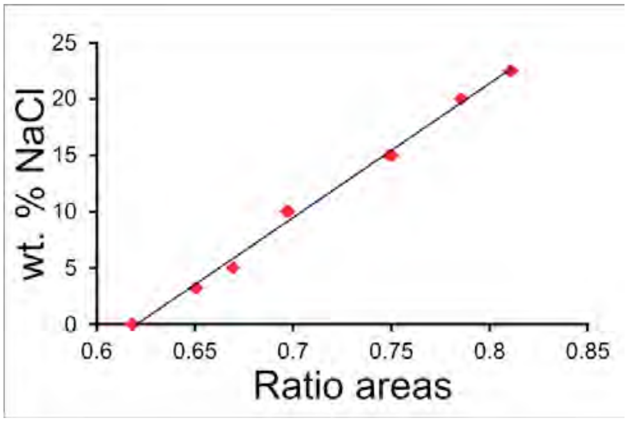

Figure 1. Peak area ratios obtained from synthetic fluid inclusions as a function of wt. % NaCl.

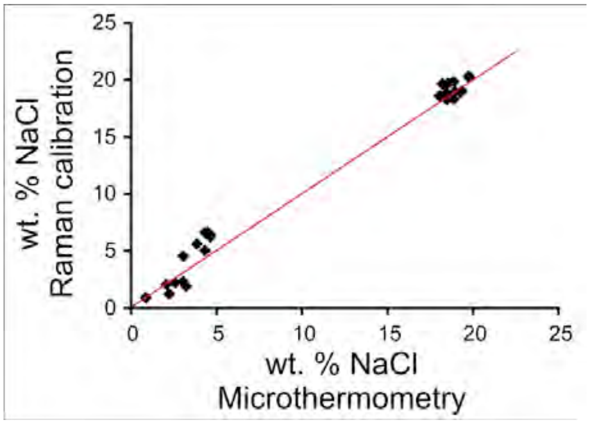

Figure 2. Conventional microthermometry versus Raman determination. Red line represents one to one relationship.

REFERENCES

Bodnar, R.J. (1993) Revised equation and table for determining the freezing point depression of H_2O-NaCl solutions. Geochimica et Cosmochimica Acta. Vol. 57. 683-684.

Bodnar, R.J. (2003) Introduction to aqueous-electrolyte fluid inclusions. *In*: Fluid Inclusions: Analysis and Interpretation, (eds. I. Samson, A. Anderson, D. Marshall) Mineralogical Association of Canada Short Course. Vol. 32. 81–100.

Dubessy, J., Lhomme, T., Boiron, M.C., Rull, F. (2002) Determination of Chlorinity in Aqueous Fluids Using Raman Spectroscopy of the Stretching Band of Water at Room Temperature: Application to Fluid Inclusions. Applied Spectroscopy. Vol. 56. 99-106.

Furić, K., Ciglenečki, I., Ćosović, B. (2000) Raman spectroscopic study of sodium chloride water solutions. Journal of Molecular Structure. Vol. 550–551. 225-234.

Georgiev, G.M., Kalkanjiev, T.K., Petrov, V.P., Nickolov, Zh. (1984) Determination of Salts in Water Solutions by a Skewing Parameter of the Water Raman Band. Applied Spectroscopy. Vol. 38. 593-595.

Goldstein, R.H. and Reynolds, T.J. (1993) Systematics of fluid inclusions in diagenetic minerals. SEPM Short Course Notes. Vol. 31. 213.

Mernagh, T.P., Wilde, A.R. (1989) The use of the laser Raman microprobe for the determination of salinity in fluid inclusions. Geochimica et Cosmochimica Acta. Vol. 53. 765-771.

Sun, Q., Zhao, L., Li, N., Liu, J. (2010) Raman spectroscopic study for the determination of Cl^- concentration (molarity scale) in aqueous solutions; application to fluid inclusions. Chemical Geology. Vol. 272. 55-61.

Fluid inclusion study in coexisting quartz and enargite from Main Stage veins at Butte, Montana.

Ortelli M.*, Kouzmanov K.*, Dilles J.H.**, and Rusk B.G.***

**Earth and Environmental Sciences, University of Geneva, Geneva, Switzerland*
***Geosciences, Oregon State University, Wilkinson Hall 104, Corvallis, OR, U.S.A.*
****Department of Geology, Western Washington University, Bellingham, WA, U.S.A.*

In ore deposit research, most fluid inclusion studies are conducted on transparent gangue minerals which are assumed to be “co-genetic” with the ore mineralization. However, ore-precipitating fluids can be directly studied by analyzing fluid inclusions in opaque ore minerals that are transparent to near-infrared light, such as enargite (Campbell et al. 1984, Mancano and Campbell 1995).

In this study, we report microthermometric measurements on fluid inclusions in ore minerals (enargite, sphalerite) and adjacent quartz from the Butte district, Montana. At Butte, porphyry Cu-Mo (“pre-Main Stage”) mineralization is cut by large through-going “Main Stage” base-metal vein lodes. The Main Stage mineralization consists of intergrown sulfides (chalcocite, enargite, pyrite, ± bornite, covellite, sphalerite) and gangue minerals (quartz, carbonates). Previous fluid inclusions studies in quartz from Main Stage veins describe CO_2-bearing (0.2 to 1 mol%) liquid-rich fluid inclusions that homogenize to liquid at temperatures between 250° and 300°C, with salinities ranging from 1 to 4 wt% NaCl eq. and some rare vapor-rich fluid inclusions (Rusk et al. 2008).

Microthermometric measurements, using a Linkam FTIR-600 heating-freezing stage mounted on an Olympus BX51 infrared microscope, have been performed on enargite, quartz and sphalerite samples selected from a vertical profile in the Leonard Mine, located in the central Cu(-Ag-Zn)-rich zone of the district. The local paragenetic sequence consists of an early quartz-pyrite (± huebnerite) and enargite stage, which is followed by a Cu-rich event marked by the deposition of a second generation of pyrite, bornite, covellite and various Cu-sulfosalts, crosscut by late sphalerite-galena rhodochrosite veins.

Multiple episodes of quartz precipitation in the Main Stage veins, associated with sulfide formation (enargite, pyrite, covellite and bornite) are highlighted by scanning electron microscope-cathodoluminescence imaging (Figs. 1a-b). *Quartz-I* (light-gray) is affected by dissolution prior to the precipitation of *quartz-II* (low-luminescence), which is paragenetically related to pyrite and enargite deposition. Pseudo-secondary sub-rounded vapor and liquid-rich polyphase fluid inclusions (Figs. 1e-f) constitute a boiling assemblage in *quartz-II* (Fig. 1f) with homogenization temperature (Th) between 270° and 310°C and salinity of 2.4 ± 0.9 wt% NaCl eq. *Quartz-III (dark-gray)*, which exhibits oscillatory growth zoning pattern, is affected by a second stage of dissolution and precedes the latest *quartz-IV* generation (low-luminescent). Primary fluid inclusion assemblages in *quartz-III* (Fig. 1c) consist of liquid-rich inclusions with T_h between 260° and 290°C and low salinity - typically around 1.4 wt% NaCl eq. Late liquid-rich fluid inclusions in *quartz-IV* (Fig. 1c) indicate a slight increase of fluid salinity (3.4 ± 0.8 wt% NaCl eq.). Raman microspectrometry will be performed to determine the nature of the solid phases and the gas composition, as petrographic observations suggest the presence of muscovite (Fig.1e), and anhydrite (Fig. 1f).

Primary fluid inclusions in enargite (Fig. 1h) are liquid-rich, rectangular to tube-like, trapped along growth zones and show similar T_h and salinity to *quartz-II*-hosted fluid inclusions (Fig. 1g). Secondary fluid inclusions in enargite trapped along healed fractures (Fig. 1i) are larger in size, have lower Th (230-250°C) and distinctly higher salinity (5.1 ± 1.2 wt% NaCl eq.). High uncertainties in Th measurements are due to the decrease of the infrared transmittance of enargite at temperatures above 260-270°C. Three primary fluid inclusion assemblages in the late sphalerite (Fig. 1i) contain trapped chalcopyrite and homogenize between 300° and 330°C and have salinity of 4.4 ± 1.3 wt% NaCl eq.

Following the deposition of the enargite-pyrite assemblage at temperatures of 270-310°C from a low-salinity fluid (2.4 ± 0.9 wt% NaCl eq.), a slight decrease in salinity is registered in *quartz-III*-hosted inclusions, whereas secondary fluid inclusions in enargite could indicate later mixing with a cooler fluid of even higher salinity (Fig. 1g). Primary fluid inclusions in sphalerite, which is late in the paragenetic sequence in the Leonard Mine, indicate the incursion of high temperature fluids with similar salinity at the late stage of vein formation. To better understand the fluid evolution and composition within the studied sequence Raman microspectrometry and LA-ICP-MS analyses of fluid inclusions will be performed.

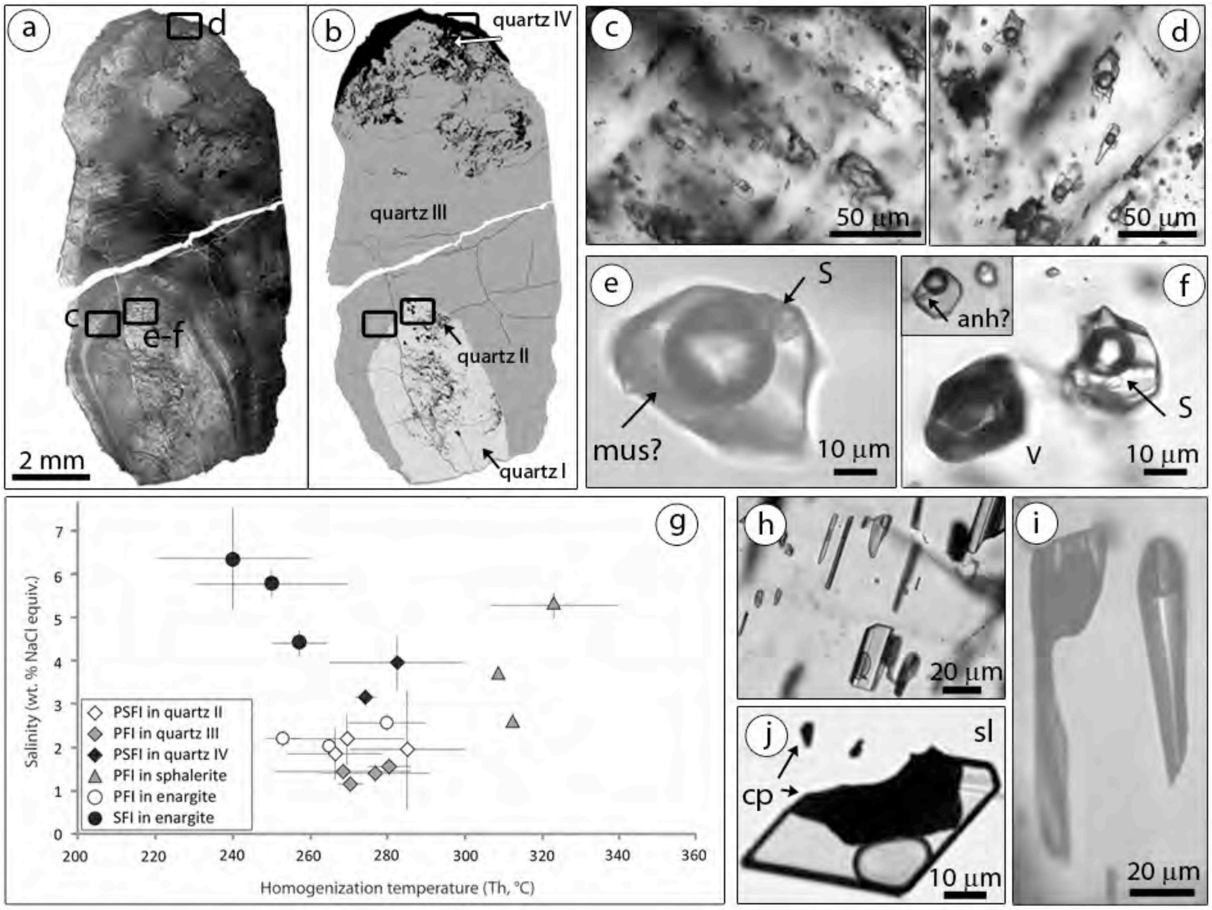

Figure.1 a) SEM-CL image of quartz crystal associated with pyrite and enargite. Black squares locate figures 1c-d-e-f; b) Drawing of the four quartz generations: quartz-I (light-gray) with black quartz-II, quartz-III (gray) late black quartz IV c) Transmitted-light photomicrograph of primary liquid-rich fluid inclusions in quartz-III; d) Transmitted-light photomicrograph of late fluid inclusions related to quartz-IV; e-f) Transmitted-light photomicrograph of vapor and liquid-rich polyphase fluid inclusions related to quartz-II; g) Microthermometric data on 88 single fluid inclusions from 18 FIAs in quartz, enargite and sphalerite. Error bars correspond to the standard deviation within the assemblage; h) Infra-red transmitted-light photomicrograph of primary fluid inclusions in enargite; i) Infra-red transmitted-light photomicrograph of secondary fluid inclusions in enargite; j) Transmitted-light photomicrograph of primary fluid inclusions in sphalerite with trapped chalcopyrite. Abbreviations: PSFI – pseudo-secondary fluid inclusions, PFI – primary fluid inclusions, SFI – secondary fluid inclusions, anh-anhydrite, cp-chalcopyrite, mus-muscovite, s-solid, sl-sphalerite, V-vapor.

Acknowledgements: This study was supported by the Swiss National Science Foundation (grant 20021-127123).

REFERENCES

Campbell, A. R., Hackbarth, C. J., Plumlee, G. S., Petersen, U. (1984) Internal features of ore minerals seen with the infrared microscope. Economic Geology. Vol. 79. 1387-1392.

Mancano, D. P., Campbell, A. R. (1995) Microthermometry of enargite-hosted fluid inclusions from the Lepanto, Philippines, high-sulfidation Cu-Au deposit. Geochimica et Cosmochimica Acta. Vol. 59. 3909-3916.

Rusk, B., Miller, B.J., Reed, M. (2008) Fluid-inclusion evidence for the formation of Main Stage polymetallic base-metal veins, Butte, Montana, USA. *In:* Circum-Pacific tectonics, Geologic Evolution, and Ore Deposits (eds. J.E. Spenser, S.R. Titley). Tucson, Arizona Geological Society. Digest 22. 573-581.

Pan-American Current Research on Fluid Inclusions (PACROFI-XI)
University of Windsor, Windsor, Ontario, Canada, June 18–20, 2012, Abstract Volume

Preliminary petrographic observations on fluid inclusions in the Hoidas Lake REE deposit, Saskatchewan, Canada.

Pandur, K.*, Ansdell, K.*, and Halpin, K.**

**Department of Geological Sciences, University of Saskatchewan, Saskatoon, SK, Canada*
***Great Western Minerals Group, Saskatoon, SK, Canada*

The Hoidas Lake deposit consists of light rare earth element-enriched vein-type mineralization in the Rae Province of northern Saskatchewan, Canada. The deposit is associated with the Hoidas-Nisikkatch fault, which is a splay off the larger Black Bay Fault system. The geology and complex vein paragenesis of the deposit has been described in detail by Halpin (2010). The first vein generation contains allanite, diopside, hornblende, chevkinite, titanite and hyalophane. Later veins are filled with brecciated red apatite, and then green apatite. A late coarse red apatite vein type cross-cuts earlier vein generations. Light rare earth element contents increase from the earliest apatite to the green apatite phase. Chemical composition of the vein minerals suggests that the fluids responsible for the poly-phase hydrothermal events may have been derived from a carbonatitic or alkalic magma source at depth. Hydrothermal alteration of the veins, especially the earlier apatite phases is observed, and quartz, calcite and hematite-rich veins and vugs appear to be the latest stage of hydrothermal activity.

The goal of this on-going research is to unravel the details of the hydrothermal evolution of the deposit by providing constraints on the characteristics of the fluids involved in mineralization. The first step is a fluid inclusion petrographic study of the separate vein types. All observations below are at room temperature.

The diopside-allanite veins do not contain phases transparent enough for study. However, quartz crystals in the immediately adjacent host rocks were studied for secondary fluid inclusion planes that might have formed at the time of early vein formation. The fluid inclusion planes parallel to the diopside-allanite veins mostly contain two-phase H_2O inclusions that have either 80-90 vol. % or 10-20 vol. % vapour. Light green solid inclusions are also very common in planes parallel to the veins.

Apatite crystals were examined in the later vein types. The earliest red apatites contain solid inclusion-rich centers, while their outer zones are inclusion poor. Irregularly shaped or spherulitic Fe-oxide inclusions are the most abundant in the cores of the apatites, along with some light green or transparent solid inclusions, which themselves often contain opaque phases. The fluid inclusions in the red apatite appear mostly in these solid inclusion-rich parts. The majority of these are dark-rimmed one-phase CO_2 inclusions (L_{CO2}), and less commonly two-phase CO_2 inclusions with 10-30 vol. % vapour. The oldest apatite crystals gain their red colour from the abundant Fe-oxide inclusions. In the places, where the alteration is not so strong, these apatite crystals are light green in colour. Two-phase secondary H_2O inclusions with 10-60 vol. % vapour phase are sometimes found around the strongly altered, Fe-oxide rich parts. Some of these fluid inclusions contain Fe-oxides, which are interpreted to have been accidentally trapped from the fluids. The clear rims of the red apatite crystals usually show very few solid and fluid inclusions. Quartz crystals in the matrix of red apatite breccias contain primary fluid inclusions along growth zones and along grain boundaries, and similar fluid inclusions appear in the apatite matrix in these breccias as well. These are mostly dark-rimmed, seemingly one-phase inclusions (V_{H2O} or L_{CO2}), but there are some two-phase H_2O inclusions with 10 vol. % vapour phase or 90 vol. % vapour phase. The quartz crystals also contain spherulitic Fe-oxide inclusions, often oriented into chains. Two-phase H_2O inclusions with varying vapour content (10-90 vol. %) appear near the Fe-oxide inclusions. Poly-phase H_2O inclusions (L_{H2O} + V_{H2O} + halite + opaque) with 20 vol. % vapour are found along secondary planes.

Green apatite crystals are much clearer compared to red apatite, they often contain no solid or fluid inclusions. Sometimes, dark-rimmed liquid CO_2 inclusions, or two-phase CO_2 inclusions with 20-30 vol. % vapour phase appear in them. Green apatite breccias are also affected by Fe-oxide alteration, and two-phase H_2O inclusions with variable vapour content appear near the Fe-oxide-rich parts. Light green or transparent solid inclusions also occur, usually spatially associated with the Fe-oxide inclusions. In the green apatite crystals and clearer outer zones of the red apatite crystals solid inclusions and fluid inclusions are often oriented and exhibit needle-like shapes.

The latest apatite phase consists of coarse red apatite crystals, which also contain a lot of Fe-oxide inclusions, and associated transparent and light green solid inclusions. The inclusions are often oriented and exhibit negative crystal shapes. In comparison with the earlier apatites, these apatites do not appear to contain one-phase CO_2 inclusions. However, irregularly shaped two-phase H_2O inclusions with 10-60 vol. % vapour phase were observed.

A small veinlet in the host granodiorite is filled with quartz and calcite crystals. Its quartz crystals contain several secondary fluid inclusion planes. Two-phase H_2O inclusions with varying amounts of vapour (10-90 vol. %) are present, and sometimes appear to be along the same planes as poly-phase aqueous (L_{H2O} + V_{H2O} + halite) inclusions. CO_2 inclusions are also present, mostly one-phase (L_{CO2}), partly two-phase (L_{CO2} + V_{CO2}) with 10-30 vol. % vapour, and rarely three-phase (L_{H2O} + L_{CO2} + V_{CO2}) with varying phase contents. In some secondary planes, poly-phase H_2O inclusions (L_{H2O} + V_{H2O} + halite) with 20 vol. % vapour and poly-phase CO_2-bearing inclusions (L_{H2O} + L_{CO2} + V_{CO2} ± halite) with varying phase contents appear to coexist.

Preliminary observations indicate that inclusion-rich early red apatite and green apatite might have formed in the presence of CO_2-rich fluids, as opposed to late coarse red apatite. The CO_2-rich fluids were trapped before the hydrothermal alteration that resulted in Fe-oxide precipitation. This later alteration is thought to have formed in the presence of H_2O-rich fluids, as suggested by the occurrence of two-phase H_2O inclusions with variable vapour contents, containing entrapped Fe-oxide in some cases. Quartz crystals in the matrix of the red apatite breccias might have formed partly before and partly during this process, because they also contain aqueous inclusions and Fe-oxide inclusions.

In summary, the earlier REE-bearing apatites seem to have been precipitated from CO_2-rich fluids, while these fluids were not present during the formation of late coarse red apatites. The mineralized veins were affected by later aqueous fluids, which were sometimes of high salinity, and which may have been responsible for Fe-oxide alteration. The fluid inclusion petrographic studies reported here will be followed by microthermometric studies to determine the characteristics of the fluids present during the evolution of the system. This work will provide the framework for later stable and radiogenic isotope analyses to constrain the source and age of the hydrothermal fluids.

This study is supported by funding and scholarships from Natural Science and Engineering Research Council of Canada, Great Western Minerals Group, and the University of Saskatchewan.

REFERENCES

Halpin, K. M. (2010) The characteristics and origin of the Hoidas Lake REE deposit. Unpublished M.Sc. Thesis. University of Saskatchewan. 173 p.

Hydrothermal evolution of the Recsk porphyry Cu ore system, Hungary, based on fluid inclusion studies.

Pandur, K.* and Molnár, F.**

**Department of Geological Sciences, University of Saskatchewan, Saskatoon, SK, Canada*
***Geological Survey of Finland, Espoo, Finland*

The porphyry Cu(-Mo-Au), Cu-Zn-Fe skarn and related epithermal Au deposits of the Recsk Ore Complex in Hungary are hosted by a Late Eocene-Early Oligocene intrusive-volcanic complex. The igneous unit is part of the Paleogene Magmatic Arc of the Alp-Carpathian subduction-collision belt (Molnár, 2007). The presently known reserves of the Cu(-Mo-Au) porphyry ore (109.4 Mt at 0.96% Cu) are located in a small subvolcanic intrusion, 400 m below the present surface. The porphyry stock is flanked by skarn ore zones along its contacts with the Mesozoic basement rocks. This intrusion is the northernmost unit in a series of similar mineralized intrusions in an approximately 10 km long NNE-SSW oriented zone.

Characterization of the vein system, study of wall rock alteration and fluid inclusion studies were carried out along a representative section across the northernmost mineralized intrusion. Observations were made with a special consideration of the relative chronology of veinlets, in order to use their fluid inclusion contents for evaluation of the temporal evolution of the ore forming fluid system. Classification of veinlets was based on the systematics introduced by Sillitoe (2010).

Fluid inclusion studies in the vein-filling minerals led to determination of six distinct fluid inclusion types. Type 1 inclusions show L + V + S1 (± S2) phase compositions, with 20 apparent vol.% vapour phase and halite (± sylvite) at room temperature. Type 2 fluid inclusions show L+V phase compositions, with 80-90 apparent vol.% vapour phase. Homogenization of the type 1 fluid inclusions would have been into the fluid phase at temperatures higher than 450°C, whereas dissolution of the solid phases happened before disappearance of the vapour phase. In the type 1 fluid inclusions, salinities are between 40-55 NaCl equiv. wt.%. Homogenization of type 2 fluid inclusions happened with the disappearance of the liquid phase at temperatures higher than 450°C. Type 1 and type 2 inclusions are syngenetic, because they occur in the same secondary inclusion planes, and they are thought to have been trapped from heterogeneous fluids, after boiling. Type 3 fluid inclusions show L+V phase compositions, with 10-20 apparent vol.% vapour phase, and type 4 fluid inclusions show L+V phase compositions, with 80-90 vol.% vapour phase at room temperature. Type 3 and type 4 fluid inclusions appeared syngenetically in secondary inclusion planes. In type 3 inclusions, homogenization happened with the disappearance of the vapour phase, and homogenization temperatures varied widely (T_h(LV→L) = 160-380°C). Salinities are between 0 and 15 NaCl equiv. wt.%. Type 5 fluid inclusions show L + V phase compositions, with 20-30 apparent vol.% vapour phase at room temperature. They were trapped from homogeneous fluids. They homogenized into the liquid phase, with T_h(LV→L) values between 280 and 340°C and salinities are between 5-6 NaCl equiv. wt.%. Type 6 fluid inclusions also show L + V phase compositions, with 10-20 apparent vol.% vapour phase at room temperature, and were trapped from homogeneous fluids. They homogenized with disappearance of the vapour phase, with T_h(LV→L) values between 110 and 200°C. The salinites are between 5 and 15 NaCl equiv. wt.%.

Cross-cutting relationships of the distinct vein generations show, that A-type quartz veins are the earliest, followed by B-type quartz veins. These are more abundant in the central parts of the intrusion. Younger D-type veins and the youngest C-type veins can mostly be found in the marginal parts of the system. Type 1 and type 2 fluid inclusions were found in quartz crystals of A-type veins as primary and secondary inclusions, while type 3 and type 4 fluid inclusions appear in secondary planes in the quartz of A-type veins, and as primary and secondary inclusions in the quartz of B-type veins. Type 5 fluid inclusions occur related to D-type veins, and the anhydrite and calcite crystals of D- and C-type veins contain primary, secondary and undeterminable type 6 fluid inclusions.

Combination of the homogenization temperature and salinity data shows that during the evolution of hydrothermal fluids, temperature and salinity decreased progressively. Absence of the early EDM- and M-type veins (Sillitoe, 2010) and the earliest one-phase magmatic fluids in the Recsk porphyry system indicates that the earliest stage of hydrothermal alteration took a short time, and boiling of magmatic fluids began relatively early. The earliest observed fluid inclusion assemblage (type 1 and type 2 fluid inclusions) was trapped after boiling of the primary magmatic fluids, displaying both high density and low density fluid inclusions, and A-type veins formed in the presence of these fluids. Fluid inclusions of the second assemblage (type 3 and type 4) were trapped at lower temperature and from lower salinity fluids, and also represent boiling. Multiple events of boiling might have happened due to pressure fluctuations in the system (Burnham, 1997; Fournier, 1999). Another possible way for formation of type 3 and type 4 fluids is condensation of the low density, low salinity vapour phase, separated by the earlier boiling process. B-type quartz veins formed in the presence of type 3 and type 4 fluids. Generally in porphyry Cu systems, the presence of A- and B-type veins and heterogeneous fluid inclusions is closely related to potassic alteration (Sillitoe, 2010). This may be evidence of an early potassic alteration zone in the Recsk diorite intrusion that was later entirely overprinted, as there is no direct textural evidence for it at the present time. Sericitic alteration, dominant in the studied diorite samples can be connected to the opening of the D-type veins. This happened in the presence of homogeneous, low salinity type 5 fluids. Appearance of these fluids in the system indicates that the intrusion cooled down adequately, so that meteoric waters could percolate into it and dilute magmatic fluids (Sillitoe, 2010). Further cooling and dilution by low-salinity fluids changed the composition of fluids, leading to intensive carbonate alteration in the previously sericitized rocks and carbonate precipitation in veins. Anhydrite and calcite filling of the late D- and C-type veins contains type 6 fluid inclusions. These represent a low salinity, homogeneous fluid, almost completely diluted by meteoric waters.

The European Union and the European Social Fund have provided financial support to the project under the grant agreement no. TÁMOP 4.2.1./B-09/KMR-2010-0003.

REFERENCES

Burnham, C. W. (1997) Magmas and Hydrothermal Fluids. *In:* Geochemistry of Hydrothermal Ore Deposits, third edition (ed. H.L. Barnes). John Wiley & Sons Inc., USA. 63-123.

Fournier, R. O. (1999) Hydrothermal Processes Related to Movement of Fluid From Plastic into Brittle Rock in the Magmatic-Epithermal Environment. Economic Geology. Vol. 94. 1193-1211.

Molnár, F. (2007) The Cu-Au-Ag-Zn-Pb ore complex at Recsk: a uniquely preserved and explored porphyry-skarn-epithermal system. Proceedings of the 9th Biannual SGA Meeting, Dublin, Ireland. Vol. 1. 226-240.

Sillitoe, R. H. (2010) Porphyry Copper Systems. Economic Geology. Vol. 105. 3-41.

Analysis of individual hydrocarbon fluid inclusions by femtosecond laser ablation and time of flight secondary ion mass spectrometry (ToF-SIMS).

Pottorf, R.J.*, Dreyfus, S.*, Siljeström, S.**, Pecheyran, C.***, Catalayud, B.***, Phan, N.*,
Madincea, M.*, and Reynolds, T.J.****

**ExxonMobil Upstream Research, Houston, U.S.A.*
***SP Technical Research Institute of Sweden, Boraas, Sweden*
****IPREM Laboratoire de Chimie Analytique Bio-Inorganique et Environment, UMR 5254, Pau, France*
*****FLUID INC., Denver, U.S.A.*

Femtosecond Laser Ablation

Recent advances in laser technology have led to ultrashort laser pulses capable of selectively opening and liberating oil within individual petroleum inclusions. Coupling of an on-line femtosecond laser to a gas chromatograph-mass spectrometer successfully analysed hydrocarbon compounds from individual inclusions (Volk et al, 2010), but C_{19+} compounds, including biomarkers, were undetected and potentially remained in the ablation chamber or in the transfer line. To test this hypothesis, well-characterized crude oil samples were ablated for different laser conditions, and the products were collected on Teflon filters placed at the exit of the ablation chamber. Filter extracts were then analysed by GCxGC-ToFMS. Data obtained from the extracted filters showed the presence of unaltered C_{12+} compounds including biomarkers. The success of the femtosecond technique as a sampling tool for biomarker analysis of crude oils was extended to the analysis of individual HC inclusions.

ToF-SIMS

ToF-SIMS technology has been used to detect hopanes and steranes in single oil-bearing fluid inclusions (Siljeström et al, 2010). Standard oil suites were used to calibrate the ToF-SIMS instrument for various hydrocarbon source rock facies allowing the determination of the origin of oils trapped in inclusions within the Elk Basin Field, Big Horn Basin, WY. The oils appear to be derived from a distal carbonate source (Phosphoria Formation) supporting long distance, lateral migration into the Big Horn Basin Fields from a mature Phosphoria source rock ~65-120 Ma.

REFERENCES

Siljeström, S., Lausmaa, J., Sjövall, P., Broman, C., Thiel, V., Hode, T. (2010) Analysis of hopanes and steranes in single oil-bearing fluid inclusions using time-of-flight secondary ion mass spectrometry (ToF-SIMS). Geobiology. Vol. 8. 37-44.

Volk, H., Fuentes, D., Fuerbach, A., Miese, C., Koehler, W., Barsch, N., Barcikowski, S. (2010) First on-line analysis of petroleum from single inclusion using ultrafast laser ablation. Organic Geochemistry. Vol. 41. 74-77.

Long-term adakite generation and no evidence for magma mixing at Mount St. Helens based on melt inclusion analyses.

Severs, M. S.*, Gryger, K. J.*, Makin, S.*, Fedele, L.**, Bodnar, R.J.**, and Bradford, W.*

**Environmental Science and Geology Program, Richard Stockton College of New Jersey, Galloway, NJ, U.S.A.*
***Department of Geosciences, Virginia Tech, Blacksburg VA, U.S.A.*

Adakites are unusual intermediate-felsic volcanic rocks that have traditionally been hypothesized to form by melting of a subducting mafic slab. However, as a class of rocks they are clouded by what geochemical characteristics are required to be called "adakites", as well as whether the term should refer only to rocks that may be produced by subducting slab melting or whether it can include generation by other petrogenetic mechanisms, such as melting of the underplated mafic crust. Adakites have similar geochemical characteristics to the tonalite-trondjhemite-granodiorite (TTG) suite that composes a large percentage of Archean continental crust (e.g., Martin et al., 2005). As such, they have been proposed to be modern analogues for how the TTG-suite formed, and hence, how early plate tectonics functioned. Although highly debated, several authors (e.g., Sajona and Maury, 1998) have also hypothesized that adakites may be related to Cu-Au ore deposits. Recent geochemical evidence has cast doubt upon whether adakites are slab melts (e.g., Dreher et al., 2005) and have suggested "low-silica" adakites (high-Mg andesites) may form by mixing two or more silicate melts (Streck et al., 2007). Additionally, the length of time adakites are generated and how (or if?) they transition into or from calc-alkaline non-adakitic magma is also uncertain.

This project aims at addressing these two questions by examining the previously-identified adakite location at Mount St. Helens (MSH; Defant and Drummond, 1993). MSH is an ideal location to investigate both of these questions because of the well-constrained eruptive history (e.g., Mullineaux, 1996) and its proximity in the Cascades to Mt. Shasta where magma mixing was invoked as a dominant magmatic process (Streck et al., 2007). Samples were collected from each of the eruptive units and processed to release individual phenocrysts. Melt inclusions (MI) were found in over 60% of the phenocrysts and were present in each sample. MI ranged from completely glassy (± bubble) to slightly devitrified brownish glass (± bubble). Samples containing unhomogenized MI were placed into a box furnace and homogenized over 12-24 hour time increments, with homogenization temperatures ranging from 975 to 1050°C. MI were geochemically analyzed by laser ablation-inductively coupled plasma mass spectrometry (LA-ICPMS). Additionally, phenocrysts were examined by electron microprobe (EPMA) to investigate the nature of any chemical zonation present.

The geochemistry of the samples suggests several important observations. First, all of the eruptive units at MSH display some adakitic characteristics including: ≥60.0 wt% SiO_2, Sr contents between 400-1100 ppm, high Sr/Y ratios, high La/Yb ratios, and low heavy rare earth element abundances (Fig. 1). The oldest eruptive units, Ape Canyon and Cougar stages, have the most pronounced of these characteristics. Previous authors (Defant and Drummond, 1993; Smith and Leeman 1987) had only identified the Kalama, Smith Creek, and Swift Creek stages as being adakitic in character. Second, MI within each eruptive units define strong linear to curved trends in major elements, suggesting that crystal fractionation is the dominant process. No MI with significantly different major or trace element compositions were found. This argues against magma mixing playing a significant role. Additionally, EPMA chemical zonation maps of plagioclase phenocrysts do not show major changes in composition indicative of new pulses of magma injection. Phenocrysts typically display oscillatory normal zonation with an average core composition of An_{64} and an average rim composition of An_{54}. Some crystals have elliptical, complex cores, which are suggestive of a xenocrystic origin.

The results from this study indicate that magma mixing is not a significant process in the generation of adakites and that the variability seen in their major elements is due to fractional crystallization of predominantly pyroxene, amphibole, and plagioclase. MSH has produced adakites from the beginning of its eruptive period and also across several stages of dormancy. This suggests that the mechanism of adakite generation is something that is taking place over an extended period, and slab melting fits this model of generation better than the alternatives of either melting of underplated mafic crust or complex crustal mixtures. At MSH, slab melting occurs because the subducting slab is both young and hot and its proximity to the Columbia River Embayment also favour a warmer subduction zone in contrast to the Cascades north or south of this area.

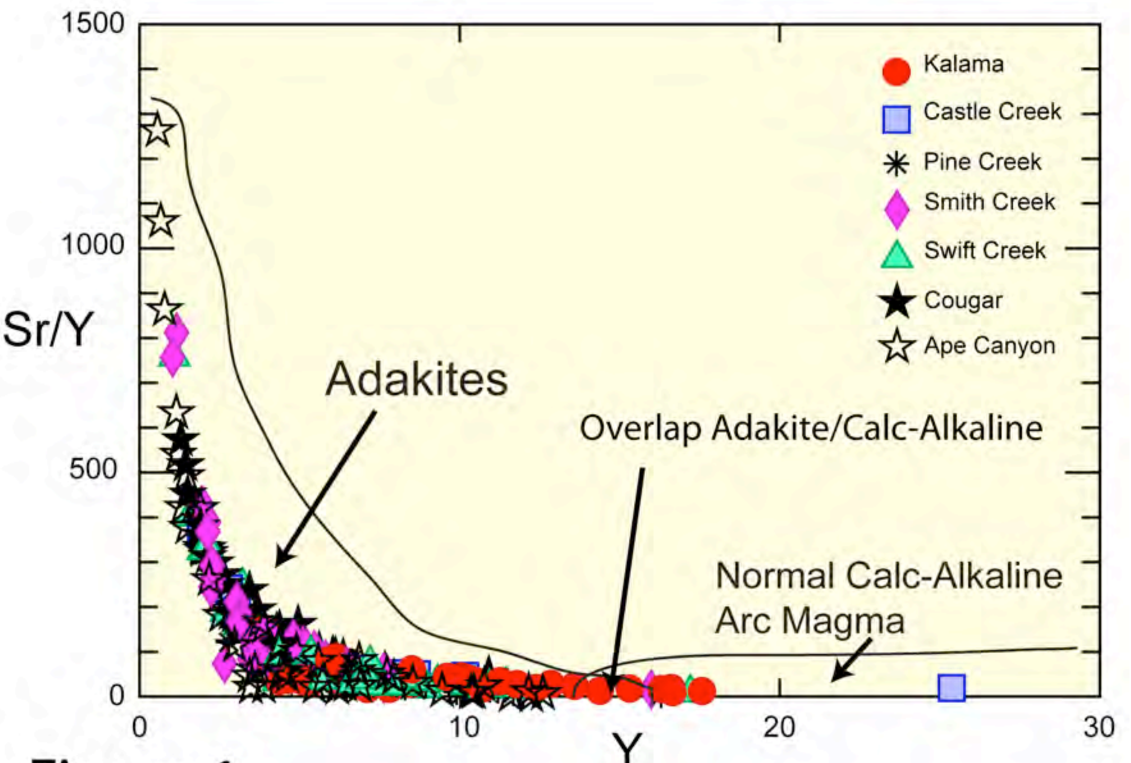

Figure 1

REFERENCES

Defant, M. J., Drummond, M. S. (1993) Mount St. Helens: Potential example of partial melting of the subducted lithosphere in a volcanic arc. Geology. Vol. 21. 547-550.

Martin, H., Smithies, R. H., Rapp, R., Moyen, J.-F., Champion, D. (2005) An overview of adakite, tonalite-trondhjemite-granodiorite (TTG), and sanukitoid: Relationships and some implications for crustal evolution. Lithos. Vol. 79. 1-24.

Mullineaux, D. R. (1996) Pre-1980 tephra-fall deposits erupted from Mount St. Helens, Washington. USGS Professional Paper. Vol. 1563. 99p.

Sajona, F. G., Maury, R. C. (1998) Association of adakites with gold and copper mineralization in the Philippines. Academie des Sciences Comptes Rendus, ser. II: Sciences de la Terre et des Planetes. Vol. 326. 27-34.

Smith, D. R., Leeman, W. P. (1987) Petrogenesis of Mount St. Helens dacitic magmas. Journal of Geophysical Research. Vol. 92. 10313-10334.

Streck, M. J., Leeman, W., Chesley, J. (2007) High-magnesian andesite from Mount Shasta: a product of magma mixing and contamination, not a primitive mantle melt. Geology. Vol. 35. 351-354.

Experimental insights into the variability of ore metal ratios in magmatic-hydrothermal systems.

Simon, A.

Department of Geoscience, University of Nevada Las Vegas, Las Vegas, NV, U.S.A.

Porphyry-type ore deposits are important sources of Cu, Au, Mo and Ag, accounting, respectively, for 57%, 9%, 99% and 13% of the total discovered quantity of each metal (Singer, 1995). There seems to be broad consensus that porphyry deposits are the result of a seemingly simple recipe with the following steps: 1) mantle-derived silicate melt(s) ponds in the shallow crust; 2) silicate melt(s) exsolves a volatile phase owing to decompression and/or crystallization; 3) metals are transferred from the melt and crystals to the volatile phase; 4) the volatile phase ascends and escapes the parent magma chamber; 5) metals precipitate from the volatile phase as it cools, decompresses and reacts with rocks above the magma chamber. This recipe is not new. Lindgren (1905) postulated the basic aspects of this recipe more than one hundred years ago, and since then, geologists have come to recognize that despite significant commonalities, there is significant variability with respect to both the total metal endowment and the ratio of ore metals among porphyry ore deposits.

A global analysis of porphyry deposits indicates that the abundances of Cu and Au range from approximately 0.1 to 1 wt. % and 0.001 to 1 ppm, respectively. These data indicate that Cu is elevated by as much as 100 times, and Au by as much as 1000 times, the typical concentrations of these metals in continental crust. These data also indicate that while the concentration of Cu in porphyry deposits is relatively constant, the concentration of Au varies by three orders of magnitude. Closer scrutiny of the global data set also indicates that some porphyry deposits are essentially devoid of Au and others are Au-rich and lack Cu, at least in economic terms. So what causes this variability in the ratio of Cu to Au among porphyry deposits? Is the variability caused by subtle changes to one step of the master recipe given above?

To answer these questions, geologists have increasingly turned to experimental petrology to explore the behaviour of Cu and Au, and other ore metals, at the pressure-temperature-composition conditions that exist throughout the entire continuum of magmatic-hydrothermal systems, from the source of metals, i.e., the upper mantle, to the shallow crust where the metals are mined.

If we start with step one of the recipe, observations of porphyry systems indicate that the parental melts range in composition from andesite to rhyolite (Seedorff et al., 2005; Sillitoe, 2010). Gold-only porphyries are commonly associated with mafic and/or alkaline intrusions, and Cu-Au porphyries are commonly associated with a more diverse range of intermediate to felsic magmas. Thus, metal abundances and metal ratios appear to be at least somewhat related to the composition of the parent magma. Recent experimental data from Li and Audétat (2012) indicate that the metal content of primitive arc magmas depends on the abundance and type of sulphide in the mantle source. They reported that Cu and Au are favourably hosted by both monosulfide solid solution (Mss) and sulphide liquid. However, the sulphide melt / silicate melt partition coefficient for Au is much higher than for Cu, which results in a greater enrichment of Au in the sulphide melt during partial melting. This observation provides a mechanism for the fractionation of Cu from Au during partial melting in the magma source and is consistent with the hypothesis put forth by Richards (2009) that two-stage partial melting results first in Cu-rich silicate melts and second in Au-rich silicate melts.

Step two of the porphyry recipe has been investigated by interrogating fluid and melt inclusions in both porphyry host rocks and plutonic rocks that are thought to represent the root zones of eroded porphyry systems, and by performing experiments to quantify the chemistry of aqueous fluid at conditions that extend from the depositional environment to those in the parent magma (Bodnar et al., 1985; Williams-Jones and Heinrich, 2005; Simon and Ripley, 2011). The chemistry of the inclusions that were trapped at magmatic conditions indicates that porphyry ore fluids in economic deposits were dominantly of low to moderate salinity (~2 to 10 wt. % NaCl eq.) and sulphur bearing (Shinohara, 1994; Webster, 1997; Williams-Jones and Heinrich, 2005).

Step three has been investigated by measuring element abundances in fluid and melt inclusions, which were trapped at magmatic conditions, and by performing experiments to assess the roles of intrinsic and extrinsic variables on the mass transfer of ore metals from silicate melt to aqueous fluid. Published experimental data suggest that oxygen fugacity (fO2) and the abundances of Cl and S in the ore fluid and coexisting silicate melt are master controls on this mass transfer process (Simon and Ripley, 2011; Zajacz et al., 2011, 2012). At fO2 < NNO+1, Cu is retained by intermediate silicate melts (i.e., $D_{Cu}^{fluid/melt} < 2$), whereas Au is strongly partitioned to the ore fluid (i.e., $D_{Au}^{fluid/melt} = 200$). The value of $D_{Au}^{fluid/melt}$ decreases significantly at fO2 > NNO+1 in intermediate melt assemblages, and $D_{Cu}^{fluid/melt}$ increases significantly in felsic assemblages.

Step four has been investigated by studying miarolitic cavities in plutonic rocks (Candela and Blevin, 1995), by computational simulations (Huber et al., 2012), and by applying knowledge of the physics of brittle-ductile transitions to magma chambers (Fournier, 1999). New data indicate that the formation of permeable pathways for the ascent of ore fluid through the parent magma is maximized at crystallinities of ≥ 50 – 60 vol.%, at which stage the advective transport of ore metals from melt to the ore fluid is increased by several orders of magnitude relative to degassing at higher melt fractions. This new finding is counter to the hypothesis that early formation of a volatile phase, at low crystallinities, is critical for the formation of a porphyry deposit.

Step five has been assessed by interpreting the chemical composition of pre-, syn- and post-ore stage fluid inclusions with deference to experimental data to asses the behaviour of Cu and Au during cooling and water rock reaction. The results, albeit limited, indicate that Cu and Au exhibit similar behaviour in ore fluids at this stage. Thus, the primary cause for the fractionation of Cu from Au must be at the magmatic stage(s) of the evolution of a porphyry ore system.

Experimental data are a key ingredient to our ability to evaluate all steps of the porphyry recipe, from the mantle source to the shallow crust. In this talk, I will present and discuss experimental data in the context of the evolution of porphyry ore deposits, with particular regard to the processes that affect ore metal ratios.

REFERENCES

Candela, P.A. and Blevin, P.L. (1995) Do some miarolitic granites preserve evidence of magmatic volatile phase permeability? Economic Geology. Vol. 90. 2310-2316.

Fournier, R.O. (1999) Hydrothermal processes related to movement of fluid from plastic into brittle rock in the magmatic-epithermal environment. Economic Geology. Vol. 94. 1193-1211.

Huber, C., Bachmann, O., Vigneresse, J-L., Dufek, J., Parmigiana, A. (*In press)* Metals extraction and transport in shallow magmatic systems. G-Cubed.

Li, Y., Audétat, A. (*Submitted*) Partitioning of ore metals between sulfide phases and silicate melt under upper mantle conditions.

Lindgren, W. (1905) The copper deposits of the Clifton-Morenci district, Arizona: U.S. Geological Survey Professional Paper. Vol. 43. 375p.

Seedorff, E., Dilles, J.H., Proffett, J.M.J., Einaudi, M.T., Zurcher, L., Stavast, W.J.A., Johnson, D.A., Barton, M.C. (2005) Porphyry deposits: characteristics and origin of hypogene features. Economic Geology 100th anniversary volume. 251-298.

Singer, D.A. (1995) World class base and precious metal deposits; a quantitative analysis. Economic Geology. Vol. 90. 88-104.

Simon A.C., Ripley, E.M. (2011) The role of magmatic sulfur in the formation of ore deposits. *In:* Sulfur in magmas and melts: its importance for natural and technical processes (eds. H. Behrens, J.D. Webster). Reviews in Mineralogy and Geochemistry. Vol. 73. 513-578.

Webster, J.D. (1997) Exsolution of magmatic volatile phases from Cl-enriched mineralizing granitic magmas and implication for ore metal transport. Geochimica et Cosmochimica Acta. Vol. 61. 1017-1029.

Williams-Jones, A.E., Heinrich, C.A. (2005) Vapor transport of metals and the formation of magmatic-hydrothermal ore deposits. Economic Geology. Vol. 100. 1287-1312.

The chemistry of fluid inclusions from the Waiorongomai epithermal Au-Ag vein deposit, Hauraki goldfield, New Zealand.

Simpson, M. P.*, Mauk, J. L.*, and Bodnar, R. J.**

**School of Environment, University of Auckland, Auckland, New Zealand, ma.simpson@auckland.ac.nz.*
***Fluids Research Laboratory, Virginia Tech, Blacksburg, VA, U.S.A.*

The Buck Reef at the Waiorongomai epithermal Au-Ag deposit in the Hauraki goldfield, New Zealand has an exceptional strike length of 3.2 km, but is essentially barren (<0.2 g/t Au). Minor historic production totals 28,453 oz Au and 40,478 oz Ag and is restricted to small ore shoots (<50 m in length) from the New Find, Colonist, and Premier sections of the Buck Reef at its junction with smaller splay veins. The Buck Reef consists of near vertical sheeted and interconnecting quartz veins (0.1 to 10 m wide) and quartz-cemented breccias composed predominantly of massive to coarsely crystalline and vuggy quartz. Splay veins also have brecciated fragments and thin bands of sphalerite with galena, chalcopyrite, pyrite, minor tetrahedrite and electrum. Fluid inclusions from the Buck Reef were studied by microthermometry and laser ablation-inductively coupled plasma-mass spectrometry (LA-ICP-MS) to determine the temperature, apparent salinity and composition of individual inclusions in order to characterise the composition of trapped fluids and to provide insight as to why this vein is poorly mineralized.

Most fluid inclusions studied are hosted in quartz with those in a single sample of sphalerite also measured. Four fluid inclusions types are distinguished based on phase relationships at room temperature: 1) two-phase liquid-rich (liquid + vapor), 2) two-phase liquid-rich with included mineral grains of clay and/or calcite, 3) two-phase vapor-rich and 4) single-phase vapor-only. The two-phase inclusions with included mineral grains of clay are relatively common, although not all inclusions in a fluid inclusion assemblage (FIA) contain this mineral. The main clay based on K and Al responses in LA-ICP-MS profiles appears to be illite. However in some inclusions the clay minerals gave a Ca and Al response and these may be smectite. Rare vapor-rich inclusions that occur with liquid-rich inclusions were likely trapped under boiling conditions.

Microthermometric measurements were made on liquid-rich inclusions with the homogenization (T_h) and final ice melting temperatures (T_m) determined for 716 and 249 fluid inclusions, respectively. Several FIAs were measured in each sample and these show overlapping T_h values for primary, pseudosecondary and secondary fluid inclusions, and also for liquid-rich and liquid-rich inclusions with included mineral grains. The T_h values range from 195° to 298°C, although narrower ranges are associated with different section of the Buck Reef: Buck Rock (214° to 241°C), New Find (~227° to 281°C), Colonist (~241° to 281°), and Premier (238° to 260°C). Cooler temperatures are recorded for the Buck Rock section, which is located 1.4 km south of the New Find, Colonist and Premier sections that occur at similar elevations. Individual FIAs have narrower T_h ranges that are typically less than 20°C. The T_h ranges for quartz and sphalerite from the Hero splay vein are essentially identical at 238° to 270°C (ave. 251°C) and 232° to 263°C (ave. 246°C), respectively. Collectively the fluid inclusions have trapped dilute fluids with less than 3.4 weight percent NaCl equivalent. Detailed analyses of individual samples reveal that some show variations in apparent salinity among FIAs. For example, a quartz crystal from the Colonist Loop vein has four pseudosecondary FIAs with salinity ranges of 1.7 to 2.4, 0.2 to 0.4, 3.2 to 3.4 and 1.9 to 2.1 weight percent NaCl equivalent and two large isolated suspected primary inclusions with salinities of 0.2 weight percent NaCl equivalent. While these differences do not appear vastly different based on the bulk salinity, the Na content for each FIA determined by LA-ICP-MS can differ by an order of magnitude, as described below.

Microanalysis by LA-ICP-MS was carried out on over 200 liquid-rich inclusions and was biased towards relatively large inclusions (10 to 50 microns), because these contained greater amounts of liquid that produced better signals. For all inclusions, Na, Li, Mg, Al, Si, K, Ca, Mn, Fe, Cu, Zn, As, Se, Rb, Sr, Ag, Sb, Te, Ba, Au, Tl and Pb (n=22) were measured using a dwell time of 10 milliseconds; except for Au, which was scanned for 40 milliseconds. Signal integrations and element concentration calculations were made using Analysis Management System software. Elements commonly detected in the host quartz include Li, Al, Sb and minor Ba. Elevated concentrations of Na appear in several quartz samples and may be due to intra-crystalline water. Elements detected in fluid inclusions include Na, K, Ca, Sb, As, minor Sr, Rb, Ba and rare Li and Al (Table 1). Concentrations of the other elements are below or near the limit of detection. All inclusion fluids have Na with many containing K, and a lesser number Ca in decreasing concentrations; those with elevated K and Ca generally contain trace amounts of Rb and Sr. Antimony is the second most common element and ranges in concentration from 0.9 to 1,124 ppm. However, the absolute concentration of Sb in the inclusion fluids is difficult to quantify because Sb is commonly incorporated into quartz. Where quartz lacks Sb, the inclusion fluids contain up to 113 ppm Sb. Arsenic is detected in fewer inclusions and in concentrations up to 166 ppm. Most inclusions that contain As also have more enriched concentrations of Sb, but rare FIA have more enriched concentrations of As than Sb. Detailed analyses of several FIA in a single quartz crystal from the Colonist Loop vein reveal trapped fluids with different element constitutions and concentrations (Table 2). Both FIA_1 and FIA_5 contain Na, K, Rb, Ba, Li and rarely Sb, however FIA_1, which has a slightly lower salinity, also contains Ca and As. In contrast, Na is the only cation that can be detected in FIA_3 and FIA_4, although these inclusions have very low salinities, which may impact the number of elements detected. In sphalerite the main elements detected are Zn, Fe and Mn together with more variable Cu, Pb and Ag. Fluids in the inclusions contain Na, K, Ca and Sb; the latter up to 217 ppm.

Gold and Ag are below the detection limit (ppm level) in the liquid of pseudosecondary and secondary fluid inclusions in late crystalline quartz from the Buck Reef, although this does not preclude their presence at the ppb level. On the one hand, the general lack of Au in veins may indicate that the parent fluid had low Au concentrations. On the other hand, the general lack of minerals and textures indicative of boiling (vein adularia, platy calcite and pseudomorphed equivalent, widespread replacement adularia) suggests restricted fluid flow and only localised boiling conditions conducive for Au deposition. Detailed microthermometric measurement of different FIA in some individual crystals reveals the trapping of fluids with different suites of elements and different element concentrations. While some variability can potentially be attributed to boiling resulting in element concentration or mixing resulting in dilution, the presence or absence of some elements (i.e. Ca) can only be attributed to different fluid compositions that could be due to the trapping of different fluid pulses.

Table 1. Summary LA-ICP-MS results with minimum and maximum element concentrations for fluid inclusions in quartz and sphalerite from the Buck Reef and adjacent splay veins, Waiorongomai deposit.

Sample	Vein	Mineral	Elements in host	Elements in fluid inclusions (ppm)							
				Na	K	Ca	Rb	Sr	Ba	As	Sb
W002 plate 1a	Buck Reef- Buck rock	Quartz	Li, Al, Sb	1,092 to 3,423	212 to 551	-	-	3.74 to 12.7	0.39 to 1.68	-	36.5 to 198
W003	Pride of the South vein	Quartz	Li, Al, Sb	983 to 2,660	30 to 31	14 to 37	-	-	-	13.1 to 33.0	34.9 to 129
W012 plate 2	Buck Reef- New Find	Quartz	Li, Al	444 to 4,656	78 to 1,361	12 to 577	2.34 to 6.65	0.14 to 15.4	0.11 to 16.2	13.1 to 23.1	0.9 to 52
W013 plate 1a	Buck Reef- New Find	Quartz	Local Al	762 to 2,717	291 to 847	49 to 482	9.49 to 38.4	1.00 to 42.2	0.87 to 10.3	-	13.8 to 195
W013 plate 1b	Buck Reef- New Find	Quartz	Local Sb	366 to 2,118	-	49 to 76	-	-	-	-	32.2 to 62
W016 plate 3	Hero vein	Sphalerite	Zn, Fe, Mn, Cu, Pb, Ag	1,991 to 3,166	427 to 454	148 to 251	-	3.44 to 3.47	-	-	45.8 to 217
W016 plate 4	Hero vein	Quartz	Li, Al, Sb, (Na)	623 to 3,101	110 to 593	34 to 99	-	0.79 to 5.27	0.31 to 5.15	27.7 to 167	68.1 to 1,124
W017 plate 1	Buck Reef- Colonist	Quartz	Li, Al, Sb, Ba, (Na)	1,250 to 3,256	42 to 2,061	8 to 78	-	0.47 to 4.06	0.12 to 8.67	14.6 to 37.0	9.2 to 188
W018 plate 2	Buck Reef- Colonist	Quartz	Li, Al, Sb, Ba, (Na)	1.053 to 6,141	317 to 501	191 to 517	-	0.26 to 2.04	6.03 to 8.67	36.2 to 132	330.8 to 466
W019 plate 1	Colonist Loop vein	Quartz	Li, Al, Sb, Ba, (Na)	1,166 to 6,048	245 to 863	43 to 60	-	0.87 to 4.31	4.38 to 35.8	32.7 to 157	34.2 to 450
W019 plate 2	Colonist Loop vein	Quartz	Local Al	490 to 9,200	83 to 4,170	245 to 577	9.17 to 44.7	21.5 to 44.7	0.10 to 2.44	8.6 to 58.2	1.2 to 27.9
W020 plate 1	Buck Reef- Premier	Quartz	Li, Al, (Sb)	404 to 2,659	27 to 348	13 to 61	-	-	0.17 to 3.83	2.1 to 16.6	3.5 to 83

Table 2. Summary LA-ICP-MS results for FIA in a single quartz crystal from the Colonist Loop vein.

Sample	FIA	Salinity	Elements in fluid inclusions (ppm)								
		(wt. % NaCl)	Li	Na	K	Ca	Rb	Sr	Ba	As	Sb
W019 plate 2	FIA_1	1.7 to 2.4	72 to 141	4,830 to 7,468	602 to 1,428	245 to 577	9.17 to 13.6	2.15 to 13.6	0.10 to 2.4	22.8 to 58.2	1.19 to 7.8
	FIA_3	0.2	-	505	137	-	-	-	-	-	-
	FIA_4	0.2 to 0.4	-	490 to 1,292	83 (n=1)	-	-	-	-	-	-
	FIA_5	3.2 to 3.4	195 to 254	8,590, 9,200	3,024 to 4,170	-	21.6 to 44.7	-	0.94 to 2.4	8.6 (n=1)	16.8 to 27.9

Petrography of fluid inclusions from the Marathon Cu-Pd deposit: the role of hydrothermal fluids in mineralization.

Smoke, R.P.S.*, Linnen R.*, Corcoran, P.*, Samson, I.**, Shahabi-Far, M.**, Good, D.***, and Ames, D.****

**Western University, London, ON, Canada*
***University of Windsor, Windsor, ON, Canada*
****Stillwater Canada Inc., Thunder Bay, ON, Canada*
*****Geological Survey of Canada, Ottawa, ON, Canada*

The Marathon Cu-Pd deposit is hosted by the Two Duck Lake Gabbro, which has intruded the Eastern Gabbro of the Mesoproterozoic Coldwell Complex. There is controversy as to whether the deposit formed from strictly magmatic processes or if hydrothermal fluids played a part in mineralization. Knowledge of the timing of fluid infiltration, the composition of the fluids that were present, and at the pressure and temperature at the time of mineralization will provide important information about how the deposit formed. Fluid inclusion analysis is one of the direct methods to do this.

In order to ascertain what fluids were present at the time of mineralization, a timing sequence of the fluid inclusions in relation to the mineralization event must be determined. Apatite is a useful host mineral because: it is hard and refractory, which decreases the chance of post entrapment modification; it is common throughout the deposit; and chlorapatite and fluorapatite are known to form under different conditions. Chlorapatite is typically formed from aqueous fluids and fluorapatite is magmatic. Petrographic microscopy, cathodoluminescence (CL) spectroscopy and microscopy, and scanning electron microscopy (SEM) in conjunction with energy dispersive spectroscopy (EDS) were used to establish phases of apatite, fluid inclusion types, their relationship with chlorapatites versus fluorapatites, and ultimately with sulphide mineralization events.

Fluid inclusion petrography was completed on ten samples from three zones in the deposit; the W-Horizon, the Main Zone, and the Footwall Zone (Fig. 1). The W-Horizon contains early fluorapatite and chlorapatite, the Main Zone contains early and secondary chlorapatite; and the Basal Zone contains primary chlorapatite and fluorapatite. Six fluid inclusion types are present: 1) vapour (V); 2) liquid-vapour (LV); 3) liquid-solid (LS); 4) liquid-vapour-solid (LVS); 5) liquid-only (L); and 6) an indeterminate type that is either LS or melt inclusions. What makes type 6 significant is that the solid within these inclusions is chalcopyrite. Most are secondary with the exception of some rare primary type 2, and psudosecondary type 1 and 2 inclusions. Type 1 and 2 inclusions commonly occur in the same plane. In several examples of both fluorapatite and chlorapatite, secondary type 1 and 2, or type 2 inclusions occur in the same plane as chalcopyrite. This is significant because platinum group minerals are commonly found within chalcopyrite. There is no variation in the chlorine and fluorine composition of apatites within each thin section, with only one exception. In one sample from the Footwall Zone, areas of relatively higher chlorine concentration in chlorapatites are associated with increased fluid inclusion abundance, and where chalcopyrite occurs in the same trace as the fluid inclusions. This relationship was used to assign a psuedosecondary origin for these type 1 and 2 inclusions.

This study is distinctive in that there is a common association of fluid inclusions with chalcopyrite mineralization, which may aid in constraining the timing of these fluid inclusions to the PGE mineralization event. This will be dependent on, and future studies will establish, whether there are any PGM in the sulphides. Microthermometry and other types of analyses, including Raman spectroscopy, are planned to determine whether the coeval existence of V and LV inclusions represent fluid immiscibility and to determine the composition of the inclusions, as well as the pressure and temperature conditions at the time of entrapment.

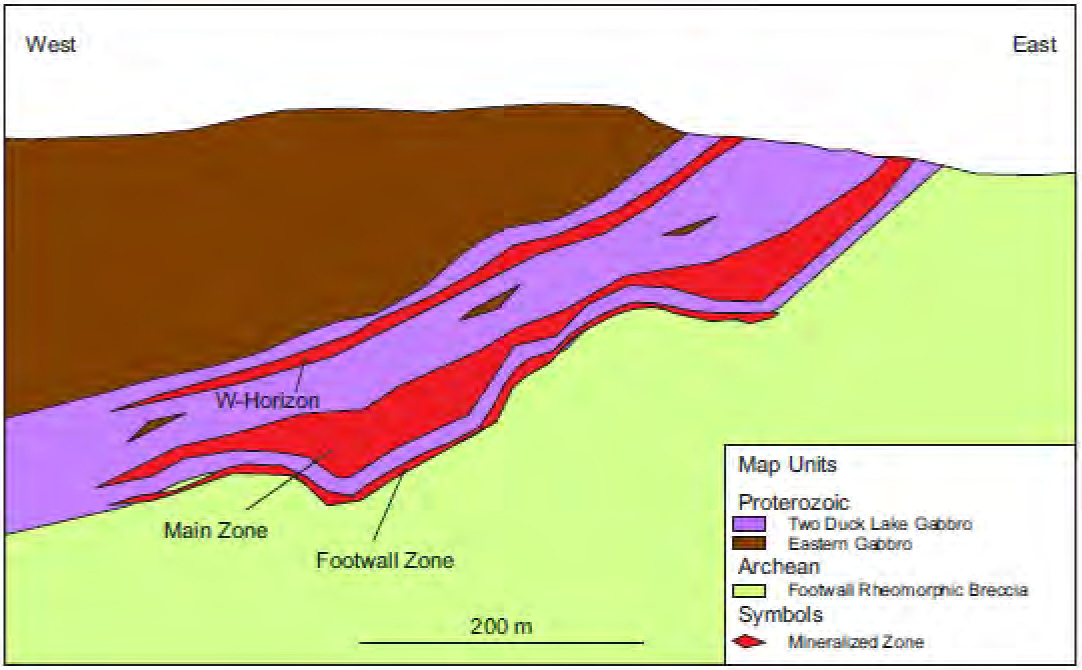

Figure 1. Generalized cross section showing the major mineralized zones of the Marathon Cu Pd deposit. (Ruthart, MSc thesis, 2012).

REFERENCES

Balhaus, C. G., Stumfl, E. F. (1986) Sulfide and platinum mineralization in the Merensky Reef: evidence from hydrous silicates and fluid inclusions. Contributions to Mineralogy and Petrology. Vol. 94. 193-204.

Boudreau, A. E. (1992) Chlorine as an exploration guide for the platinum-group elements in layered intrusions. Journal of Geochemical Exploration. Vol. 48. 21-37.

Good, D., Crocket, J.H. (1994) Genesis of the Marathon Cu-Platinum-Group Element Deposit, Port Coldwell Alkalic Complex, Ontario: A Midcontinent Rift-Related Magmatic Sulphide Deposit. Economic Geology. Vol. 89. 131-149.

Puritch, E.J., Orava, D., Armstrong, T., Yassa, A., Gowans, R., Wislesky, I., Jacobs, C. (2009) Technical report on the updated mineral resource estimate and feasibility study for the Marathon PGM-Cu project, Marathon, Ontario, Canada, Micon International Limited. 225p.

Watkinson, D.H., Ohnenstetter, D. (1992) Hydrothermal origin of platinum-group mineralization in the Two Duck Lake Intrusion, Coldwell Complex, Northwestern Ontario. Canadian Mineralogist. Vol. 30. 121-136.

The numerical tool HOKIEFLINCS_H2O-NACL and its application in interpreting H_2O–NaCl fluid inclusion microthermometric data.

Steele-MacInnis, M., Lecumberri-Sanchez, P., and Bodnar, R.J.

Department of Geosciences, Virginia Tech, Blacksburg, VA, U.S.A.

HOKIEFLINCS_H2O-NACL is a new spreadsheet-style application based in Microsoft Excel, designed to interpret microthermometric data from H_2O-NaCl fluid inclusions (Steele-MacInnis et al., in press). The numerical tool comprises a collection of published models which together fully characterize H_2O-NaCl fluid inclusion properties over the *PVTX* range relevant to hydrothermal systems. HOKIEFLINCS_H2O-NACL estimates fluid inclusion properties based on the temperature of dissolution of the last solid phase, T_m, and the liquid-vapor homogenization temperature, T_h, obtained during microthermometry. The program calculates fluid density and salinity, and estimates the slope of the isochore of the inclusion, allowing the user to calculate a pressure correction. The program is designed such that the user can quickly and easily reduce large datasets.

The program HOKIEFLINCS_H2O-NACL represents a single comprehensive spreadsheet tool combining available numerical models into a single format. Depending on the mode of homogenization, different models may be required to interpret microthermometric measurements from H_2O-NaCl fluid inclusions. For inclusions in which ice is the last solid phase to dissolve during heating, salinity is determined using the equation of Bodnar (1993). If the last solid phase to dissolve (in the presence of vapor) is either hydrohalite or halite, equations from Sterner et al. (1988) are used to determine the liquid composition. For homogenization in the absence of solids, pressure at T_h and liquid density are represented by equations of Atkinson (2002) and Bodnar (1983), respectively. The dP/dT slopes of isochores in the liquid field are modeled using equations of Bodnar and Vityk (1994). For inclusions with $T_h < T_m$ (inclusions that homogenize by halite disappearance), the salinity, pressure at homogenization, density and dP/dT slope of the isochore in the liquid field are represented by the model of Lecumberri-Sanchez et al. (in press).

The Excel spreadsheet, HOKIEFLINCS_H2O-NACL (Steele-MacInnis et al., 2012; available from the authors), does not require iterative procedures to interpret microthermometric data. The user inputs a value of T_m (specifying which solid phase, either H_2O-ice, hydrohalite or halite, is the last to dissolve) and T_h, in °C (Fig. 1). The fluid salinity, density and the isochore slope are output (Fig. 1). To calculate a pressure correction, the user may input an estimate of either *P* or *T* of trapping, and the other quantity is computed based on the isochore slope. The program can be used with any version of Excel, on both Mac and PC platforms.

As an example of the steps involved in using HOKIEFLINCS_H2O-NACL, consider a fluid inclusion that contains liquid and vapor at room temperature, has final ice melting (in the presence of vapor) at -10°C, and homogenizes by vapor bubble disappearance at 300°C. To analyze these data, the value “-10” is entered into the cell for T_m (column C, row 30, Fig. 1), and “ice” is entered into the adjacent cell (cell D30, Fig. 1). The equation of Bodnar (1993) returns a salinity of 13.9 wt% NaCl (cell H30, Fig. 1). To determine the density of the inclusion and pressure at homogenization, the homogenization temperature (“300”) is entered into the cell E30 (T_h), and the program applies the equations of Bodnar (1983) and Atkinson (2002) to estimate a bulk density of 0.86 g/cm^3 (cell J30; Fig. 1) and *P* at homogenization of 78 bar (cell I30; Fig. 1). Using the equation of Bodnar and Vityk (1994), the isochore dP/dT slope for this inclusion is 12.1 bar/°C (cell K30; Fig. 1). The isochore slope can be used along with an independent estimate of the trapping temperature to determine the trapping pressure. For example, if mineral equilibria indicate that the host phase for the FI formed at 600°C, the pressure of formation would have been ~3700 bar (Fig. 1).

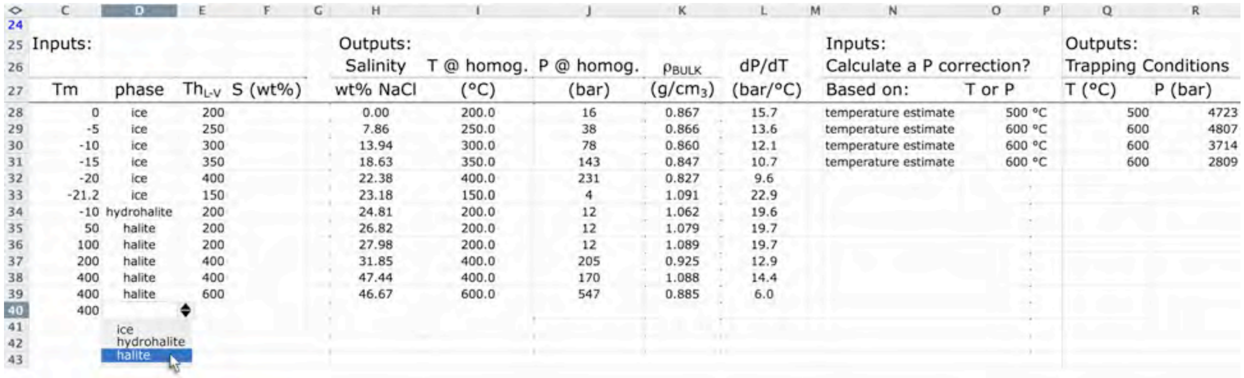

Inputs:				Outputs:					Inputs:		Outputs:	
				Salinity	T @ homog.	P @ homog.	ρ_{BULK}	dP/dT	Calculate a P correction?		Trapping Conditions	
Tm	phase	Th_{L-V}	S (wt%)	wt% NaCl	(°C)	(bar)	(g/cm$_3$)	(bar/°C)	Based on:	T or P	T (°C)	P (bar)
0	ice	200		0.00	200.0	16	0.867	15.7	temperature estimate	500 °C	500	4723
-5	ice	250		7.86	250.0	38	0.866	13.6	temperature estimate	600 °C	600	4807
-10	ice	300		13.94	300.0	78	0.860	12.1	temperature estimate	600 °C	600	3714
-15	ice	350		18.63	350.0	143	0.847	10.7	temperature estimate	600 °C	600	2809
-20	ice	400		22.38	400.0	231	0.827	9.6				
-21.2	ice	150		23.18	150.0	4	1.091	22.9				
-10	hydrohalite	200		24.81	200.0	12	1.062	19.6				
50	halite	200		26.82	200.0	12	1.079	19.7				
100	halite	200		27.98	200.0	12	1.089	19.7				
200	halite	400		31.85	400.0	205	0.925	12.9				
400	halite	400		47.44	400.0	170	1.088	14.4				
400	halite	600		46.67	600.0	547	0.885	6.0				
400												

Figure 1. Screenshot of HOKIEFLINCS_H2O-NACL.

The range of conditions over which HOKIEFLINCS_H2O-NACL is valid varies somewhat depending on the nature of the input data (depending on the particular numerical model(s) used to interpret the data). In general, the program is valid from -21.2 to 700°C, from the liquid-vapor curve to 6000 bar and from 0 to 70 wt% NaCl for FI that homogenize by vapor bubble disappearance; and from T_h of 100 to 600°C, the liquid-vapor-halite curve to 3000 bar and 28-75 wt% NaCl for inclusions that homogenize by halite disappearance. Additional details of the range over which the tool is valid are described by Bodnar and Vityk (1994) and Lecumberri-Sanchez et al. (in press). The model ranges are clearly identified within the spreadsheet, and the program includes a series of "if/then" statements to alert the user to potentially invalid input data. For example, if the user inputs a value of -25°C for ice melting temperature, the program recognizes that this value is less than the H_2O-NaCl eutectic temperature (-21.2°C) and a warning message is displayed. Similarly, the program verifies that T_m, T_h and all estimated fluid properties (density, isochore slope, etc.) are within the ranges of validity of the various numerical models.

A major advantage of HOKIEFLINCS_H2O-NACL compared to other available programs for interpreting fluid inclusion microthermometric data is the speed and ease with which the user can interpret large datasets. Fluid inclusion data (T_m and T_h) stored in a spreadsheet format can be directly copied and pasted into HOKIEFLINCS_H2O-NACL to reduce the data. Because all computations are direct, the results are immediately displayed when T_m and T_h are entered.

REFERENCES

Atkinson, B. (2002) A model for the PTX properties of H_2O-NaCl. MSc. Thesis. Virginia Tech. 133 pp.

Bodnar, R.J. (1983) A method of calculating fluid inclusion volumes based on vapor bubble diameters and P-V-T-X properties of inclusion fluids. Economic Geology. Vol 78. 535-542.

Bodnar, R.J. (1993) Revised equation and table for determining the freezing point depression of H_2O-NaCl solutions. Geochimica et Cosmochimica Acta. Vol 57. 683-684.

Bodnar, R.J., Vityk, M.O. (1994) Interpretation of microthermometric data for H_2O-NaCl fluid inclusions. *In:* Fluid Inclusions in Minerals, Methods and Applications (eds. B. De Vivo, M.L. Frezzotti). Virginia Tech, Blacksburg VA. 117-130.

Lecumberri-Sanchez, P., Steele-MacInnis, M., Bodnar, R.J. (*In press*) A numerical model to estimate trapping conditions of fluid inclusions that homogenize by halite disappearance. Geochimica et Cosmochimica Acta.

Steele-MacInnis, M., Lecumberri-Sanchez, P., Bodnar, R.J. (*In press*) HOKIEFLINCS_H2O-NACL: A Microsoft Excel spreadsheet for interpreting microthermometric data from fluid inclusions based on the PVTX properties of H_2O–NaCl. Computers & Geosciences.

Sterner, S.M., Hall, D.L., Bodnar, R.J. (1988) Synthetic fluid inclusions. V. Solubility relations in the system NaCl-KCl-H_2O under vapor-saturated conditions. Geochimica et Cosmochimica Acta. Vol 52. 989-1005.

PVTX properties of H_2O-$FeCl_2$ fluids.

Steele-MacInnis, M., Lecumberri-Sanchez, P., and Bodnar, R.J.

Department of Geosciences, Virginia Tech, Blacksburg, VA, U.S.A.

Iron chloride is a significant component of saline aqueous fluids in many geologic environments, reaching concentrations of several wt% in some hydrothermal systems (Yardley, 2005). However, the *PVTX* and phase equilibrium properties of iron-bearing aqueous fluids are mostly uncharacterized (Liebscher, 2007), owing to the inherent difficulties resulting from the redox sensitivity of Fe. For example, if Fe^{2+} in the starting materials is oxidized to form Fe^{3+} during the run, then the nominally binary H_2O-$FeCl_2$ system may be complicated by the formation of additional species such as Fe_3O_4, HCl and H_2 (Chou and Eugster, 1977). Despite this potential complexity, the effect of $FeCl_2$ on the phase equilibria of aqueous fluids is a significant concern in iron-rich environments. Partitioning of $FeCl_2$ between coexisting liquid and vapor in the H_2O-NaCl-KCl-$FeCl_2$ system has been determined at 800°C by Simon et al. (2004). However, little is known about the *PVTX* properties and liquid-vapor equilibria of binary H_2O-$FeCl_2$ fluids.

In the present study we apply the synthetic fluid inclusion technique (Bodnar and Sterner, 1987) to investigate the *PVTX* properties of H_2O-$FeCl_2$ fluids. To control the oxidation state of iron during the experiments, we load $FeCl_2$ solution prepared using de-oxygenated water. Oxygen fugacity is buffered by the pressure-vessel material, which is a nickel alloy with fO_2 close to Ni-NiO, where Fe^{2+} is the dominant aqueous iron species. Fluid compositions are confirmed after each experiment using low-temperature microthermometry. In addition to the quantitative verification of $FeCl_2$ concentration based on the freezing-point depression, the stability of the Fe^{2+} species is qualitatively assessed after each experiment by the green color of the fluid released when the capsule is opened (solutions containing ferric iron would be yellowish-orange in color).

Inclusions have been synthesized containing between 10 and 35 wt% $FeCl_2$ (in 5 wt% increments). Reconnaissance work is underway to identify *PVTX* points along the locus of critical points and to constrain the critical properties, using methods similar to those described by Knight and Bodnar (1989). These results will help to interpret the formation conditions of inclusions with significant iron chloride contents, up to 10 wt% $FeCl_2$ or more, which occur in some porphyry-type systems (e.g., Landtwing et al., 2005).

REFERENCES

Bodnar, R.J, Sterner, S.M. (1987) Synthetic fluid inclusions. *In:* Hydrothermal Experimental Techniques (eds. G.C. Ulmer, H.L. Barnes). Wiley Interscience, New York NY. 423-457.

Chou, I.M., Eugster, H.P. (1977) Solubility of magnetite in supercritical chloride solutions. American Journal of Science. Vol. 277. 1296-1314.

Knight, C.L., Bodnar, R.J. (1989) Synthetic fluid inclusions: IX. Critical PVTX properties of NaCl-H_2O solutions. Geochimica et Cosmochimica Acta. Vol. 53. 3-8.

Landtwing, M.R., Pettke, T., Halter, W.E., Heinrich, C.A., Redmond, P.B., Einaudi, M.T., Kunze, K. (2005) Copper deposition during quartz dissolution by cooling magmatic-hydrothermal fluids: The Bingham porphyry. Earth and Planetary Science Letters. Vol. 235. 229-243.

Liebscher, A. (2007) Experimental studies in model fluid systems. Reviews in Mineralogy and Geochemistry. Vol. 65. 15-47.

Simon, A.C., Pettke, T., Candela, P.A., Piccoli, P.M., Heinrich, C.A. (2004) Magnetite solubility and iron transport in magmatic-hydrothermal environments. Geochimica et Cosmochimica Acta. Vol. 68. 4905-4914.

Yardley, B.W.D. (2005) Metal concentrations in crustal fluids and their relationship to ore formation. Economic Geology. Vol. 100. 613-632.

Pan-American Current Research on Fluid Inclusions (PACROFI-XI)
University of Windsor, Windsor, Ontario, Canada, June 18–20, 2012, Abstract Volume

Nature, origin, and role of fluids trapped in the Granophyre Unit of the 1.85 Ga Sudbury Igneous Complex, Canada.

Stewart, R. C. and Kontak, D. J.

Department of Earth Sciences, Laurentian University, Sudbury, ON, rx1_stewart@laurentian.ca

The 1.85 Ga Sudbury Igneous Complex (SIC) is a differentiated impact melt sheet and host to one of the largest Ni-Cu-PGE mineralized districts in the world. The SIC contains four major lithologies, which, from bottom to top, are: the contact sublayer, norite, quartz gabbro, and granophyre. These units are overlain by the crater-fill breccias of the Onaping Formation and the overlying, subaqueous sedimentary strata of the Whitewater Group. Significantly, massive sulphide (Zn-Cu-Pb-Ag) ore bodies occur at the top of the Onaping Formation and represent products of the regional-scale circulation of hydrothermal fluids (200-250°C) fuelled by the cooling SIC. The granophyre accounts for about 50 vol. % of the SIC, is 1.5 km thick, and is interpreted to have cooled separately from the norite and quartz gabbro. The granophyre is dominated (80-98% modal mineralogy) by quartz, alkali feldspar, and plagioclase and contains abundant (to 50%) granophyric texture. The rest of the unit consists of variable % of biotite, amphibole, apatite, titanite, and oxides. Alteration phases include biotite, amphibole, chlorite, epidote, and re-equilibrated feldspars. SEM-EDS analyses of the silicate phases indicates the presence of several amphibole types, both primary and secondary, that plagioclase is An_{0-5}, and that orthoclase is Or_{95-100}, hence, both the feldspar phases record subsolidus, metasomatic exchange with fluids down to <300°C. Furthermore, the feldspars are characterized by pitted textures, the pits often lined with secondary mineral phases (e.g. zircon, baddeleyite, thorite), and also contain fluid inclusions. These latter features are indicative of dissolution-precipitation reactions in the feldspars (e.g. Putnis, 2002).

In order to determine the chemistry and origin of the hydrothermal fluids responsible for the metasomatism in the granophyre and to compare these to fluids implicated in the Cu-Ni-PGE mineralization in the footwall of the SIC, a fluid inclusion study of quartz-hosted inclusions was undertaken. Petrographic examination indicates three aqueous type FIAs are present, in order decreasing abundance these are: (1) L-V with about 10% V. These inclusions are associated with monophase L types which become L-V types upon cooling; (2) L-V-Halite ± Solids with halite the most common solid; and (3) L-V with about 20-30% V. Of these inclusion types, type 1 is by far the most abundant. Preliminary microthermometric analyses indicate the following: (1) type 1 FIAs have T_h = 100-112°C and are saline with 20-25 wt. % eq. NaCl. For these inclusions, T_e = -50°C combined with ice-hydrohalite melting relationships indicates the presence of $CaCl_2$ with $X_{Na} \sim 0.8$; (2) type 2 FIAs have halite dissolution at 105°C and total T_h = 131-140°C; salinities are estimated at 28 wt. % eq. NaCl and ice-hydrohalite melting indicates these fluids are very calcic. These inclusions also contain several unidentified solid phases; and (3) type 3 FIAs have T_h of about 320°C and melting of ice and hydrohalite indicate salinities near 23 wt. % eq. NaCl.

The solute chemistry of the fluid inclusions was characterized by SEM-EDS analysis of evaporate salt mounds (see Figs. 1 and 2). For the samples used, type 1 inclusions dominated the samples, thus it is inferred that the mounds reflect the chemistry of these inclusions. The data indicate the mounds are dominated by Na with lesser Ca and K in an average proportion of 70:20:10; the main anion was Cl, however, significant amounts of F (5-20 wt. %) are present. Using a uniform salinity of 20 wt. % and the Na:Ca:K proportions from Figure 1, the general composition of the North Range fluid is estimated at 56,000 ppm Na, 15,000 ppm Ca and 10,000 ppm K, and for the South Range fluid 45,000 ppm Na, 15,000 Ca, and 20,000 ppm K. Other points to note are: (1) minor to trace amounts of Mn and Fe also occur in 5-25% of the mounds; (2) fluorine occurs in most North Range mounds, and (3) Fe is much more abundant in the North Range mounds.

These preliminary data suggest that the secondary fluid inclusions in quartz of the granophyre represent two thermally distinct, but chemically similar fluid systems. Types 3 fluids represent trapping of a high-temperature fluid potentially responsible in part for the pervasive alteration of the granophyre, whereas types 1 and 2 fluids are lower temperature and may, therefore, relate to the collapse of the once higher temperature, larger, and more regional-scale hydrothermal fluid circulation cell fuelled by the cooling SIC. This same hydrothermal cell likely gave rise to the massive sulphide deposits found at the top of the Onaping Formation (Ames and Farrow, 2007). If this latter assumption is correct, this is the first time that the Onaping hydrothermal system has been identified within the underlying SIC environment.

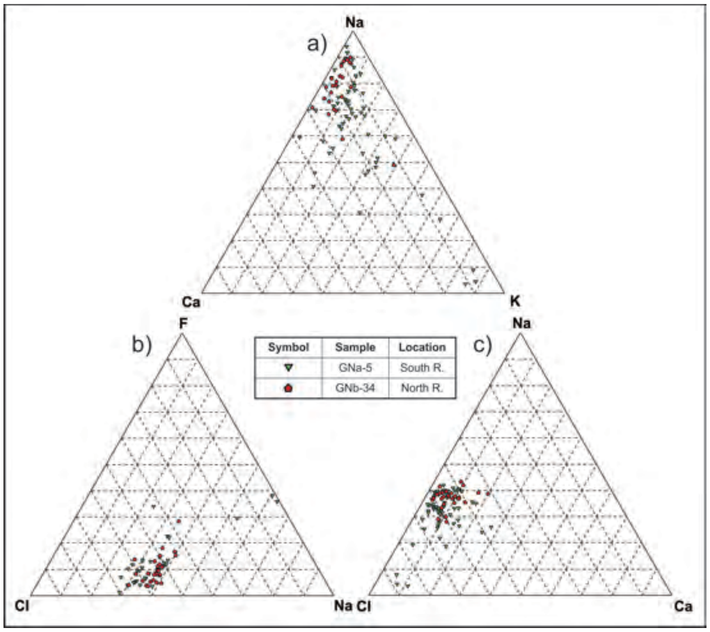

Figure 1. SEM-EDS evaporate mound data plotted on ternary diagrams: (a) Na-Ca-K; (b) F-Cl-Na; (c) Na-Cl-Ca. Note separation of the two samples from the North and South ranges based on their Na:K ratios.

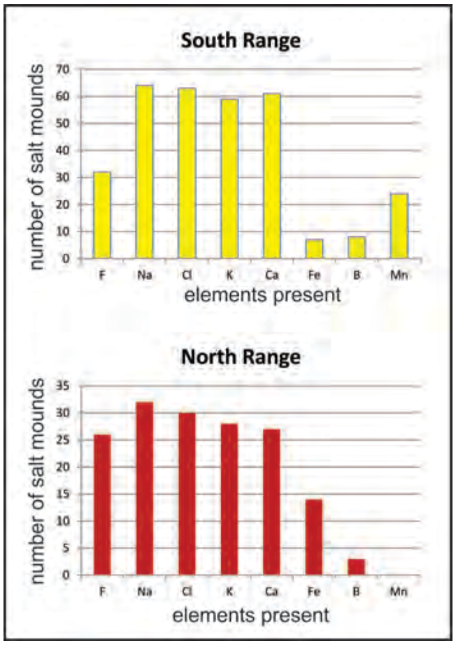

Figure 2. Summary of evaporate mound data broken into the North and South ranges. Data summarized (in wt. % normalized to 100%) are, from left to right, F, Na, Cl, K, Ca, Fe, B, and Mn.

REFERENCES

Ames, D.E., Farrow, C.E.G. (2007) Metallogeny of the Sudbury mining camp, Ontario. *In:* Mineral Deposits of Canada: A Synthesis of Major Deposit-Types, District Metallogeny, the Evolution of Geological Provinces, and Exploration Methods (ed. W.D. Goodfellow). Geological Association of Canada, Mineral Deposits Division, Special Publication. 329-350.

Putnis, A. (2002) Mineral replacement reactions: from macroscopic observations to microscopic mechanisms. Mineralogical Magazine. Vol. 66. 689–708.

A new method for calculation of molar volume and bulk composition of CH_4-H_2O-NaCl fluid inclusions.

Sun, R.

State Key Laboratory of Continental Dynamics, Department of Geology, Northwest University, Xi'an, China

In addition to the CO_2-H_2O-NaCl system, fluids in the CH_4-H_2O-NaCl system are also frequently encountered in hydrothermal systems, sedimentary terranes, and low- to medium-grade metamorphic environments. Thus, it is important to be able to determine the bulk composition and molar volume (*V-x* properties) of CH_4-H_2O-NaCl inclusions for the exploration of ore deposits, oil and natural gas, and for modelling heat and mass transfer in various geological environments.

In general, the *V-x* properties of fluid inclusions can be determined from microthermometric and other analytical data. For instance, the salinity of H_2O-NaCl inclusions is determined from the final melting temperature of ice, hydrohalite or halite. The salinity of CO_2-H_2O-NaCl inclusions is determined from the final melting temperature of CO_2 clathrate hydrate at the clathrate-liquid water-liquid CO_2-gas CO_2 equilibrium. For the calculation of x_{CO2} and molar volume of CO_2-H_2O-NaCl inclusions, the volume fraction of the CO_2 phase, estimated from dimensional measurements, is also needed. However, the uncertainty in estimation of the volume fraction of fluid inclusions may be large, especially for those inclusions of irregular shape.

Parry (1986) proposed that the molar volume and bulk composition of CO_2-H_2O-NaCl inclusions can be determined based only on microthermometric data (i.e., the homogenisation temperature and mode of the carbonic phase and the temperature and mode of total homogenisation of the fluid inclusion). It is unnecessary to estimate the volume fraction of the CO_2 phase for Parry's method. However, Parry's method is not useful for CH_4-H_2O-NaCl inclusions because the homogenisation temperature of the CH_4 phase is below the freezing point of water. The salinity of the CH_4-H_2O-NaCl inclusion cannot be determined by following the method used for CO_2-H_2O-NaCl inclusions for the same reason. Dubessy (1992) proposed that the salinity of the CH_4-H_2O-NaCl inclusion can be calculated from the melting temperature of ice ($T_{m,ice}$), the melting temperature of CH_4 clathrate hydrate($T_{m,cla}$), and the volume fraction of CH_4 gas phase at $T_{m,cla}$, when $T_{m,cla}$ is higher than $T_{m,ice}$.

This study proposed a new method to calculate the *V-x* properties of CH_4-H_2O-NaCl inclusions. Based on the basic assumption that the bulk composition and the volume of fluid inclusions are constant after entrapment, an iterative method was used to determine the molar volume and bulk composition from $T_{m,ice}$, $T_{m,cla}$, and the total homogenisation temperature and homogenisation mode of the fluid inclusion. It is unnecessary to use the volume fraction of the CH_4 phase as input data for the new method. Instead, it can be calculated from this method. The equation of state developed by Duan et al. (2003) was used to calculate the vapour-liquid equilibria and *PVTx* properties of the CH_4-H_2O-NaCl system, and the model proposed by Duan and Sun (2006) was used to calculate the pressure of stability for CH_4 hydrate. Based on this new method, a FORTRAN 77 computer package was written that allows calculation of the *V-x* properties of CH_4-H_2O-NaCl inclusions with total homogenisation temperatures of greater than 573 K.

REFERENCES

Duan Z., Moller N., Weare J. H. (2003) Equations of state for the NaCl-H_2O-CH_4 system and the NaCl-H_2O-CO_2-CH_4 system: Phase equilibria and volumetric properties above 573 K. Geochimica et Cosmochimica Acta. Vol. 67. 671-680.

Duan Z., Sun R. (2006) A model to predict phase equilibrium of CH_4 and CO_2 clathrate hydrate in aqueous electrolyte solutions. American Mineralogist. Vol. 91. 1346-1354.

Dubessy J., Thiery R., Canals M. (1992) Modelling of phase equilibria involving mixed gas clathrates: Application to the determination of molar volume of the vapour phase and salinity of the aqueous solution in fluid inclusions. European Journal of Mineralogy. Vol. 4. 873-884.

Parry W.T. (1986) Estimation of X_{CO2}, P, and fluid inclusion volume from fluid inclusion temperature measurements in the system NaCl-CO_2-H_2O. Economic Geology. Vol. 81. 1009-1013.

Significance of fluid, silicate and sulfide melt inclusions in mantle xenoliths from the Carpathian-Pannonian Region.

Szabó, Cs.

Lithosphere Fluid Research Lab, Institute of Geography and Earth Sciences, Eötvös University, Budapest, Hungary

Lithospheric mantle beneath the Carpathian-Pannonian Region (CPR), transported to the surface by Plio-Pleistocene alkali basalt as peridotite and pyroxenite xenoliths, provides a great opportunity to study deep-seated fluid, silicate and sulfide melt inclusions, and to obtain insight into their nature and behaviour under upper mantle conditions. Within the CPR, five volcanic fields (Styrian Basin, Little Hungarian Plain, Bakony-Balaton Highland, Nógrád-Gömör, and Persany Mountains) are known, which contain large amount of upper mantle xenoliths. Based on petrologic, geophysical, geochemical, tectonic, sedimentological, structural and volcanological studies over the last few decades, the deep lithospheric mantle of this region, which covers approximately 300 000 km^2, is one of the best studied mantle portions in the world. To better understand processes such as mantle metasomatism, fluid-melt immiscibility, incompatible element and volatile transport, and element partitioning, all of which are related to melt/fluid migration and interaction with mantle, we have selected a set of representative mantle xenoliths from each volcanic field to study their fluid, silicate and sulfide inclusions, focusing on “primary” (early stage) silicate and sulfide melt inclusions, as well as spherical and negative crystal-shaped fluid inclusions. It is more than interesting that such silicate and fluid inclusions are highly characteristic of xenoliths occurring in the central part of the CPR (Bakony-Blaton Highland) and northern (Nógrád-Gömör) and eastern edge (Persany Mountains) of the studied region. In contrast, sulfide blebs occur in xenoliths collected at the edge (Styrian Basin, Nógrád-Gömör, Persany Mountains) of the CPR.

Silicate melt inclusions in pyroxene consist of partially crystallized glass, and show post-entrapment crystallization on the inclusion walls. They are characterized by alkali-rich intermediate major element compositions. Fluid inclusions, present as either isolated inclusions or coexisting with silicate melt inclusions, are enclosed in pyroxene and contain generally one observable fluid phase at room temperature. Experiments on low- and high-T heating-freezing stages, coupled with Raman spectroscopy, confirmed that both the coexisting and the isolated fluid inclusions are high-density CO_2-dominated fluids, which also contain H_2O and rarely H_2S molecules. The FIB-SEM (focused ion beam-scanning electron microscopy) exposure technique revealed a thin glass film, covering the wall of the fluid inclusions, which provides direct evidence that the silicate components were formerly dissolved in the CO_2-rich fluid phase. Also, tiny magnesite and quartz step-daughter crystals are common in these fluid inclusions, and reflect a moderate-T reaction between fluids and the host mantle mineral. The distribution of trace elements in silicate melt inclusions and fluid inclusions indicates that both the isolated H_2O-bearing, CO_2-rich fluid inclusions and those coexisting with silicate melt inclusions contain similar and characteristic trace elements, such as LILE, MREE, Nb and Zr. Consequently, volatile-bearing silicate melt and silicate-bearing CO_2-rich fluids, formed by immiscibility, could act as metasomatic agents in the deep lithosphere to produce the characteristic incompatible trace element enrichment observed in metasomatized lithospheric mantle.

Sulfide blebs, enclosed in olivine, generally consist of monosulfide solid solution, pentlandite and chalcopyrite. The compositions of the Fe-Ni-Cu-rich multiphase sulfide inclusions, which also contain minor amounts of Co and Pt-group elements (Os, Ir, Ru, Rh, Pt and Pd), were determined by LA-MC-ICP-MS. The total concentrations of PGE range between 4 and 796 ppm. The majority of sulfide inclusions show high and variable abundances of Os, Ir, and Ru, and decreasing negatively sloped PPGE (Rh, Pt, Pd) patterns, in some cases with very low Pt concentrations, which is particularly characteristic for the rare sulfide blebs in the Bakony-Balaton Highland xenoliths. This discrepancy in PGE distributions could be explained by different degrees of partial melting and metasomatism in the CPR mantle.

Pan-American Current Research on Fluid Inclusions (PACROFI-XI)
University of Windsor, Windsor, Ontario, Canada, June 18–20, 2012, Abstract Volume

Determination of CO_2/H_2S ratios by Raman spectroscopy and model stability of mixed CO_2-H_2S clathrates in fluid inclusions.

Tattitch, B.C.*, Candela, P.A.*, Piccoli, P.M.*, and Bodnar, R.J.**

**Laboratory for Mineral Deposits Research, University of Maryland, College Park, MD, U.S.A.*
***Fluids Research Group, Virginia Tech, Blacksburg, VA, U.S.A.*

In-situ analysis of gas chemistry in natural and synthetic fluid inclusions provides data for characterizing hydrothermal fluids. In porphyry ore deposits, the dominant volatile phase component is water, although CO_2 is often present as an appreciable (0 to 10 mol%) component. Magmatic hydrothermal fluids in arc environments can have much higher concentrations of CO_2, with H_2O/CO_2 ratios near 1 at shallow levels (<10 km), and more CO_2-rich compositions at depth. Sulfur is also present in volatile phases derived from arc magmas. These hydrothermal fluids often rise under reduced conditions where H_2S is a significant and often the dominant sulfur-bearing phase component.

Methods for fluid inclusion analysis often rely on microthermometric measurements of salinity for accurate analyses. However, in the presence of CO_2, aqueous inclusions often nucleate clathrate upon cooling, preventing accurate salinity measurements by using the ice melting point. Recent work presented by Fall et al. (2011) provides a new model for determining the density of liquid or vapor CO_2 present in fluid inclusions at pressures below 10 MPa based on Raman Fermi-diad splitting measurements. Identifying the appropriate isochore for fluid inclusions that contain CO_2 present as vapor allows for accurate measurement of inclusion salinity by clathrate melting whereas other analytical methods have relied on inherently imprecise measurements such as bubble volume. Here we discuss measurements of CO_2 density that can be used to determine the salinity of synthetic fluid inclusions. These inclusions were generated to investigate the role of CO_2 in the formation of porphyry copper deposits. Sulfur is also a critical component of many ore-forming fluids, and at magmatic conditions most of the sulfur present in volatile phases will be present as H_2S. Sulfur-bearing magmatic fluids that are both CO_2-bearing and H_2S-bearing may produce fluid inclusions that nucleate clathrate formed from CO_2 - H_2S -H_2O – salt mixtures. We present a model for the stability of these mixed CO_2-H_2S clathrates and their relevance to the characterization of sulfur-bearing ore fluids.

Vapor-rich fluid inclusions were generated by trapping, in quartz, a boiling assemblage of vapor and brine at 800°C and 100 MPa. The NaCl-KCl-H_2O-CO_2 volatile phase assemblage was generated by using oxalic acid dihydrate and an aqueous solution of NaCl + KCl. An in-situ fracturing technique similar to that presented by Sterner and Bodnar (1991) was used to promote equilibrium prior to trapping the magmatic fluids. Unfractured quartz cores were added to the starting materials; after 3 days at run conditions the vessel was rotated through 180^{o}, thereby exposing the capsule to cooler fluid (~400°C), and fracturing the quartz. Regions of quartz containing fluid inclusions with similar phase proportions (bubble size and no daughter halite or sylvite) were selected for analysis of vapor-rich inclusions with minimal brine contamination. The selected inclusions ranged in size from 5 µm to 50 µm and comprised a CO_2-dominated vapor bubble (~80%), condensed aqueous liquid (20%), and, in sulfur-bearing experiments, a sulfide daughter mineral (opaque ~ 2%).

Raman analyses of the vapor-rich inclusions were completed using the JY Horiba LabRam HR (800 mm) spectrometer and a 514.53 nm Laser Physics 100S-514 Ar^+ Laser at Virginia Tech. The Raman laser was focused on the CO_2-rich vapor bubble in each inclusion, and a spectrum was collected that included both CO_2 peaks. The position of each peak was then determined after making a baseline correction, and the splitting between the peaks (Δ) was calculated for each inclusion. The CO_2 density (ρCO_2) was then calculated by using the model presented by Fall et al. (2011). Clathrate melting temperatures (T_m^{Clath}) were then obtained by using a USGS fluid inclusion stage via cyclical heating and cooling of inclusions over a temperature range of -10 to +15°C. The CO_2 density is then correlated with the pressure of the fluid inclusion at the clathrate melting temperature (P_{FI}) according to a NIST equation of state for pure CO_2 (Lemmon et al. 2012). The salinity of each inclusion was then obtained by comparing the intersection of the T_m^{Clath} and the P_{FI} with the salinity-dependent model for CO_2 clathrate presented by Duan and Sun (2006). The P_{FI} values determined using this method are also consistent with isochoric quench calculations by using a model density for the high-temperature vapor and the salinity determined from microthermometry.

Calculation of inclusion salinity in H_2S-bearing vapor-rich inclusions required several additional steps. The Raman spectra for these inclusions were expanded to include both CO_2 peaks ($1V_1$~1286 cm^{-1} and $2V_2$~1389 cm^{-1}) along with the Raman active $H_2S_{(v)}$ peak (~ 2611 cm^{-1}) in a single analysis. The intensity of each of these peaks is a function of the mole fraction of each gas in the vapor bubble (X_{CO2} and X_{H2S}) and the scattering efficiency of each vibrational mode (CO_2: $1V_1$=1.0 and $2V_2$=1.5, H_2S: $1V_1$=6.4) (Burke 2001). By integrating the area under each peak and correcting for scattering efficiencies, we can obtain the composition of the vapor bubble at room temperature in each inclusion. The appropriate isochore for each CO_2/H_2S mixture (Stouffer at al. 2001) can then be used to obtain the pressure at T_m^{Clath}, in a manner similar to that employed for sulfur-free inclusions. Diamond (2003) notes that both CO_2 and H_2S form clathrate with the same structure and that a continuous solid solution exists for clathrate at any CO_2/H_2S ratio. The limited experimental data on the effect of chlorides on pure H_2S clathrates suggests that the magnitude of the change on the clathrate stability boundary is similar to that of pure CO_2 clathrate (Bond and Russell 1949). Given these similarities, we have modeled the stability of mixed CO_2-H_2S clathrate at low X_{H2S} as an ideal mixing between the pure end-member clathrates.

The difference between the stability of the mixed clathrate and the pure-CO_2 clathrate (between 0.5 and 1°C) was then used as a correction factor in calculating the salinity for the H_2S-bearing inclusions. The calculated salinities of the H_2S bearing inclusions are similar to H_2S-free inclusions synthesized at the same H_2O/CO_2 ratio and experimental conditions. The addition of small amounts of H_2S to the volatile phase assemblage should not affect the salinity of the coexisting vapor and brine. However, this model demonstrates that ignoring the 2 to 6 mol% H_2S in the inclusion would result in a 30% to 50% error in the salinities calculated using clathrate melting temperatures.

These data provide a foundation for determining the salinity of vapor-rich inclusions containing $CO_2 \pm H_2S$ in sufficient quantity to stabilize clathrate upon cooling. The salinity of vapor-rich fluid inclusions is now commonly used as a standard for characterization of fluid compositions. As analyses of fluid inclusions from natural systems and experimental analogues become more complete, the influence of secondary components such as CO_2 and H_2S are becoming more important. In-situ measurements of gas composition and models for mixed gas clathrate stability will provide more accurate measurements of fluid composition and its effect on processes from metal partitioning to phase stability and solubility. As additional experimental information on mixed gas clathrate stability becomes available, the combination of Raman spectroscopy and clathrate stability will allow for accurate characterization of salinity for a wide variety of fluid compositions.

REFERENCES

Burke, E.A.J. (2001) Raman microspectrometry of fluid inclusions. Lithos. Vol. 55. 139-158.

Diamond, L.W. (1994) Salinity of multivolatile fluid inclusions determined from clathrate hydrate stability. Geochimica et Cosmochimica Acta. Vol. 58. 19-41.

Duan, Z.H., Sun, R. (2006) A model to predict phase equilibrium of CH_4 and CO_2 clathrate hydrate in aqueous electrolyte solutions. American Mineralogist. Vol. 91. 1346-1354.

Fall, A., Tattitch, B., Bodnar, R.J. (2011) Combined microthermometric and Raman spectroscopic technique to determine the salinity of H_2O-CO_2-NaCl fluid inclusions based on clathrate melting. Geochimica et Cosmochimica Acta. Vol. 75. 951-964.

Lemmon, E.W., McLinden, M.O., Friend, D.G. (2012) Thermophysical Properties of Fluid Systems. *In:* NIST Chemistry WebBook, NIST Standard Reference Database Number 69 (eds. P.J. Linstrom, W.G. Mallard). National Institute of Standards and Technology. Gaithersburg MD.

Sterner S.M. & Bodnar R.J. (1991) Synthetic fluid inclusions. X. Experimental determination of P-V-T-X properties in the CO_2-H_2O system to 6 kb and 700°C. American Journal of Science. Vol 291. 1-54.

Stouffer, C.E., Kellerman, S.J., Hall, K.R., Holste, J.C. (2001) Densities of carbon dioxide plus hydrogen sulfide mixtures from 220 K to 450 K at pressures up to 25 MPa. Journal of Chemical and Engineering Data. Vol. 46. 1309-1318.

Preliminary results of thermometric analysis of high temperature fluid inclusions in quartz in lithophysae agates from Nowy Kosciol (Sudety Mts., Poland).

Wolkowicz K.*, Jackowicz E.**, and Rzymelka J.***

*Polish Geological Institute-Polish Research Institute, Warsaw, Poland, *krystyna.wolkowicz@pgi.gov.pl, **elzbieta.jackowicz@pgi.gov.pl, ***jan.rzymelka@pgi.gov.pl*

Fluid inclusions in the oldest quartz in Polish lithophysae agates from Nowy Kosciol in the Kaczawa Mts (Sudety Mts, SW Poland) were investigated. The studied agates come from J. Rzymelka's collection.

The research included: fluid inclusion petrography with microphotography (Nikon, Eclipse LV100 POL; Nikon, Coolpix 8400 camera); fluorescence analysis (microscope Nikon with adding UV); fluid inclusion microthermometry on THMS600 heating-freezing stage (Linkam Scientific Instruments Ltd, UK). Heating-freezing runs were conducted in the temperature range between 26 and 412°C and to -196°C. The precision of measurements in the positive range equals 1°C, and in the negative range is 0.1°C.

In the Sudety Mts., agates are found in various Permian volcanics, but lithophysae agates (known as thundereggs) occur only in rhyolites, which create covers and subvolcanic forms, sometimes in association with rhyoitic tuffs. Agates form infilings in cavities, connected with megaspherulites, which appear in the weathering zone of felsic volcanics. Agate nodules can reach sizes of over 60 cm in diameter; they contain mainly chalcedony and quartz, arranged in concentric and occasionally horizontal bands. From rim to core, agates display repetitive textures with alternate layers of fibrous chalcedony and granular, mainly microcrystalline, quartz layers. The fibres in chalcedony are elongated toward the centre of agates, perpendicular to the banding pattern. The presence of red- or orange-coloured bands is caused by finely dispersed hematite between chalcedony fibres. The latest stage of formation of agate bands is represented by a coarse crystalline quartz layer.

Previous studies have shown that the temperature interval of crystallization of silica minerals in agates from magmatic environments ranges from < 50 to > 400°C (e.g., Götze et al., 2001). The vast majority of data has been obtained on the basis of isotopic studies of oxygen and hydrogen. Temperatures above 375°C were obtained using a geothermometer based on the size of crystallites (Moxon, 1996). These temperature estimates partly overlap with the Sudetes agate data: fluid inclusion homogenization temperatures (100-215°C) (Kozlowski, 1985) and values calculated based on the results of isotopic studies (20-120°C) (Möckel et al., 2010).

In the examined lithophysae agates, there are several generations of quartz with sufficiently large crystals to allow for fluid inclusion analysis. Homogenization temperatures ranging from 412 to 26°C were obtained. The highest temperatures, ranging from 412 to 238°C, were obtained from the oldest quartz crystals growing directly on the altered rocks on the walls of geodes, as described below. Such high temperature data were not obtained in the previous thermometric analyses. These have significant meaning for the genesis of agates, especially for the initial stage of SiO_2 crystallization.

Fluid inclusions occur as: single inclusions, in small clusters, in groups located along crystal growth zones, and along different kinds of trails. They are always two-phase (L+V).

The highest homogenization temperature was achieved in an isolated inclusion. This inclusion, hypidiomorphic in shape, 10 μm in size, contains about 10% gas phase at room temperature. The homogenization occurs at temperature of 412°C by disappearance of the liquid phase.. Eutectic and melting temperature indicate very low salinity of the parent solutions (T_m close to -0.1°C) composed probably of NaCl- $MgCl_2$ with the addition of $CaCl_2$ (T_e -42°C) (Goldstein and Reynolds, 1994, Samson et al., 2003).

Fluid inclusions occur both in small clusters, as well as in groups of inclusions located along crystal growth zones. These have a primary origin. Fluid inclusions located along trails have secondary or pseudosecondary origin. These inclusions are very small. They rarely exceed 1 μm, and are only occasionally as large as 10 μm. Their predominant forms are oval or polygonal to irregular, but are often rounded. They have about 20% gas phase at room temperature. Inclusions present "loose" in small clusters homogenize into the liquid phase at temperature ranging from 238 to 361°C. Eutectic and melting temperature (T_e - 42°C, T_m close to 0°C) indicate (Goldstein and Reynolds, 1994, Samson et al., 2003) that the composition and salinity of the parent solutions are similar to the single inclusion described above. The fluid inclusions located along crystal growth zones homogenize at temperatures of 267 to 299°C by bubble disappearance. The inclusions accumulated along the trails homogenize into the liquid phase at temperatures ranging from 274 to 325°C.

The last group of described fluid inclusions, usually arranged linearly, are up to 60 µm in size. They are characterized by a large, dark bubble. They contain at maximum about 80% gas phase at room temperature. However, the inclusions show no fluorescence. They homogenize at temperatures of 375 to 400°C in the gas phase. The obtained temperatures are likely not entirely reliable, because at least some of these inclusions contain an irregular distribution of phases. Attempts to heat the frozen inclusions did not reveal any changes. Only at the lowest temperatures (below -190°C), a change in the bubble was noticed, although the nature of the phase change is not known.

The most widespread theory about the genesis of agates assumes that they originated as a result of hydrothermal, post-volcanic activity (Florke et al., 1982, Heaney, Davis, 1995, Götze et al., 2001). This view has been supported by studies of the agates from The Sudety Mts. (Kryza & Kryza, 1982; Kozlowski, 1985; Bogdanski et al., 2009). The high homogenization temperatures obtained from thermometric studies, ranging from 412 to 238°C, indicate that the oldest quartz crystallized from high-temperature hydrothermal fluids and the presence of a pneumatolitic stage during the filling of bubbles formed in degassed lava. This high-temperature generation of quartz crystallized mainly from low-salinity solutions (T_m close to 0°C), containing salts in the $NaCl-MgCl_2-CaCl_2$ system.

REFERENCES

Bogdanski, J., Praszkier, T., Siuda, R. (2009) Agaty z Płoczek Gornych (in polish only). Lwowek Sl. Wyd. Gmina i miasto Lwowek Sląski, Tow. Geol. „Spirifer". 196p.

Flörke, O. W., Köhler-Herbet, B., Lange, K., Tönges I. (1982) Water in microcrystalline quartz of volcanic origin: Agates. Contributions to Mineralogy and Petrology. Vol. 80. 324-333.

Goldstein R. H., Reynolds T. J. (1994) Systematics of fluid inclusions in diagenetic minerals. SEPM Short Course. Vol. 31. 199p.

Götze J., Plötze M., Tichomirowa M., Fuchs M., Pilot J. (2001) Aluminum in quartz as a indicator of the temperature of formation of agate. Mineralogical Magazine. v. 65. 407-413.

Heaney P. J., Davis A. M. (1995) Observations and origin of the self-organized textures in agates. Science. Vol. 269. 1562-1565.

Kozłowski A. (1985) Studies of fluid inclusions in agates from Płóczki Górne and Nowy Kościół, Poland. Fluid Inclusion Research - Proceedings of COFFI, Michigan University Press, Ann Arbor, USA. Vol. 18. 221-222.

Kryza J., Kryza R. (1982) Agate mineralization in Rotliegendes volcanic rocks in the vicinities of Nowy Kosciol (Gory Kaczawskie Mts). Przeglad Geologiczny. No. 3. 122-125.

Moxon T. (1996) Agate: microstructure and possible origin. Terra Publications, Doncaster, UK. 106pp.

Möckel R., Götze J., Sergeev S. A., Kapitonov, I. N., Adamskaya, E. V., Goltsin N. A., Vennemann T. (2010) Trace-Element Analysis by Laser Ablation Inductively Coupled Plasma Mass Spectrometry (LA-ICP-MS): a Case Study for Agates from Nowy Kościoł, Poland. Journal of the Siberian Federal University Engineering and Technologies. Vol. 2. 123-138.

Samson I., Anderson A., Marshall D. (ed.) (2003) Fluid inclusions: Analysis and interpretation. Short Course Mineralogical Association of Canada. Vol. 32. 374p.

Fluid inclusion study on vein gold-copper mineralization at the Qiaxia-Sarekoubu area, southern Altaides, China.

Xu, J.H., Xiao, X., Yang, R., and Lin, L.H.

Resource Engineering Department, University of Science and Technology Beijing, Beijing, China

The southern margin of the Altaides had undergone intensive NW-SE compression since the Late Devonian to the Early Permian, which resulted in syn-orogenic metamorphism, deformation and hydrothermal mineralization. This was an important mineralizing epoch that followed Early Devonian VMS mineralization (Xiao et al, 2008). Not only had VMS ores undergone deformation and metamorphism, but gold-copper-bearing sulfide-quartz veins formed during orogeny or post-orogeny. The Sarekoubu vein gold deposit and the Qiaxia copper-gold vein deposit, located to the east of Altai town of northwest China, occur in metamorphic volcaniclastic rocks of the lower Devonian Kangbutiebao Formation (Fig.1A). These quartz veins can be divided into two groups. The first group of quartz occurs as lensoid or streaked quartz veins (QI) which are parallel to the foliation of the biotite-chlorite (Fig.1B) or garnet-chlorite schists. The second group is gold-chalcopyrite-bearing quartz veins (QII) which cross-cut the metamorphosed volcanic rocks at small angles, and represent a younger, metamorphic-related overprinting event.

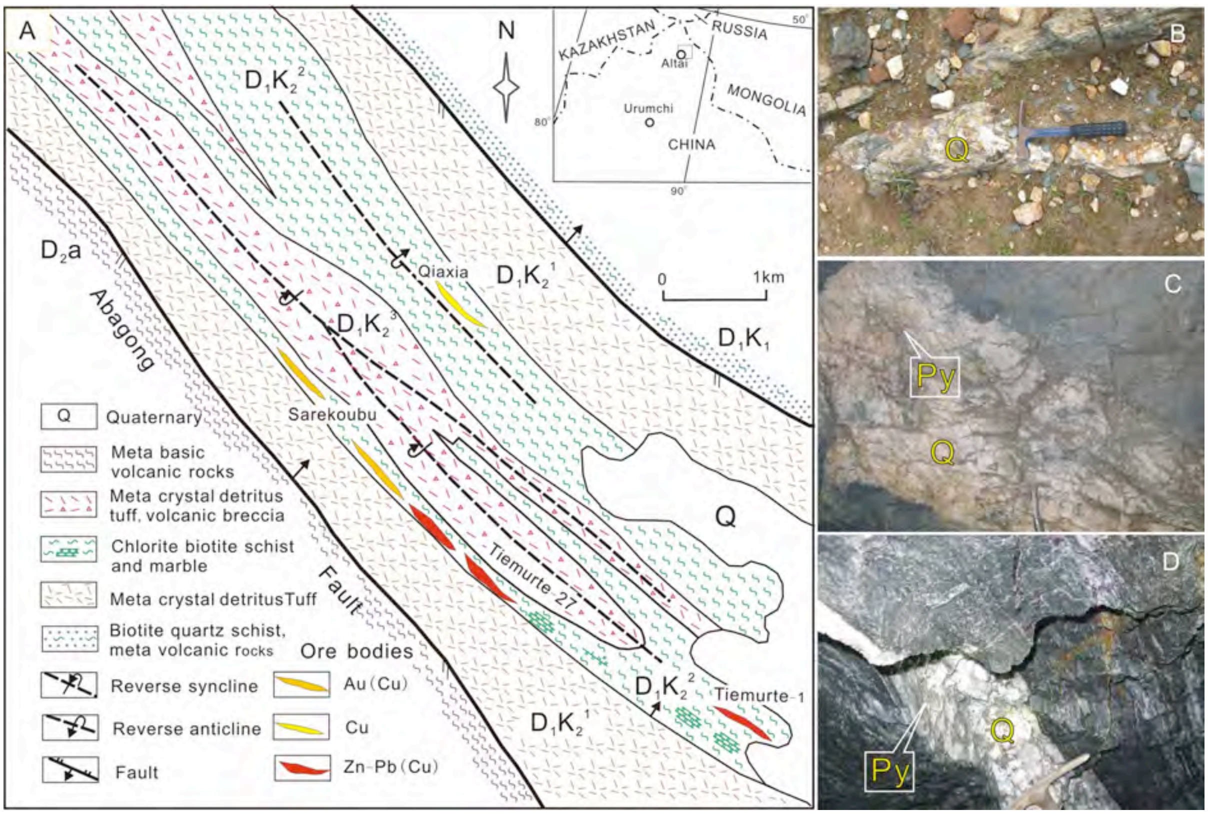

Figure 1. Sketch map of the Sarekoubu and Qiaxia deposits (A) in southern Altaides, China, and characteristics of vein gold-copper mineralization (B, C, D).

There are three types of fluid inclusions in the quartz veins. The first type of fluid inclusions is characterized by CO_2-rich fluids (CO_2-H_2O inclusions). CO_2-H_2O inclusions occur as isolated elliptical or irregular clusters with no planar orientation, and are interpreted as primary in origin, both in QI and QII, with sizes of 2-20μm and with CO_2/H_2O ratios of 0.1 to 0.9. Some CO_2-H_2O inclusions comprise three phases at room temperature: a CO_2 liquid phase, a CO_2 vapor phase, and an aqueous phase. The second type are carbonic fluid inclusions, and are commonly observed; a few carbonic fluid inclusions may be of primary origin, especially in the chalcopyrite-quartz veins from the Sarekoubu deposit. Most of the carbonic fluid inclusions are of secondary origin in early quartz QI. There are two groups based on melting temperatures of frozen CO_2 phases ($T_{m,CO2}$). The first group comprises pure CO_2 inclusions, with $T_{m,CO2}$ = -60°C ~ -56.5°C and $T_{h,CO2}$ = -23°C ~ +31°C ; whereas the second group comprises CO_2-CH_4-N_2 inclusions with $T_{m,CO2}$ less than -57°C, to a minimum of -78.1°C, and $T_{h,CO2}$ = -33.7°C ~ -17.7°C. Based on the trapping temperatures of associated L_{CO2}-L_{H2O} inclusions, which range from 205°C to 370°C (Sarekoubu) and from 190°C to 350°C, the lowest trapping pressures of CO_2 fluids can be estimated to be 110-300 MPa, based on CO_2 densities and the CO_2 phase diagram at high *P-T* of Van den Kerkhof and Thiéry (2001). The third type of fluid inclusion is chracterized by salt-aqueous inclusions, which usually occur as secondary inclusions in early stages of quartz. Halite daughter minerals can be occasionally found in primary fluid inclusions in early quartz QI.

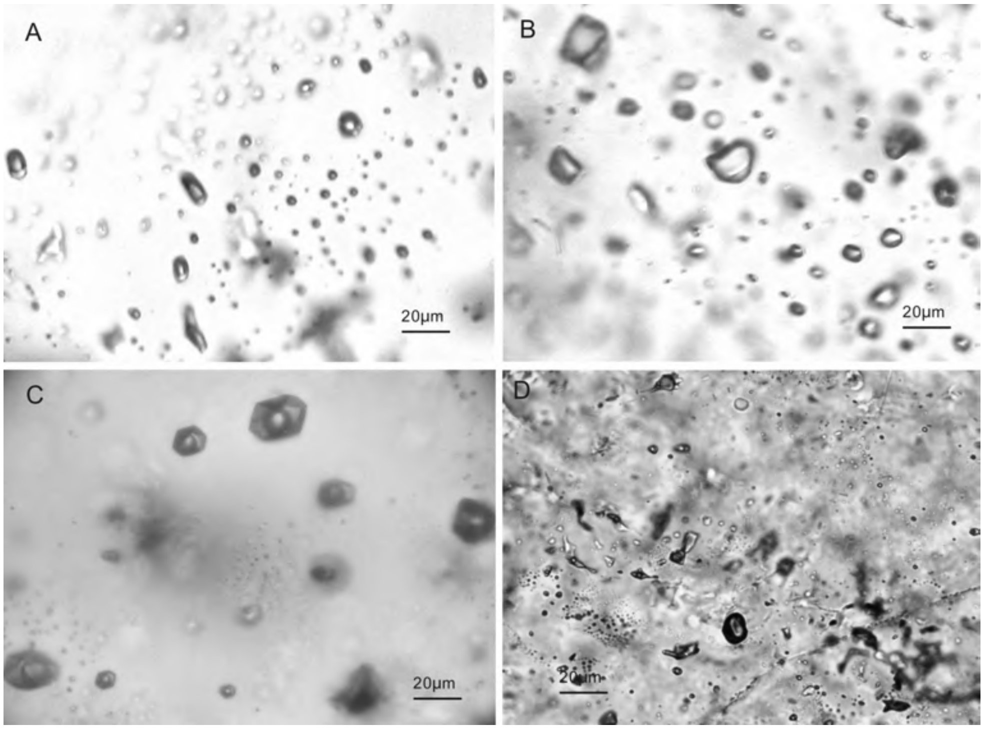

Figure 2. CO_2-rich inclusions of vein gold deposits at the Sarekoubu and Qiaxia deposits in southern Altai. A-Primary carbonic inclusions and CO_2-rich inclusions in quartz near a chalcopyrite grain, Sr21, Sarekoubu; B-Primary carbonic inclusions in a quartz grain from a chalcopyrite-quartz vein, SR4005, Sarekoubu; C-Primary CO_2-H_2O inclusions in a pyrite-quartz vein, SR805, Sarekoubu; D-CO_2-rich inclusions in lenticular quartz from a mylonite, QI106, Qiaxia.

Measured $\delta^{18}O$ values of quartz are 10.3 ~ 14.6‰ (QI) and 9.1 ~ 13.1‰ (QII), which result in fluid $\delta^{18}O$ values of 7.54 ~ 11.84‰ (QI) and 3.82 ~ 7.82‰ (QII), using the fractionation equation of Clayton et al. (1972). Measured δD values of water in fluid inclusions are -84.7 ~ -98.2‰ (QI) and -75.8 ~ -108.8‰ (QII). It is suggested that the source of the ore-forming fluids could be related to regional metamorphism and associated magmatism based on field geology and this fluid inclusion study.

REFERENCES

Clayton R.N., O'Neil J.R., Mayeda T.K. (1972) Oxygen isotope exchange between quartz and water. Journal of Geophysical Research. Vol. B77. 3057-3067.

Van den Kerkhof, A. Thiéry R. (2001) Carbonic inclusions. Lithos. Vol. 55. 49-68.

Xiao W.J., Pirajno F., Seltmann R. (2008) Geodynamics and metallogeny of the Altaid orogen. Journal of Asian Earth Sciences. Vol. 32). 77-81.

Reconstructing Permian hydrosphere, lithosphere, biosphere, and atmosphere from fluid inclusions in lacustrine halite: preliminary results from the Rebecca Bounds core, western Kansas.

Zambito, J.J. and Benison, K.C.

Department of Earth and Atmospheric Science, Central Michigan University, Mt. Pleasant, MI, U.S.A.

Primary fluid inclusions in halite crystals provide an ideal window for the preservation of hydrosphere, lithosphere, biosphere and atmosphere. Here, we present preliminary results of our petrographic studies and chemical analyses of fluid inclusions in redbed-hosted bedded halite from a core drilled in western Kansas containing Middle and Late Permian (~265 million years ago) saline lake deposits at depths of 1900 to 2600 feet. Analyses include plane-, reflected-, and polarized-light petrography, homogenization of artificially nucleated vapor bubbles, ultraviolet light microscopy (UV-visible microscopy), and laser Raman microscopy. Other types of analyses are currently being considered for obtaining enhanced data about these halites in the future. Our goal is to obtain high-resolution and quantitative data on Permian environmental conditions at various temporal scales, including lake water depths, lake water chemistry (including pH), surface air temperatures, surface atmospheric chemistry, and the presence of microorganisms and organic compounds. Comparisons with fluid inclusion data from modern acid saline lake halite from Western Australia may help refine our interpretations.

Petrographic observations show that much of the bedded halite formed in saline pans. Fluid inclusions oriented along growth bands in cm-scale crystals help define chevron halite crystals, indicative of precipitation from shallow (less than ~ 0.5 meter) surface water. Less common, randomly-oriented mm-scale halite crystals with primary fluid inclusions were also observed. Most fluid inclusions are all-liquid, but some of the largest inclusions have large dark bubbles interpreted as trapped air. Gypsum, anhydrite, and some unidentified crystals have also been observed within some fluid inclusions. Gypsum and anhydrite crystals also exist as solid inclusions within halite. Hematite-coated quartz silt and sand grains trapped as solid inclusions within bedded halite likely were transported into the saline lakes by wind. Dissolution pipes filled with clear halite and dissolution surfaces that truncate chevron crystal tops strongly suggest occasional flooding of shallow lakes with fresher water. Desiccation is indicated by microcrystalline crystal crusts containing halite and gypsum.

Homogenization of artificially nucleated vapor bubbles in fluid inclusions from chevrons reflect temperatures of shallow surface waters. Limited preliminary measurements yield temperatures of 20 – 30°C. Microstratigraphic control within and among chevron growth bands is allowing for preliminary interpretations of trends in shallow lake water temperatures within single days and over the course of approximately one week. Because modern water temperatures in shallow saline environments is very close to surface air temperatures, these data may be considered proxies for Permian air temperatures.

Suspect biological materials have been observed with plane-light and UV-vis microscopy and laser Raman spectroscopy. Rare 1-2 μm cocci shapes and pale orange ~10 μm spheres in fluid inclusions are suggestive of bacteria/archaea and algae, respectively. Very faint yellow and green fluorescence from UV-vis petrography of suspect microbes has been observed. Preliminary laser Raman spectroscopy yields spectra suggestive of some organic compounds.

Although fluid inclusion study of this Permian lacustrine halite has only recently begun, preliminary results promise an advanced and robust knowledge of specific Permian environmental conditions for the midcontinent of North America. These fluid inclusion data will strengthen models for depositional environment, paleoclimate, and past life.

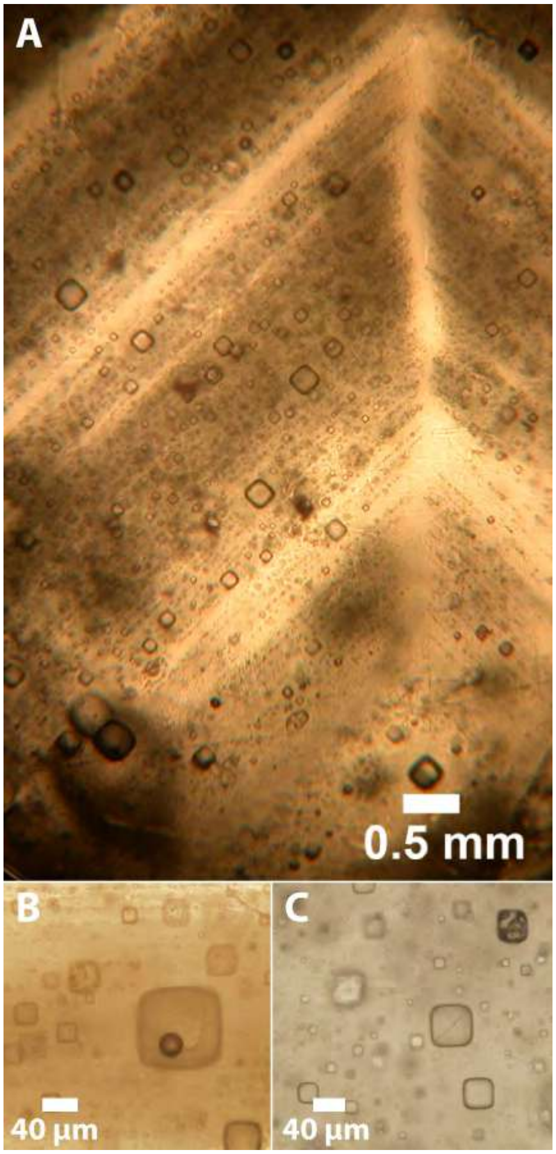

Figure 1: Fluid inclusions in Permian halite. A) Chevron crystal composed of alternating inclusion-rich and inclusion-poor growth bands. B) Primary inclusion containing large vapor bubble associated with one-phase fluid inclusions. C) Primary inclusion containing anhydrite crystals associated with one-phase fluid inclusions.

Analysis of direct samples of early solar system aqueous fluids.

Zolensky, M.E.*, Bodnar, R.J.**, Fedele L.**, Yurimoto, H.***, Itoh, S.***, Fries, M.****, and Steele, A.*****

**ARES, NASA Johnson Space Center, Houston, TX, U.S.A.*
***Fluids Research Laboratory, Department of Geosciences, Virginia Tech, Blacksburg, VA, U.S.A.*
****Natural History Sciences, Hokkaido University, Sapporo, Japan*
*****Planetary Science Institute, Tucson, AZ, U.S.A.*
******Geophysical Laboratory, Carnegie Institute of Science, Washington, DC, U.S.A.*

Over the past three decades we have become increasingly aware of the fundamental importance of water, and aqueous alteration, on primitive solar-system bodies. Some carbonaceous and ordinary chondrites have been altered by interactions with liquid water within the first 10 million years after formation of their parent asteroids. Millimeter to centimeter-sized aggregates of purple halite containing aqueous fluid inclusions were found in the matrix of two freshly-fallen brecciated H chondrite falls, Monahans (1998, hereafter simply “Monahans”) (H5) and Zag (H3-6) (Zolensky et al., 1999; Whitby et al., 2000; Bogard et al., 2001). In order to understand the origin and evolution of the aqueous fluids inside these inclusions, we must measure the actual fluid composition, and also determine the O and H isotopic composition of the water. It has taken a decade for laboratory analytical techniques to catch up to these particular nanomole-sized aqueous samples. We have recently been successful in (1) measuring the isotopic composition of H and O in the water in a few fluid inclusions from the Zag and Monahans halite, (2) mineralogical characterization of the solid mineral phases associated with the aqueous fluids within the halite, and (3) carrying out the first minor element analyses of the fluid itself.

A Cameca ims-1270 equipped with a cryo-sample-stage of Hokkaido University was specially prepared for the O and H isotopic measurements. The cryo-sample-stage (Techno. I. S. Corp.) was cooled down to c.a. -190°C using liquid nitrogen, at which point the aqueous fluid in inclusions was frozen. We excavated the salt crystal surfaces to expose the frozen fluids using a 15 keV Cs^+ beam and measured negative secondary ions. The secondary ions from deep craters of ~10 μm in depth emitted stably, but the intensities changed gradually during measurement cycles because of shifting states of charge compensation, resulting in rather poor reproducibility of multiple measurements of standard fluid inclusions of ±90‰ (2σ) for δD, and ±29‰ (2σ) for δ^{18}O. On the other hand, the reproducibility of Δ^{17}O is ±8‰ (2σ) because the observed variations of isotope ratios follow a mass dependent fractionation law. Variations of δD of the aqueous fluids range over 330(90; 2σ) to +1200(90)‰ for Monahans and 300(96)‰ to +90(98)‰ for Zag. Δ^{17}O of aqueous fluids range over δ16(22)‰ to +18(10)‰ for Monahans and +3(10)‰ to +27(11)‰ for Zag. These variations are larger than the reproducibility of standard analyses and suggest that isotope equilibria were under way in the fluids before trapping into halite. The mean values of δD and Δ^{17}O are +290‰ and +9‰, respectively. The mean values and the variations of these fluids are different from the representative values of ordinary chondrites, verifying our working hypothesis that the fluid inclusion-bearing halites were not indigenous to the H chondrite parent-asteroid but rather represent exogenous material delivered onto the asteroid from a separate cryovolcanically-active body. This initial isotopic work has demonstrated the feasibility of the measurements, but also revealed sample processing and analytical shortcomings that are now being addressed.

Examination of solid mineral inclusions within Monahans and Zag halite grains by confocal Raman spectroscopy at the Carnegie Geophysical Laboratory has revealed them to be metal, magnetite, forsteritic olivine (Fo≈98), macromolecular carbon (MMC), pyroxenes, feldspar with Raman spectral affinity to anorthoclase and, probably, fine-grained lepidocrocite (FeO(OH)). In addition, one inclusion features aliphatic material with Raman spectral features consistent with a mixture of short-chain aliphatic compounds.

We have initiated analyses of the bulk composition of the fluids within the inclusions in Zag and Monahans halites at Virginia Tech by LA-ICPMS using an Agilent 7500ce quadrupole ICPMS and a Lambda Physik GeoLas 193 nm excimer laser ablation system. Preliminary results reveal that the inclusion aqueous fluids contain highly charged cations of Ca, Mg and Fe.

The minerals and compounds discovered thus far within Monahans/Zag halites are indicative of an originating body at least partly composed of unequilibrated anhydrous materials (high Fo olivine, pyroxenes, feldspars, possibly the metal) which were subjected to aqueous alteration (the halite parent brine) and containing a light organic component (the short-chain aliphatic compounds). This material was ejected from the originating body with little or no disruption, as evidenced with the presence of fluid inclusions. An actively geysering body similar to modern Enceladus (Postberg et al., 2011) may be a reasonable analogue in this respect. Also, the originating body should have been within close proximity to the H chondrite parent in order to generate the number of halite grains seen in Monahans and Zag. Other candidates for Monahans/Zag halite parent bodie(s) may include a young Ceres with its possible liquid ocean, or Main Belt comets.

REFERENCES

Bogard D., Garrison D., Masarik J. (2001) The Monahans chondrite and halite; aron-39/argon-40 age, solar gases, cosmic-ray exposure ages, and parent body regolith neutron flux and thickness. Meteoritics and Planetary Science. Vol 36. 107-122.

Postberg F., Schmidt, J., Hillier, S., Kempf, S., Srama, R. (2011) A salt-water reservoir as the source of a compositionally stratified plume on Enceladus. Nature. Vol. 474. 620-622.

Whitby J.,Burgess, R., Turner, G., Gilmour, J., Bridges, J. (2000) Extinct ^{129}I in halite from a primitive meteorite; evidence for evaporate formation in the early solar system. Science. Vol. 288. 1819-1821.

Zolensky M.E., Bodnar, R.J., Gibson, E.K., Nyquist, L.E., Reese, Y., Shih, C-Y., Wiesmann, H. (1999) Asteroidal water within fluid inclusion-bearing halite in an H5 chondrite, Monahans (1998). Science. Vol. 285. 1377-1379.